AD-A171 571 EFFECT OF GRAIN SIZE ON THE INTERNAL FRACTURING OF POLYCRYSTALLINE ICE(U) COLD REGIONS RESEARCH AND ENGINEERING LAB HANOVER NH D M COLE JUL 86 CRREL-86-5 1/1

UNCLASSIFIED F/G 8/12 NL

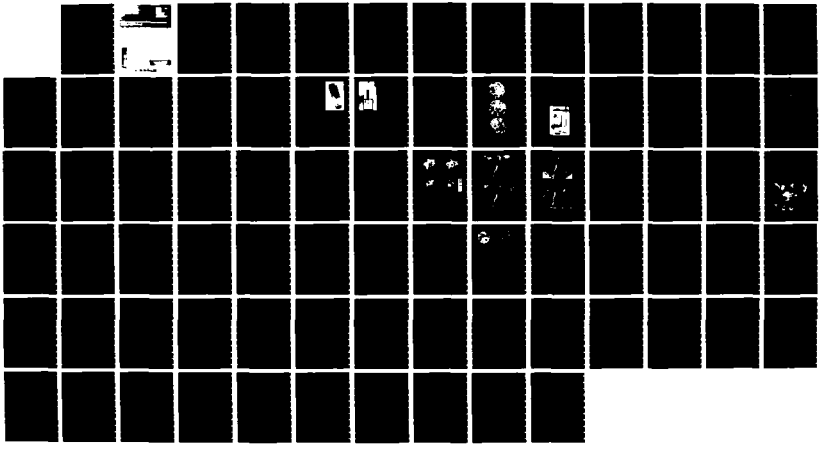

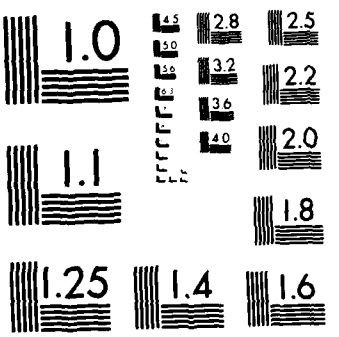

MICROCOPY RESOLUTION TEST CHART

Unclassified

SECURITY CLASSIFICATION OF THIS PAGE (When Data Entered)

REPORT DOCUMENTATION PAGE		READ INSTRUCTIONS BEFORE COMPLETING FORM
1. REPORT NUMBER CRREL Report 86-5	2. GOVT ACCESSION NO. AD-A171 571	3. RECIPIENT'S CATALOG NUMBER
4. TITLE (and Subtitle) EFFECT OF GRAIN SIZE ON THE INTERNAL FRACTURING OF POLYCRYSTALLINE ICE		5. TYPE OF REPORT & PERIOD COVERED 6. PERFORMING ORG. REPORT NUMBER
7. AUTHOR(s) David M. Cole		8. CONTRACT OR GRANT NUMBER(s)
9. PERFORMING ORGANIZATION NAME AND ADDRESS U.S. Army Cold Regions Research and Engineering Laboratory Hanover, New Hampshire 03755-1290		10. PROGRAM ELEMENT, PROJECT, TASK AREA & WORK UNIT NUMBERS DA Project 4A762730AT42 Task A, Work Unit 004
11. CONTROLLING OFFICE NAME AND ADDRESS Office of the Chief of Engineers Washington, DC 20314-1000		12. REPORT DATE July 1986 13. NUMBER OF PAGES 79
14. MONITORING AGENCY NAME & ADDRESS(if different from Controlling Office)		15. SECURITY CLASS. (of this report) Unclassified 15a. DECLASSIFICATION/DOWNGRADING SCHEDULE

16. DISTRIBUTION STATEMENT (of this Report)

Approved for public release; distribution is unlimited.

17. DISTRIBUTION STATEMENT (of the abstract entered in Block 20, if different from Report)

18. SUPPLEMENTARY NOTES

19. KEY WORDS (Continue on reverse side if necessary and identify by block number)

Acoustic emissions
Creep tests
Fracture (mechanics)
Grain size
Ice
Polycrystalline

20. ABSTRACT (Continue on reverse side if necessary and identify by block number)

This work presents the results of a study to examine the effects of grain size on the number and size of internal microfractures in polycrystalline ice. Laboratory-prepared specimens were tested under uniaxial, constant-load creep conditions at -5°C. Grain size ranged from 1.5 to 6.0 mm. This range of grain size, under an initial creep stress of 2.0 MPa, led to a significant change in the character of deformation. The finest-grained material displayed no internal cracking and typically experienced strains of 10^{-2} at the minimum creep rate $\dot{\epsilon}_{min}$. The coarse-grained material experienced severe cracking and a drop in the strain at $\dot{\epsilon}_{min}$ to approximately 4×10^{-3}. Extensive post-test optical analysis allowed estimation of the size distribution and number of microcracks in the tested material. These data led to the development of a relationship between the average crack size and the average grain size. Additionally, the crack

DD FORM 1 JAN 73 1473 EDITION OF 1 NOV 65 IS OBSOLETE

Unclassified

SECURITY CLASSIFICATION OF THIS PAGE (When Data Entered)

20. Abstract (cont'd).

size distribution, when normalized to the grain diameter, was very similar for all specimens tested. The results indicate that the average crack size is approximately one-half the average grain diameter over the stated grain size range. A dislocation pileup model is found to adequately predict the onset of internal cracking. The work employed acoustic emission techniques to monitor the fracturing activity. This information shed light on the time and strain at which the fracturing began and when the peak fracturing rate occurred. Other topics covered in this report include creep behavior, crack healing, the effect of stress level on fracture size and the orientation of cracked grains. Theoretical aspects of the grain size effect on material behavior are also given.

PREFACE

This report was prepared by David M. Cole, Research Civil Engineer, of the Applied Research Branch, Experimental Engineering Division, U.S. Army Cold Regions Research and Engineering Laboratory. Funding for this research was provided by DA Project 4A762730 AT42, *Research in Snow, Ice and Frozen Ground,* Task A, *Properties of Cold Regions Materials,* Work Unit 004, *Strength Characteristics of Ice and Frozen Ground.*

The author would like to express his appreciation to Dr. Erland Schulson for his help and support in the research described in this report. He also thanks Dr. Samuel Colbeck, Stephen Ackley, and Dr. Harold Frost for their help and useful suggestions, and for their technical review of this report.

The author is indebted to many members of the CRREL staff for their support in various aspects of this work. In particular, thanks are given to Dr. Ronald Liston for his encouragement throughout this program, and to Dr. Anthony Gow for many helpful suggestions. Special thanks are given to Gary Decoff for invaluable help in the computer aspects of this work, Nancy Richardson for her tireless efforts in typing the manuscript and Matthew Pacillo for drafting the illustrations.

CONTENTS

	Page
Abstract	i
Preface	iii
Background	1
Present research in perspective	2
Explanations of the grain-size dependency	2
Grain size effects on the ductile to brittle transition	3
Nucleation mechanisms and modeling	4
Characteristic size of nucleated crack	6
Cracking in ice	8
Detection of internal fracturing by acoustic emission techniques	10
Test methods	12
Specimen preparation	12
Creep testing apparatus	12
Crack length and crack density measurements	13
Crack healing measurements	14
Thin section photographs	14
Grain size determination	14
Acquisition of acoustic emission data	16
Presentation of results	18
Specimen characteristics	18
Microcrack measurements	18
Creep behavior	22
Crack healing	26
Slip plane length distribution	27
Acoustic emission observations	27
Grain orientation	28
Analysis and discussion	33
Thick section observations	34
The grain size vs crack size relationship	35
Crack nucleation condition	38
Crack density and specimen strain	40
Creep behavior	40
Normalized crack length	43
Location of cracks	44
Acoustic emission activity	45
Summary and conclusions	48
Suggestions for future work	48
Literature cited	49
Appendix A: Crack length histograms	53
Appendix B: Crystal orientations	71

ILLUSTRATIONS

Figure — Page

1. Stress/grain-size relationship showing transition grain size for ductile to brittle behavior 4
2. Most favorable crack orientation 5
3. Typical untested specimen 12
4. Creep testing apparatus showing displacement transducer and mounting clamps on specimen 13
5. Schematic showing typical locations of thick sections in the cylindrical ice specimens 13
6. Typical thin sections of test material 15
7. AE transducer mounted on specimen 16
8. Idealized acoustic emission waveforms 17
9. Typical crack length histogram 19
10. Mean crack length vs mean grain diameter 19
11. Mosaics formed from enlarged thick section photographs 20
12. Crack density vs grain diameter 21
13. Crack density vs axial strain for several ranges in grain size 23
14. Strain-time plots for several tests 23
15. Creep curves for all tests 24
16. Minimum creep rate vs grain diameter 26
17. Strain at minimum creep rate vs grain diameter for 10 specimens 27
18. Time-lapse photographs of crack healing, face view 28
19. Time-lapse photographs of crack healing, edge view 29
20. Crack length vs time 31
21. Slip plane length distribution 31
22. Typical acoustic emission data 32
23. Acoustic emission rate data 33
24. Thick section photograph taken parallel to the axis of applied stress 34
25. Distribution of the angle between the axis of compressive stress and the plane of the observed crack 35
26. Theoretical prediction and observed relationship for the average crack size/grain size relationship 38
27. Creep curve for a fine-grained specimen under high load 42
28. The effect of grain growth on grain size 43
29. Normalized fracture length distribution for all tests 44
30. Maximum normalized crack length vs grain diameter for all tests 44
31. Normalized crack length histograms 45
32. Mean AE amplitude vs mean crack length 47

TABLES

Table

1. Creep data 17
2. Grain size estimates and seed grain sizes 18
3. Crack location 19
4. Results of microfracture observations 21
5. Results of acoustic emission observations 32

EFFECT OF GRAIN SIZE ON THE INTERNAL FRACTURING OF POLYCRYSTALLINE ICE

David M. Cole

Ice exhibits brittle behavior at high temperatures under a variety of loading conditions. A key factor causing this brittleness is the lack of a sufficient number of independent slip systems; five are required to satisfy the von Mises criterion for an arbitrary change in shape. Slip is likely on the basal and prismatic planes (Goodman 1977), but these do not provide the needed five systems. So, given the inability of the lattice to accommodate plastic deformation by slip alone, and given a loading condition sufficiently rapid to prevent diffusional mechanisms from operating effectively, ice will develop cracks. The size and extent of the cracks at a given temperature depend on the applied stress and structural characteristics of the polycrystalline aggregate, such as the orientation, shape and size of the grains. Microstructural differences such as those between freshwater ice and sea ice also influence cracking activity.

The internal shear stress generated during either tensile or compressive loading nucleates cracks. Under certain conditions, these cracks propagate only a short distance before coming to rest within the material. Given sufficiently high stress levels, the cracks thus nucleated can propagate through the material to cause brittle fracture.

The nucleation of stable, non-propagating cracks is of interest for a number of reasons. These cracks are the flaws that can propagate under subsequent tensile loading. In compression, when the cracks do not propagate, they are responsible for the gradual weakening of the structure as straining proceeds. Gold (1970) noted that ice passes directly from primary to tertiary creep as a result of the structural damage caused by internal cracking.

This report concentrates on the effect of grain size on the internal cracking of polycrystalline ice with equiaxed grains. Relatively little research has been done in this area, although considerable work exists on the cracking of columnar grained ice, and such work is examined in detail. Additionally, some relevant contributions regarding cracking in materials other than ice are covered.

Initial discussions center on the root of the grain-size dependency in material behavior. The effect of grain size on the ductile/brittle nature of deformation is then addressed. Subsequent sections give attention to crack nucleation mechanisms and the cracking activity observed in ice. The final sections describe acoustic emission techniques for crack detection and their application to the field of ice mechanics.

BACKGROUND

This work primarily examines the dislocation pileup mechanism for crack nucleation. While the operation of a mechanism based on stress concen-

trations arising from grain anisotropy is recognized, it is felt that the pileup mechanism will dominate at the strain rates and temperatures investigated in this work.

Present research in perspective

The role of grain boundaries in crack formation has long been recognized. However, very little has been done to quantify the relationship between grain size and crack size, primarily due to the difficulty in making the appropriate observations in most materials.

A primary objective of this research was to develop a crack size/grain size relationship for ice. Because of its optical properties and its propensity to develop cracks under conditions of practical concern, polycrystalline ice was ideally suited to such a study of internal cracking activity. The optical techniques employed allow the estimation of the crack size distribution as well as the number of cracks per unit volume in the tested material.

Another objective was to demonstrate the effect of grain size relative to the onset of internal cracking. As noted above, earlier work clearly demonstrated the influence of stress or strain rate on the tendency of ice to develop cracks, but the influence of grain size alone in this regard has not been clearly demonstrated. This objective was accomplished by monitoring the extent of cracking in specimens of increasing grain size while such variables as stress, temperature and the amount of strain were held constant. The conditions for the onset of cracking were analyzed in terms of established crack nucleation theory.

Additionally, this research addressed several peripheral topics germane to the experimental methods employed and to the mechanical properties of ice in general. These topics included the observation of microcracks at various times after formation to monitor shape change (the crack healing process), an examination of the effect of grain size on creep behavior, acoustic emissions activity, and observations on the orientation of grains containing cracks and the orientation of the cracks themselves relative to the axis of compressive stress.

The information obtained by the accomplishment of these objectives will be useful in several respects. The crack size/grain size relationships will enhance our understanding of the effect of grain size on the fracture strength of unflawed ice. Knowledge of the size distribution and number of cracks will allow a more precise examination of the effects of stress/strain history on the mechanical properties of the material. Verification of the crack nucleation model will allow its application with greater confidence.

The crack healing observations will be useful in that the results indicate the change in crack geometry with time. This makes it possible to assess the period for which a newly formed crack is a significant source of internal stress concentration.

Explanations of the grain-size dependency

Armstrong (1979) pointed out the broad applicability of the Hall-Petch relationship between strength and grain size:

$$\sigma = \sigma_0 + Kd^{-1/2} \tag{1}$$

where σ = stress
σ_0 = frictional stress
K = Hall-Petch slope
d = grain diameter.

He summarized results demonstrating the validity of the Hall-Petch relationship for tensile yield and brittle fracture stresses and for the flow stress at various levels of strain. Equation 1 is essentially an empirical relationship and much work has been carried out in efforts to develop a firm theoretical basis for its veracity.

Li and Chou (1970) review the major theoretical arguments that have been put forth to explain the $d^{-1/2}$ dependency. Early work (see Stroh 1957 for a useful summary) led to the wide acceptance of a dislocation pileup model to explain the observed grain size dependency. Direct observations of dislocation pileups at grain boundaries made a very convincing case for this. Arguments for the dislocation pileup model are based on the supposition that shear deformation passes from grain to grain when dislocations, acting under an imposed stress, pile up at a grain boundary and produce a stress concentration that is capable of producing slip in the adjacent grain.

A pileup at the edge of one grain of diameter d induces a shear stress τ at a distance r in the adjacent grain according to the relationship

$$\tau = \tau_i (d/r)^{1/2} \tag{2}$$

where τ_i is the applied shear stress. Given that a stress τ_d is required to generate slip in the adjacent grain, and that a frictional stress τ_i must be overcome, eq 2 may be rewritten:

$$\tau_d = (\tau_i - \tau_i)(d/r)^{1/2}. \tag{3}$$

Solving for the applied shear stress,

$$\tau_s = \tau_i + \tau_d (r/d)^{1/2}. \quad (4)$$

Thus arises the $d^{-1/2}$ dependency according to the dislocation pileup mechanism.

Interestingly, as Li and Chou (1970) pointed out, materials in which no pileups are observed have been found to obey the Hall–Petch relationship. This has led to a search for alternative explanations of the observed stress/grain-size relationship, namely work hardening and grain boundary source theories.

The work hardening theory derives a $d^{-1/2}$ dependency by using the experimentally established fact that the yield or flow stress is a function of the square root of the dislocation density, ϱ:

$$\sigma = \sigma_0 + \alpha\mu b\sqrt{\varrho} \quad (5)$$

where α = a numerical constant
σ_0 = the ordinate intercept in a plot of σ vs $d^{1/2}$
μ = the shear modulus
b = the Burgers vector.

Other experimental observations indicate that the dislocation density at yield varies inversely with grain size, thus explaining the $d^{-1/2}$ dependency.

The grain boundary source theory considers grain boundaries capable of generating dislocations. The length of the dislocation lines generated in this manner is directly proportional to the grain boundary area. When this is normalized to grain volume to give a dislocation density, a d^{-1} dependency arises. Substitution into eq 5 again yields the $d^{-1/2}$ dependency.

Stroh's (1957) work developed a crack nucleation model based on the dislocation pileup mechanism. In order to proceed with complete confidence in the use of such a model, direct evidence of dislocation pileups in the material in question would be necessary. Sinha (1978) presented photographic evidence of dislocations in polycrystalline ice. Using an etching and replication technique, he demonstrated the existence of dislocation pileups at grain boundaries through the observation of etch-pits on carefully prepared surfaces. Furthermore, Sinha's results clearly indicated the glide of basal dislocations under an applied stress. He noted the appearance of dislocations on the $\{11\bar{2}0\}$ surface parallel to the basal plane. However, work by Gold (1972) indicates that the pileup mechanism may not be the only one to cause cracking in ice.

Gold (1972) demonstrated that two independent crack distributions exist in columnar-grained ice. One was strain-dependent and was consistent with a dislocation pileup mechanism. The other appeared to be essentially independent of strain, was mainly composed of grain boundary cracks and represented approximately 24% of the total crack population. Gold (1972) speculated that cracking represented by the latter distribution dominated at high rates of loading, thus associating grain boundary cracking with brittle behavior. Furthermore, he suggested that the balance between these two crack distributions determines the transition from ductile to brittle behavior in compression.

The mechanism of this strain-independent crack distribution is not clear but appears to be more closely associated with elastic behavior than with plastic behavior. If this is indeed the case, the pileup mechanism should be adequate when significant plastic flow occurs. However, its applicability is liable to diminish as behavior becomes more brittle.

It is very difficult to discern the crack nucleation mechanism from gross specimen observations. As Stroh (1957) pointed out, the dislocation pileup model predicts the likelihood of cracking at strains on the order of those expected for cracks caused by elastically generated stress concentrations.

In light of the above, while the dislocation pileup mechanism may not be the only source of stress concentrations of sufficient magnitude to generate cracks, it reflects the bulk of the cracking activity of ice when the behavior is not purely brittle.

Grain size effects on the ductile to brittle transition

Through its influence over the internal distributions of stress, grain size exerts a significant influence over many aspects of material behavior. Most germane to the present work is the influence of grain size on the ductile/brittle character of deformation.

Armstrong (1970) explained the effect of grain size on the ductile-to-brittle transition in mild steel. Due to the thermal effects on the stress required to cause either yielding or fracture, the failure stress generally increases as temperature decreases. At a constant strain rate, the material undergoes a transition from ductile to brittle behavior at some temperature T_c. An increase in

grain size lowers the peak stress experienced under constant strain rate and increases T_c. The drop in peak stress follows the slope of the Hall–Petch relationship. The rise in T_c results from the relationship between grain size and the temperature-dependent frictional stress term of the Hall–Petch relationship, σ_0.

At constant temperature and strain rate a critical grain size may be determined above which the material is brittle and below which the material is ductile. Stroh (1957) arrived at a relationship between transition temperature and grain size by using a stochastic method:

$$1/T_c = -\tfrac{1}{2}(k/u)\log(d) + c \qquad (6)$$

where T_c = transition temperature
k = Boltzmann constant
c = a constant independent of temperature and strain rate
u = activation energy.

More recently, Schulson (1979) derived a relationship for the tensile case between the critical grain size and material characteristics of the form

$$d_c = \left(\frac{1.6K_{Ic} - K}{\sigma_0}\right)^2 \qquad (7)$$

where K_{Ic} is the critical stress intensity factor. This expression stems from the fact that, at some particular grain size, both slip-propagation controlled yield (ductile behavior) and crack-nucleation controlled fracture (brittle behavior) are equally likely. Figure 1 shows the stress vs grain size curves for the ductile and brittle cases. The intersection defines the critical grain size. In the present work, grain size varies about the critical grain size and the resulting material behavior changes in character accordingly.

The relationship between grain size and T_c can be seen in Figure 1. A lower T_c results from a higher value of σ_0 in the Hall–Petch expression describing curve 1. This has the effect of raising curve 1a in Figure 1 to curve 1b and thus shifting the intercept with curve 2 to a lower grain size. The expression for curve 2 is much less sensitive to temperature variations. Consequently, it does not shift appreciably and the effect of temperature on the point of intersection is not significantly diminished.

An increase in grain size over the critical value brings about the reduction in overall specimen strain prior to fracture often associated with increased brittleness. Results given by Mendiratta et al. (1976) show a reduction in strain to fracture in a titanium alloy from 0.21 to 0.02 arising only from an increase in grain size. For this change to take place, grain size was increased an order of magnitude from 9 to 90 μm, and the fracture mode changed from ductile dimple to brittle cleavage.

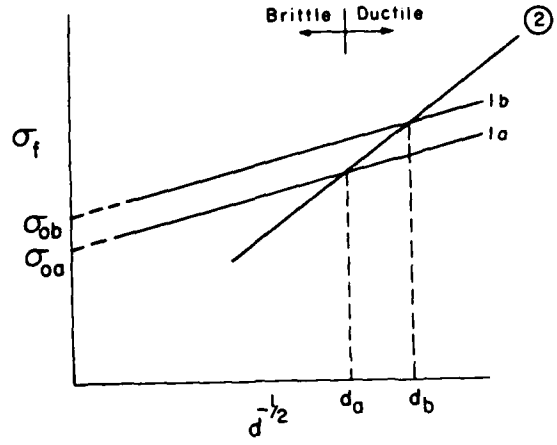

Figure 1. Stress/grain size relationship showing transition grain size for ductile (curve 2) to brittle (curves 1a and 1b) behavior. Shift from curve 1a to 1b shows effect of decreasing temperature on σ_0 and on the critical grain size.

According to work by Terlinde and Luetjering (1982) grain size exerted an influence on fracture strain of the form

$$\epsilon_f \propto d^{-1}. \qquad (8)$$

In this work, as in the abovementioned results of Mendiratta et al. (1976), a reduction in grain size changed the behavior of a titanium-aluminum alloy from primarily brittle to primarily ductile, with a significant increase in failure strain.

Nucleation mechanisms and modeling

Most current thought on crack nucleation stems from a model given by Zener (1948). According to this model a crack nucleates when the normal stress generated by a dislocation pileup reaches a critical level; this causes the material to fracture and allows the dislocations to coalesce, relieving the local strain energy. A relatively strong barrier must be present in order for the pileup to build to a sufficient stress to nucleate the crack. Lattice orientation changes at grain boundaries or hard inclusions may serve as effective barriers.

Stroh (1957) presented an extensive analysis of the stresses required to nucleate a crack. Stroh based his development on the concept of a disloca-

tion pileup on a slip plane, acted upon by a shear stress, which generates a sufficient normal stress in a neighboring grain to produce a cleavage fracture. He derived the expression

$$\sigma_E^2 = 3\pi\gamma\mu/8(1-\upsilon)\ell \tag{9}$$

for the resolved shear stress on the slip plane and, by using

$$\ell = \mu b n/\pi(1-\upsilon)\sigma, \tag{10}$$

showed the nucleation condition to be

$$n\sigma_E b = {}^3/_8\,\pi^2\gamma \tag{11}$$

where σ_E = resolved effective shear stress on the slip plane
γ = surface energy
μ = shear modulus
υ = Poisson's ratio
ℓ = length of pileup
b = the Burgers vector
n = number of dislocations in the pileup.

In eq 9, coefficients have been determined for the case of the crack forming at an orientation to the slip plane which maximizes the stress on the forming crack. Stroh determined this angle to be 70.5°. He also points out that a crack length term does not appear in this expression.

In a later work, Smith and Barnby (1967) reformulated Stroh's approach to account for the effect of shear stress on the nucleation process and developed orientation factors to account for geometries other than Stroh's case of maximum normal stress.

Smith and Barnby (1967) give the nucleation condition for a pileup of edge dislocations of a single sign as

$$\sigma_t = \left(\frac{\pi\gamma\mu}{2(1-\upsilon)\ell}\right)^{1/2} \frac{1}{[F(\phi)]^{1/2}} \tag{12}$$

where $F(\phi) = (5 + 2\cos\phi - 3\cos^2\phi)/4$ and the corresponding number of dislocations required under σ_t is

$$n = \frac{\pi^2\gamma}{2\sigma_t b}\,\frac{1}{F(\phi)}\,. \tag{13}$$

Nucleation conditions for more elaborate configurations of dislocation sign and slip plane-crack geometry are also given. Again, as in Stroh's analysis, the crack length does not appear in the nucleation criterion, only the pileup length.

The fact that the nucleation condition does not contain a crack length term is a key point. The length of the crack is determined by both the normal stress component and the presence of obstacles to its growth such as grain boundaries. In other words, once the separation of atom planes is initiated, it will continue as long as sufficient normal stress exists to propagate it. This would be the case, for example, in a tension test if the pileup were of sufficient size to generate a Griffith crack. The background tensile stress could drive the crack (nucleated via shear stresses) through the material to cause fracture. If the nucleated crack is not favorably oriented to the backgound stress or if the stress is of insufficient magnitude, it will come to rest within the material.

In compression, the nucleated cracks generally do not propagate. Initially, the background compressive stress generates shear stresses along favorably oriented slip planes, giving rise to dislocation pileups, as in the tensile case. Once the crack is nucleated, the compressive stress is not capable of propagating the crack. Instead, the crack comes to rest when the strain energy associated with the pileup is dissipated or when the leading edge of the crack reaches a barrier that it cannot overcome, such as the change in lattice orientation occurring at a grain boundary.

Visual observations (St. Lawrence and Cole 1982, Currier 1983) reveal a strong tendency for non-propagating cracks to form roughly parallel to the loading axis in uniaxial compression tests on randomly oriented, equiaxed polycrystalline ice.

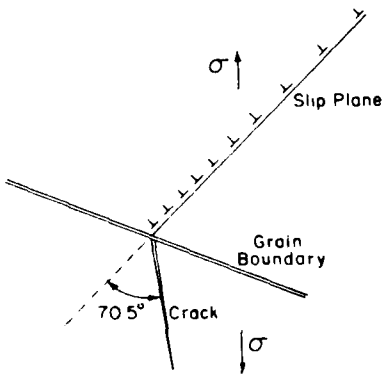

Figure 2. Most favorable crack orientation (after Stroh 1957).

This is reasonable considering Stroh's determination of the most favorable angle between the slip plane and the nucleated crack. Figure 2 shows the geometry of this situation. The slip plane is taken at an angle of 45° to the loading axis.

Although the slip plane (i.e. basal plane) could be at an angle other than the 45° shown, the planes of maximum resolved shear stress will tend to cluster about this value. Also, Smith and Barnby (1967) have shown that, while Stroh's optimum value of $\phi = 70.5°$ is correct, ϕ may easily range from 0 to 90° when shear stresses are considered in the analysis. Even when these values are used as a maximum range of crack orientation, the cracks thus nucleated will tend to lie within about 45° of the stress axis and have no strong tendency to form perpendicular to it under uniaxial stress.

Characteristic size of nucleated crack

In examining fracture mechanisms in metals, Gandhi and Ashby (1979) designated cracking with no pre-existing flaw as "cleavage 2." Here fractures are nucleated by slip or twinning. They noted that these cracks were proportional to the grain diameter and attributed this to control by the grain size of the wavelength of the internal stress.

Physically, this proportionality comes about as a result of the obstacle nature of the grain boundary. When a polycrystalline aggregate is subjected to, say, a uniaxial stress, the material experiences a uniform stress field in a macroscopic sense. Microscopically, however, this is far from the case: the internal stress and strain fields are very inhomogeneous.

Irregularities in the stress and strain fields are brought about, in a pure polycrystalline aggregate, by crystal anisotropy and by dislocation movement. Furthermore, the internal stress field is in a constant state of flux as highly localized deformation accompanies both the buildup and dissipation of stress concentrations within the material. The frequency with which these stress concentrations occur throughout the material depends primarily on the size of the constituent grains for the following reasons.

The most likely site for such stress concentrations is a grain boundary since it offers a significant obstacle to the propagation of shear deformation from grain to grain. The most likely slip plane is the uninterrupted basal plane extending across an individual grain. The slip plane length may or may not equal, but in general will scale as, the grain size. Thus, if deformation occurs via the propagation of slip bands, the stress concentrations and their associated local stress fields occur in the material at spacings proportional to the grain size. The slip occurs under the action of shear stress. However, the stress concentration resulting from slip generates a complex field of tensile, compressive and shear stresses.

Gandhi and Ashby (1979) give the expression for a critical stress σ^* above which a nucleated fracture will propagate and below which the crack will come to rest with length proportional to the grain diameter, d:

$$\sigma^* \approx (EG_c/\pi d)^{1/2} \tag{14}$$

where E is Young's modulus and G_c is toughness.

This is a propagation criterion, not a nucleation criterion, in that it assumes the nucleation of a Griffith crack proportional to d. However, the use of a crack size on the order of d should be noted.

According to Stroh (1957), a nucleated crack will attain a length, when normal background stresses are absent, determined by the number of dislocations which enter it. Once the crack is nucleated, dislocations enter it more easily because the back stress of the pileup is relieved. The more dislocations that enter, the wider and hence the longer the crack becomes. In the compression case, the only driving force for the crack is the rapidly relaxing force from the dislocation pileup. Thus, the length of the crack primarily is a function of the number of dislocations causing it to nucleate.

Generally, the analytical approach has been to assume that the favorably oriented slip planes are activated most frequently, and these will in turn nucleate cracks most easily. If these slip planes have a characteristic length, say on the order of the grain diameter, under a given nominal stress they will all tend to contain about the same number of dislocations. The associated cracks will thus tend to have a charcteristic length (see Gold 1966, for example). Stroh (1957) has indicated that cracks will nucleate and propagate to a length on the order of ℓ, the pileup length, in the absence of other driving stresses.

However, the above should be stated more precisely in terms of distributions of the quantities under consideration rather than average or characteristic values. Briefly, an estimate of the distribution of nucleated crack sizes can be obtained if an appropriate distribution, rather than an average value, is used to represent the slip plane length. However, for the purpose of demonstra-

tion of the relationship between the dislocation pileup size and the nucleated crack size, average quantities are used.

As mentioned above, grain boundaries can limit crack length. In the case of a uniaxial compression test, crack orientation can result in little or no tensile stress normal to the crack face, and a forming crack may not have a sufficient driving force to overcome the crystal reorientation at a grain boundary. Additionally, Cottrell (1958) viewed the grain boundary as a likely stopping point for a nucleated crack because a change in orientation of the cleavage plane effectively represents a region of higher surface energy to the propagating microcrack. Thus, since grain boundaries are both likely nucleation and termination sites for cracks, the crack size is expected to correlate with the grain dimension.

Actual crack length distribution data are uncommon in the literature. However, work by McMahon and Cohen (1965) shows crack size bar graphs for F4 ferrite after repeated straining in tension. They found that microcracks approximately equal to or less than the grain diameter formed first, and cracks up to three times the grain diameter formed after several loading cycles. Under certain test conditions, twin formation was prevalent and the authors attributed a reduction in the number of large cracks to the obstacle nature of the twins. Interestingly, rough calculations based on the bar graphs of McMahon and Cohen (1965) indicate that the average crack size is slightly over one grain diameter both with and without twin formation. They also note that small cracks continue to form when the large cracks begin to appear as the number of stress cycles increases.

Gold (1966) develops a quantitative approach to the relationship between grain size and nucleated crack size by using theory developed by Stroh (1954) and Bullough (1964). Gold performed uniaxial compression tests on columnar grained ice and made detailed observations on the size and number of microcracks formed during testing. Gold's analysis considers the energy of a cracked dislocation under an applied stress, and uses an energy balance method that leads to the determination of a critical or Griffith crack. The concept of a cracked dislocation as explained by Bullough (1964) allows the development of a fracture criterion given a dislocation pileup and an associated in-plane crack under an applied stress. The fracture criterion is then based on this crack achieving a critical length for propagation. Gold (1967) considers two cases when the crack forms in a grain adjacent to the grain containing the pileup: 1) the crack forms at an angle to the slip plane containing the pileup and 2) the crack forms in plane with the pileup.

Based on the equations of Stroh (1954) the energy associated with case 1 is

$$W = \frac{n^2 b^2 \mu}{4\pi(1-\upsilon)} \ln \frac{4L}{a} - \frac{\sigma_n n b a}{2} - \frac{\sigma_n^2 \pi a^2 (1-\upsilon)}{8\mu} + 2a\gamma \qquad (15)$$

where W = energy of the crack per unit length
L = effective radius of influence of the dislocations ($L \gg a$)
σ_n = tensile stress perpendicular to the plane in which the crack forms
a = crack width.

For case 2 (Bullough 1964),

$$W = \frac{n^2 b^2 \mu}{4\pi(1-\upsilon)} \ln \frac{4L}{a} - \frac{\pi a^2 (1-\upsilon)\sigma_n^2}{8\mu} + 2a\gamma. \qquad (16)$$

Gold (1966) derives critical values of crack width a for the two cases:

Case 1 $$a_{crit} = \frac{2\mu\gamma}{\pi(1-\upsilon)\sigma_n^2} \qquad (17)$$

Case 2 $$a_{crit} = \frac{4\mu\gamma}{\pi(1-\upsilon)\sigma_n^2}. \qquad (18)$$

After assuming that σ_n is equal to but of opposite sign than the applied axial compressive stress, Gold arrives at values of $a_{crit} = 5.7 \times 10^{-4}$ and 11.4×10^{-4} m for cases 1 and 2, which are in reasonable agreement with the experimental observations. Gold (1967) performed tests on replicate specimens and thus did not address the issue of grain size effects on the cracking activity of the ice. Indeed, if the assumption regarding the value of σ_n being equal and opposite to the applied stress is maintained, the above expressions for critical crack size are independent of grain size. This is a reasonable result when crack propagation is considered. The cracked dislocation is viewed as a preexisting flaw and examined in terms of its potential to propagate under a given stress field. The potential (or likelihood) for propagation is a function of material constants and flow characteris-

tics, but not specifically of grain size. Grain size exerts only an indirect influence in that it has an effect on the production of flaws in the material. Thus, if consideration begins with the material in a flawed state, grain size is not a primary consideration.

The material in the present work is considered to be unflawed and the grain size-dependent nucleation equations given earlier apply. In a subsequent section, a simple method is used to relate the nucleated crack size to the grain size through strain energy and surface energy considerations in a manner similar to the above.

Cracking in ice

A series of papers by Gold (1960; 1965a,b; 1966; 1967; 1970a,b; 1972; 1977) represent the most extensive investigations into the internal cracking of ice. The experimental work primarily involves columnar-grained ice, but many of the observations made are germane to the behavior of equiaxial-grained ice.

In his early work, Gold (1960) noted the formation of cracks parallel to the long dimension of grains in rectangular ice specimens. The test material was grown to result in random *c*-axis orientation in the plane perpendicular to the long axis of the grains. Cracks formed parallel to the grain boundaries and the planes of the cracks were within 45° of the stress axis. A detailed analysis of a number of cracks indicated that 30% were on grain boundaries, 59% were transcrystalline and the remaining 11% were of mixed character.

Gold (1960) also noted a change in the cracking activity for stresses greater than approximately 1.5 MPa at a temperature of -10°C. Specimens were tested under creep conditions and the material was columnar-grained freshwater ice. The average grain diameter perpendicular to the long axis of the grains was approximately 4 mm. Below the 1.5-MPa stress, cracks were relatively sparse and uniformly distributed; above this stress, cracking activity increased significantly and the cracks tended to cluster along planes of maximum shear. Cracking activity also tended to peak early in the tests.

Continuation of work along the same lines (Gold 1967) demonstrated that cracks generally involved only one or two grains and that they tended to propagate either parallel or perpendicular to the basal planes. The number of cracks that formed in a particular test depended mainly on stress and creep strain levels and was substantially independent of temperature. The test material in this work was again columnar-grained freshwater ice having basal planes parallel to the long dimensions of the grains. Compressive loads were applied perpendicular to the long dimensions of the grains.

Gold (1967) also suggests that the strength of ice experiencing purely brittle failure is determined by the level of elastic stresses that the material can sustain. In this case, rapid loading rates disallow significant plastic flow. Plastic flow can occur, however, at slower rates of loading, and internal stress concentrations capable of initiating cracking eventually develop.

Gold (1967) found considerable scatter in the time to first crack formation under a given creep stress. In general, the time for a crack to form showed an exponential decay with increasing creep stress. Some straining occurred after load application during which no cracks formed. For high stresses, some small cracks appeared upon and immediately following loading.

At a level of creep strain between 3×10^{-4} and 3×10^{-3}, large cracks (i.e. greater than 2 mm wide $\times$ 2 mm long) began to form. The rate of formation built up to a peak and then gradually declined as straining proceeded. Results indicated that the nucleation of a crack depended mainly on the level of creep strain and "not on factors controlling the rate at which the deformation occurs." Gold (1967) also noted that cracks tended to form in grains having their basal planes either perpendicular or parallel to the axis of applied stress. It was in this work, as mentioned earlier, that Gold demonstrated the applicability of a dislocation pileup mechanism to polycrystalline ice.

In subsequent work, Gold (1970a,b) quantified the cracking activity he observed in columnar-grained ice. He also noted, for creep stresses less than about 1 MPa at temperatures between -4.8 and -31 °C, that cracking was confined mainly to primary creep and that a clear secondary creep stage developed. For stresses over about 1.2 MPa, however, continuous cracking activity resulted and the material passed directly from primary to tertiary creep within 2.5×10^{-3} strain. He attributed the onset of tertiary creep in his columnar-grained material to the breakdown of the structure by internal cracking. However, it should not be inferred from this that cracking is necessary for tertiary creep to occur in ice in general. Mellor and Cole (1982) present test results that show a smooth transition from primary to tertiary creep in the absence of internal cracking in tests on equiaxed polycrystalline ice.

Gold (1970a,b) monitored the crack density by counting the number of cracks intersecting a plane perpendicular to the stress axis. Values were re-

ported in the number of cracks per unit area. By deforming specimens under various loads or strain rates (as well as at several temperatures) to given levels of strain, Gold was able to determine the increase in crack density as straining proceeded for a wide range of test conditions. These tests yielded the following additional information. The nucleated cracks did not appear to propagate with additional straining. The cracking rate depended on stress, strain and temperature. The maximum cracking rate tended to occur between axial strains of 1.5×10^{-3} to 2.5×10^{-3}. For stresses below about 1 MPa, the cracking rate tended to zero as straining proceeded. At greater stresses, cracking continued at a reduced rate after the cracking rate maximum was reached. Cracks were randomly distributed in the ice at low strains under all test conditions. But at higher stresses they tended to form in bands or "fault planes" after the maximum cracking rate had occurred.

Although Gold did not observe fully brittle behavior in these tests, he did find a decrease in the strain at which the strain rate minimum occurred with increasing cracking. As cracking became more severe, the strain associated with the transition to tertiary creep decreased from levels over 10^{-2} to less than 2.5×10^{-3}. He noted, however, that even when the lowest strains were observed, the material response was still significantly ductile in character.

Additional work (Gold 1972) reinforced his earlier observations on cracking activity. He also developed the stress dependency of cracking and investigated the statistics of the cracking activity. He found that the crack sites are not truly random throughout the specimen, but rather that the probability of a crack nucleating in a region decreases if that region already contains a crack.

Using Weibull statistics, Gold (1972) inferred the existence of two separate crack distributions. One, believed to represent cracks generated by the pileup mechanism, was strain dependent. The other distribution represented cracks formed by processes essentially independent of specimen strain; these cracks formed mainly at grain boundaries. The probability of their occurrence increased with increasing applied stress. Gold speculates that, given sufficient stress, the type of strain-independent cracking could be extensive enough to be the sole cause of specimen failure. In this work, Gold also noted that crack density decreased with temperature for a given strain at constant stress.

In a review paper, Gold (1977) pointed out the need for an increased understanding of the factors influencing the cracking activity in ice as it relates to the ductile-to-brittle transition, emphasizing ice type, temperature, loading conditions, grain size and specimen size. Some Soviet workers have conducted work along a similar line to that of Gold. Zaretsky et al. (1976) presented the results of a study on microcrack formation in columnar-grained ice. As in Gold's work, load was applied perpendicular to the long axes of the grains and the *c*-axes were randomly oriented in a plane perpendicular to the long axes of the grains. They relied heavily on the acoustic emissions (AE) monitoring technique to quantify the cracking activity. This technique was first used on ice by Gold (1960), who subsequently abandoned it and relied on visual methods to estimate the number of internal fractures.

The AE technique employs piezoelectric transducers to monitor stress waves generated by the initiation of a microcrack. The intensity of the stress wave is assumed proportional to the magnitude of the event that generates it. Electronic devices analyze the transducer output and characterize the signals in various ways, depending on the level of sophistication of the particular system. A subsequent section examines the AE method in greater detail.

Zaretsky et al. (1976) assumed a one-to-one correspondence between acoustic pulses and crack formation. Furthermore, the amplitude of the AE pulse was taken as proportional to the area of the crack that generated it. These assumptions were substantiated in subsequent work (Zaretsky et al. 1979).

Experimentally, the Soviet workers found much the same ice behavior as did Gold. Zaretsky et al. (1976) found a threshold stress for crack nucleation (denoted as σ_∞). The cracks tended to form along the grain boundaries of the columnar-grained test material. The ice deformed primarily in two dimensions—as also noted by Gold. Complete breakup of the specimens occurred at some appropriate level of crack density. The number and rate of formation of microcracks increased with increasing applied stress.

Zaretsky et al. (1976) developed an equation for the short-term ice creep rate in terms of the accumulated number of defects (microcracks), stress and two parameters. By relying heavily on there being a relatively constant number of cracks at the point of "breakup," they developed expressions for the time to break up under a given stress.

By coupling ice straining solely with the occurrence of internal cracking (as detected by AE), this work inherently recognizes cracking as the only deformational mechanism.

Zaretsky et al. (1979) expanded on much of the work presented in Zaretsky et al. (1976). The threshold stress σ_∞ was viewed as the stress above which the "progressive accumulation of structural defects occurs." Since the accurate assessment of the extent of internal cracking was critical to the evaluation of the analytical expressions of this work, Zaretsky et al. (1979) presented the results of a detailed petrographic analysis on tested specimens. The results showed structural changes (i.e. the breakup of large grains) as straining proceeded. This gave an indication of the extent of internal cracking since it was crack formation that broke up the large original grains into smaller grains.

Zaretsky et al. (1979) concluded that the threshold stress σ_∞, in uniaxial compression, is independent of temperature. Furthermore, from measurements of crack areas, it appeared that the mean crack size increased with the extent of cracking (and thus with creep stress). Crack size was given in arbitrary units, however, and thus a direct comparison between crack size and the grain size (which ranged from 2 to 12 mm) is not possible. The analytical result was an expression for creep strain as a function of stress, temperature and a cracking-related term based on AE data.

Detection of internal fracturing by acoustic emission techniques

Information provided by acoustic emissions (AE) monitoring can contribute significantly to the understanding of material behavior. Microfracturing activity especially lends itself to interpretation by AE techniques because pressure waves generated during fracture formation are easily detected. The main concern in handling AE data is that of interpretation—determining the appropriate correlation between the characteristics of the source event and the recorded AE signal. In the present case, the source event is the formation of a microcrack within the ice and the relevant AE characteristic is signal amplitude.

Evans (1979) gave a theoretical treatment of acoustical pulses generated by microfracture in brittle solids. He showed that the amplitude of such a pulse is a function of crack geometry, applied stress, material properties, and distance from the source. The fracture event generates a "ringing" or oscillation in the crystal lattice that decays in time and has a characteristic frequency spectrum. Frequency analysis is often used to differentiate source mechanisms where more than one mechanism is operating. In the present case, however, only the dislocation pileup mechanism is assumed to be operating and hence a frequency analysis is not deemed critical to the investigation. The work concentrates primarily on the analysis of AE pulse amplitude.

When the size of the AE source (i.e. microfracture) varies, the peak AE signal strength varies as well, all other factors being equal. Such factors as crack orientation and distance from the sensor can cause significant differences in the signal recorded for otherwise identical sources. Thus it should be kept in mind that the distributions generally given for AE amplitude reflect not only variations in the source itself but, to some extent, second-order variables as well.

AE amplitude data are best manipulated in the form of distribution functions. Pollock (1981) described the most commonly used distributions and discussed their pros and cons. Among those presented were the Weibull and the log-normal distributions as well as the extreme value distributions. That work also traced the development of several models developed specifically for AE data analysis. He emphasized that the amplitude distribution can be considered a property of the source mechanism. This last point is a common thread in much AE work.

Ono et al. (1978) showed close correlation between the particle size distribution of Mn-S inclusions in steel and the AE amplitude distribution found when the particles fractured during testing. Thus, the particle size governed the crack size, which in turn governed the amplitude distribution. Wadley et al. (1981) and Cousland and Scala (1981) are other examples of work directed at linking acoustic activity and specific microstructural characteristics.

In certain cases, AE also proves useful in eliminating certain deformational mechanisms from consideration. For example, in Cousland and Scala (1981), inclusion fracture was observed in tension testing and produced very high amplitude emissions. When the same material was tested in compression, inclusion fracture did not occur and no high amplitude AE signals were observed, thus giving a clear indication of the source mechanism in the tensile case. With such information on the material, the extent of inclusion fracture could be reliably determined under other test conditions without extensive metallographic investigation. Note, however, that quantitative applications of

AE require a correlation between specific characteristics of both the deformational process and the recorded AE signals.

Wadley et al. (1981) indicated the capability of AE analysis to discriminate between two possible event sources on the basis of differences in the AE signatures. By examination of cleavage and intergranular crack sizes they noted that intergranular cracks were significantly larger on average and they corresponded well with the observed number of high amplitude emissions. The particular equipment settings used, however, prevented proper acquisition of the low amplitude signals resulting from the smaller cleavage fractures.

Several studies have explored the grain size effect on internal fracturing using AE techniques. Khan et al. (1982) found AE activity to increase with grain size for several types of steel. Scruby et al. (1981) found similar trends for aluminum and an aluminum-magnesium alloy.

The optical clarity of ice and its propensity for microfracture under conditions of practical interest make it ideally suited to study with AE techniques. Gold (1960) recognized this fact and was the first to use a piezoelectric transducer to monitor cracks in ice. Interpretational difficulties, however, led him to estimate internal cracking by direct visual means in subsequent work. The potential benefit of the AE method was clear, but the equipment of the day did not prove adequate.

Work by Zaretsky et al. (1979), mentioned earlier in another connection, used AE data directly in a constitutive relationship for ice. This was possible because, for certain test conditions, the accumulated acoustic pulses followed the form of the accumulated creep strain. This 1979 paper refers to Zaretsky et al. (1976) for the development of a functional relationship between the AE signals and the corresponding formation of microcracks. The expression for creep strain was formulated as the product of the number of acoustic pulses, the mean crack size and a proportionality factor. The mean crack size was determined through an analysis of the acoustic event amplitudes by assuming that AE amplitude is a function of microcrack size.

Zaretsky et al. (1979) also show a close correlation between the microcrack surface area and the number of accumulated defects. The expected surface area increased linearly with the number of acoustic pulses recorded. The final expression given for ice creep in this work showed time-dependent strain as a function of defect accumulation measured by AE, temperature, stress and time.

The success of this approach relies heavily on the ability to determine precisely the number of cracks occurring in time from the AE data. This is a difficult task given the variability of AE monitoring systems. Additionally, this approach is valid only when processes other than crack formation do not significantly contribute to straining.

More recently, St. Lawrence and Cole (1982) and Cole and St. Lawrence (1984) applied AE techniques to monitor microfracturing in polycrystalline ice having equiaxed grains (in contrast to the columnar-grained material tested in the abovementioned works). Initial grain size was held constant in these experiments at 1.2 mm as determined by the intercept method. Equipment limitations prevented a direct correlation between AE amplitude and crack size. Instead, AE activity recorded at two sensitivity levels was only assumed to parallel the actual cracking activity. The expression developed for acoustic activity showed a dependency on stress and time. In the creep tests reported in the former paper, the AE rate reached a maximum at 1.8×10^{-3} axial strain and then dropped sharply as deformation proceeded. For stresses of less than about 2.35 MPa, the AE rate after the initial 4×10^{-3} strain was extremely low. Stresses over 3.26 MPa, on the other hand, induced considerable AE activity after the rate peak, indicating a significant amount of additional microfracture.

In this study, the acoustic activity ranged over some three orders of magnitude as stress increased from 0.8 to 3.67 MPa. Interestingly, although the test material reached virtually complete saturation with internal cracks, the overall behavior could be reasonably described as ductile since typical creep behavior was still evidenced and the strain at the creep rate minimum did not decrease.

In the constant rate of deformation tests reported in Cole and St. Lawrence (1984), the highest strain rates did bring about substantially brittle behavior. For stresses in excess of 5 MPa and strain rates over 10^{-4} s^{-1}, characteristic failure strains dropped to values as low as 2.3×10^{-3}. Ductile-type failures occur near 10^{-2} axial strain. Strain rates near 10^{-6} s^{-1} at -5°C resulted in virtually no visible cracking. An increase to roughly 10^{-4} s^{-1} results in a significant loss in ductility as indicated by the occurrence of both a high degree of internal fracture and a reduction in the axial strain associated with the peak stress.

In both the creep and strength tests reported, the onset of cracking as indicated by the AE activity occurred at approximately 10^{-3} axial strain.

Stress at the onset of visible cracking was generally near 2.0 MPa at -5°C.

In other recent work, Sinha (1982) monitored the acoustic activity in columnar-grained ice in uniaxial compressive strength tests. He noted fairly uniformly distributed cracks that were comparable in size to the grains. Visible cracking generally began at 2.4×10^{-4} strain and at stress near 0.8 MPa.

Sinha (1982) associated visible cracking with acoustic event amplitudes of 79 dB with his particular system. He used visual observation during testing to help establish this cutoff level.

As in St. Lawrence and Cole (1982), Sinha (1982) found some low level AE activity at the small strains prior to the onset of visible cracking.

TEST METHODS

This section describes the testing methods and procedures employed in the laboratory work. The specimen preparation procedure and the creep testing equipment have been described in detail elsewhere (Cole 1979, Mellor and Cole 1982) and are covered only briefly here. However, the method of grain size analysis and the post-test analysis of internal cracking receive close scrutiny.

Specimen preparation

The specimen preparation method developed by Cole (1979) produces polycrystalline ice with randomly oriented, equiaxed grains and densities of 0.917 ± 0.003 Mg/m^3. Grain size can vary up to the practical limit established by the mold size and is controlled by the grain size of the seed crystals. The specimens are 50.8 mm in diameter and 127 mm long.

The method calls for filling a cylindrical aluminum mold with the appropriate size seed grains, sealing the mold and applying a vacuum of 13–26 Pa for 2.5 hr. Distilled, degassed water at 0°C then fills the mold under the action of the vacuum. Once this flooding is complete, the mold is placed in a freezing coil which carries fluid from a temperature bath at -5°C. The degassed water is flushed up through the mold as the radial freezing progresses at an average rate of 2.8 μm/s. The continuous flushing helps prevent bubble nucleation and/or growth by keeping the dissolved gas concentration low in the pore water.

The freezing process often results in a thin column of fine bubbles along the axis of the specimen. This occurs when the freezing process prematurely closes off the path of the flushing water near one end of the specimen. The bubbles form when the remaining gas-laden pore water freezes.

Figure 3. Typical untested specimen.

Figure 3 shows a typical fine-grained specimen produced by this method. The end caps are fixed in the mold to assure proper alignment. They are made from a fabric-based phenolic material. The ice bonds well to this material once the factory finish has been roughened to expose the fabric.

Specimens emerged from this procedure near a temperature of -5°C and were placed in the creep apparatus at -5°C if they were to be tested immediately. If short-term storage was required, they were wrapped in several layers of polyethylene film and placed in ice-filled bags and kept at -12°C. Such specimens equilibrated at the -5°C test temperature for at least 24 hr prior to testing.

Creep testing apparatus

The creep apparatus and environmental control cabinet are described in Mellor and Cole (1982). The end caps bolt into the base and loading piston of the test fixture. A pneumatically actuated cylinder applies the desired load to the specimen

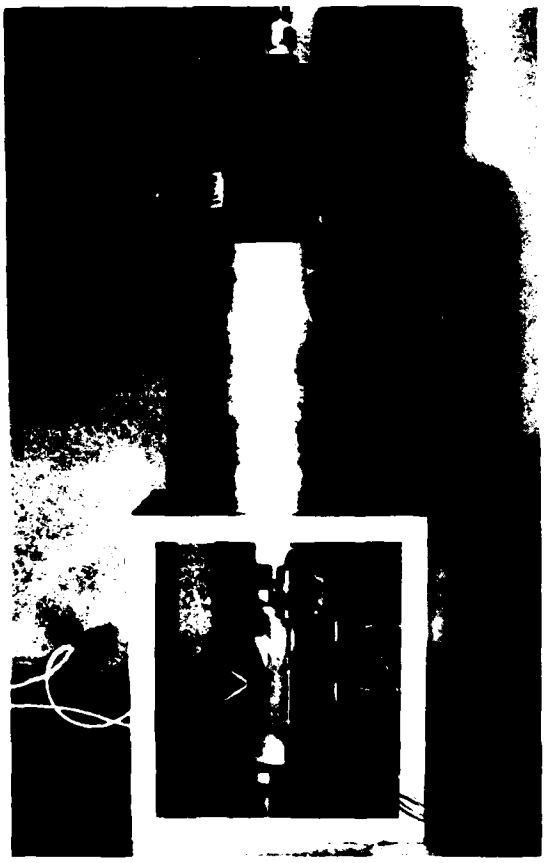

Figure 4. Creep testing apparatus showing displacement transducer and mounting clamps on specimen.

through a 50.8-mm-diameter steel piston. The piston is mounted in a large linear ball bushing to ensure virtually friction-free movement.

The calibration procedure associated the output of a transducer, which monitored the supply pressure to the actuator, to the load exerted by the piston on a standard load cell. This method accounted for all frictional losses in the system.

The test fixture maintained the end caps parallel during deformation. Therefore, only one transducer was required to monitor the axial deformation. A direct current displacement transducer (DCDT) with a linear range of ±3.175 mm was employed. Two circumferential clamps held the DCDT core and barrel. Figure 4 shows the complete creep testing apparatus along with the DCDT and mounting configuration.

An analog to digital data logger recorded the DCDT output along with the output of the pressure transducer and the time of each reading. The sampling time of the data logger ranged from 15 s at the start of a test to as high as 300 s at higher strains and slow strain rates. A separate system continuously monitored the test temperature, which varied less than ±0.1°C during testing.

Crack length and crack density measurements

After testing, specimens were moved to a -10°C work room for sectioning and photographing. Specimens were generally cut on a band saw to generate horizontal and vertical sections (see Fig. 5). These thick sections were approximately 10 mm thick, but thickness varied depending upon crack density. High crack density required thinner sections in order to distinguish individual cracks. Thicker sections could be used when the crack density was low.

The horizontal sections, taken perpendicular to the stress axis, were used to estimate crack densities and to measure crack lengths. Since the cracks tended to form parallel to the stress axis, the horizontally oriented sections showed the cracks in an edge-on view. From this vantage point, the cracks generally appeared as well-defined lines and were easily measured. The vertically oriented sections, while allowing measurement of crack dimensions parallel to the stress axis to a certain extent, did not provide an accurate means of counting and measuring every crack in the section. Inaccuracies arose in this case because some cracks were seen face-on and tended to obscure the view of cracks which were located behind them in the section.

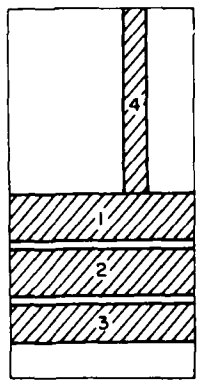

Figure 5. Schematic showing typical locations of thick sections in the cylindrical ice specimens. Numbers 1-3 are horizontal sections used for crack density measurements.

The question naturally arises as to whether the measurement of crack length in the horizontal sections is an accurate representation of the true crack length. Also, the validity of the use of one length measurement to represent the size of a crack must be established. These points will be discussed in detail and data will be presented to show the extent of the error introduced by these assumptions.

For most specimens, photographs of back-lighted thick sections were taken. From these it was possible to count and measure all visible cracks in the section. The sections were divided into roughly 200-mm² sectors and each sector was photographed with a 7× magnifying camera. It was then possible to form a mosaic of the section, and from this the number and lengths of cracks were taken.

In some cases, when the crack density was extremely low, it was possible to make direct measurement from the viewer of the camera, precluding the need of taking photographs. Also in these cases, a larger volume of material was sampled because it was considerably less time consuming to make the measurements. The volume of the section was recorded, and once the cracks were counted, the number of cracks per unit volume was calculated.

Crack healing measurements

The thick-sectioning technique described in the previous section provided a means to monitor the change in crack length with time. After photographing immediately after testing, two typical thick sections were tightly wrapped and placed in a -5 °C environment, and they were photographed several times during a period of nearly eight weeks. This was sufficient time to allow completely isolated cracks to transform from their initial "penny" shape to oblate spheroids. The lengths of the cracks were taken from each photograph, and special attention was paid to the first hours of the healing process. The results help to assess the possible change in crack length resulting from the healing process that occurred between the time of the crack's formation and the time the length measurement was made.

Thin section photographs

Photographs were taken of thin sections and provided the means of determining grain size and of discovering any anomalies in the test material (see Fig. 6). Photographs were taken of both vertical and horizontal sections in some cases, although generally only horizontal sections were taken. Figure 6 shows thin-section photographs for several specimens of various grain sizes.

The thick sections used for the crack density analysis were trimmed to a suitable thickness for the thin-section photograph immediately after the crack density measurements were taken. The amount of time between testing and the final thin section photograph was usually on the order of 2 to 4 hours. Significant grain growth was not assumed to occur within this time.

Grain size determination

There are several methods that can be used to estimate polycrystalline grain size. A summary of various methods is given by Dieter (1976) and they are briefly described below.

Mean intercept length

Grain diameter is found by dividing the total length of a test line by the number of grains intersected when the line is placed randomly on the section. This generally underestimates the true diameter of equiaxed grains, but is accurate for columnar grains viewed perpendicular to the long axes.

Grains per unit area

Assuming constant size spherical grains, the grain size may be estimated by

$$d = \sqrt{\frac{6}{\pi N_A}} \tag{19}$$

where N_A is the number of grains per unit area.

ASTM standard charts

Grain size at a fixed magnification is compared with standard ASTM grain size charts and a grain size number is established. This method will not be considered in the present work.

The apparent grain size in the plane of the section can also be estimated from measurements of grains per unit area N_A. In this case, we find the diameter which corresponds to the average area per grain $1/N_A$.

$$\text{Average area} = \frac{\pi D^2}{4}$$

$$\frac{1}{N_A} = \frac{\pi D^2}{4}$$

or

$$D = \sqrt{\frac{4}{\pi N_A}} \,. \tag{20}$$

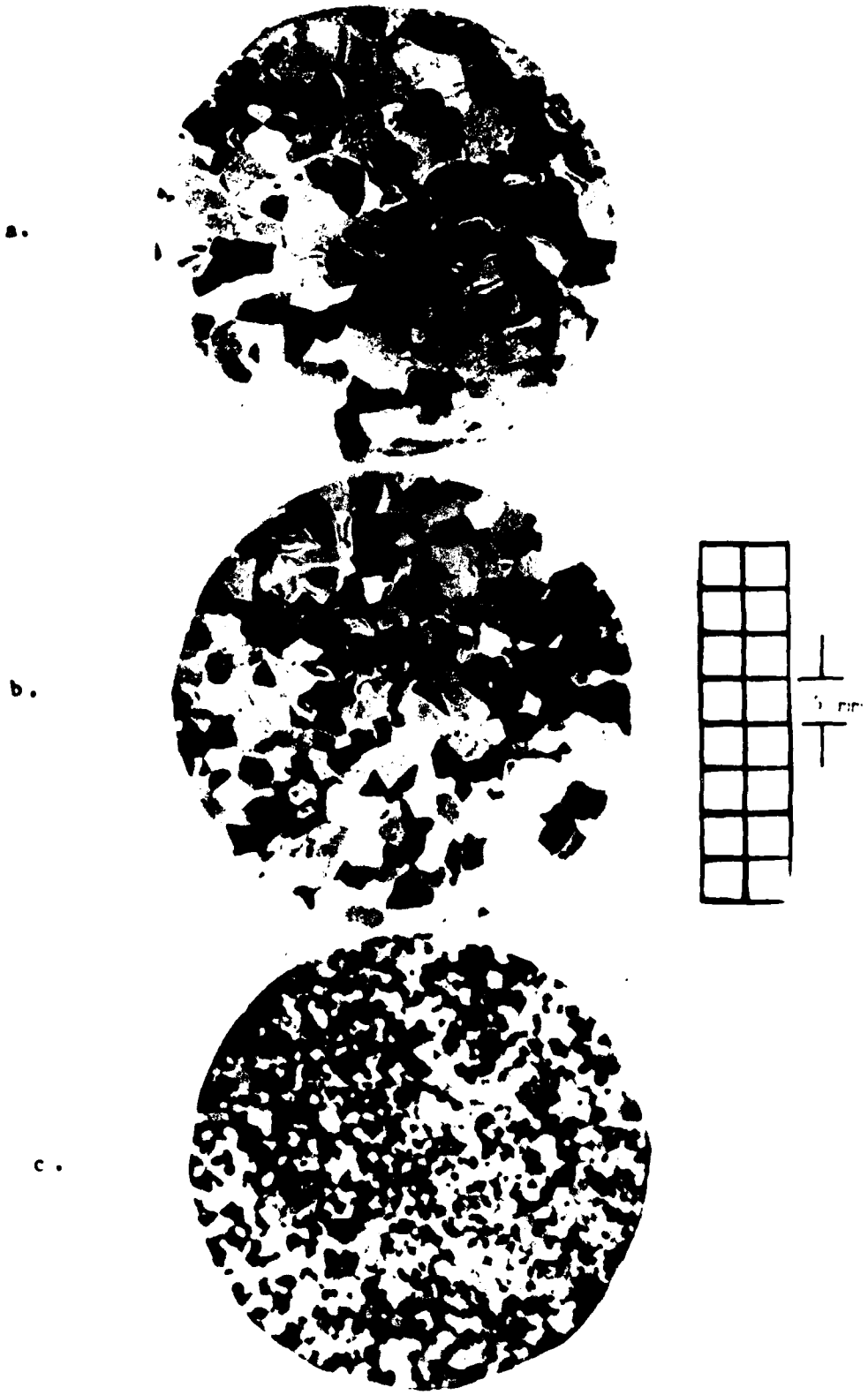

Figure 6. Typical thin sections of test material, grain sizes of a) 5.3 mm, b) 4.3 mm and c) 2.0 mm.

This results in a somewhat smaller estimate of grain size than eq 19. The test results section gives a comparison of the grain sizes obtained using each of the above methods. There are significant differences in grain size estimates depending on the method used. Since the work at hand requires estimates of the true grain size, and not merely values that scale as the grain size (such as the results of the intercept method), the estimates resulting from eq 19, which give the largest values, will be used in all analyses. The chosen method relies on the assumption that the grains are of uniform size and spherical shape. Neither of these is true; however, they appear useful because the seed grains are sieved to within ±8% of the average seed size and the seed grains are roughly equiaxed.

Caution must be exercised in comparing this work with other analyses in which grain sizes were estimated with the intercept technique. As noted, the grain sizes calculated using eq 19 are larger than those found with the intercept method for the present data. This increase is significant and should be taken into account wherever grain size measurements are of critical importance. In a related area, it should be mentioned that the method used to determine grain size will influence the slope of a Hall-Petch type plot.

Acquisition of acoustic emission data

A microcomputer-based AE system monitored the acoustic activity in all tests. The system employed two piezoelectric transducers mounted as seen in Figure 7. Elastic bands attached to the mounting shell hold the transducers in place. Ice fillets formed from distilled water served to increase the contact area between the side of the specimen and the flat transducer face. A thin layer of silicone grease between the transducer and the ice assured good acoustic coupling.

The AE system, a PAC 3400 by Physical Acoustics Corporation, recorded characteristics of the AE pulses, but not the actual pulse itself. Figure 8

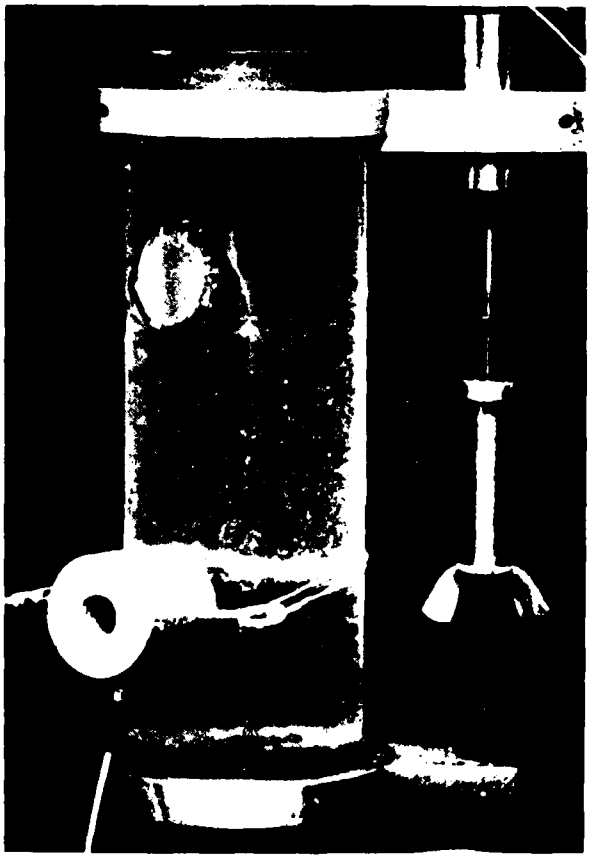

Figure 7. AE transducer mounted on specimen. Transducers are placed on flat contact points.

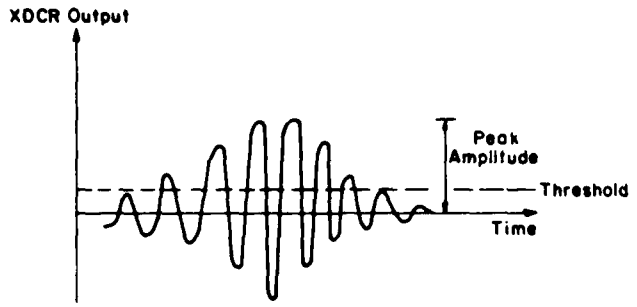

Figure 8. Idealized acoustic emission waveforms.

shows an idealized AE waveform and identifies the major characteristics recorded by the system. The gain, or amplification level, and the threshold, or cut-off voltage, together determine the overall sensitivity of the system. For these tests, the gain was set at 60 dB, which corresponds to an amplification of 1000 times the signal sensed by the transducer. The threshold setting varied somewhat depending on the AE activity level. St. Lawrence and Cole (1982) point out that, in ice, both visible cracking and deformational processes which result in no visible discontinuities generate detectable acoustic activity. Higher amplitude events, however, are expected from the visible cracks as a result of the greater strain energy associated with crack nucleation. The settings used in this work were such that the AE system responded to event amplitudes somewhat below that resulting from visible cracks, thus assuring that all the visible cracking events were recorded.

The AE amplifier band-pass filters the signal in the range 10 to 200 kHz. Earlier work (St. Lawrence and Cole 1982) showed this range to be suitable for monitoring cracks in ice.

Table 1. Creep data.

Specimen	d (mm)	σ (MPa)	ϵ_{max} ($\times 10^{-2}$)	ϵ at $\dot{\epsilon}_{min}$ ($\times 10^{-2}$)	$\dot{\epsilon}_{min}$ s^{-1} ($\times 10^{-6}$)	Time to $\dot{\epsilon}_{min}$ (s)	ϵ at $\ddot{\epsilon}_{min}$ ($\times 10^{-2}$)
69	1.5	2.0	5.0	1.00	2.85	2640	0.30
70	1.8	2.0	5.0	0.80	1.97	3180	0.12
43	1.8	2.0	1.0	0.80	1.80	2760	0.30
55	(1.8)	2.0	0.25	—	—	—	0.20
47	2.6	2.0	5.0	0.60	1.10	3900	0.16
65*	2.8	2.4	1.0	—	—	—	—
60	2.9	2.0	4.8	0.55	1.31	2483	0.20
77	3.2	2.8	1.0	0.74	5.35	697	0.30
63	3.2	2.0	1.0	0.56	1.07	3300	0.06
74	3.2	2.6	1.0	—	3.40	—	0.30
75	3.2	2.4	1.0	0.69	2.34	1546	—
64	3.3	2.0	0.5	—	(1.15)	—	0.12
44	3.3	2.4	1.0	0.80	4.37	1260	—
61	3.4	2.0	0.25	—	—	—	0.13
76	3.5	2.6	1.0	0.80	3.56	1070	0.25
78	3.5	2.6	1.0	0.60	2.50	1523	0.20
49*	3.5	2.8	0.25	(0.06)	(8.50)	35	—
56*	4.3	2.6	1.0	(0.11)	(4.60)	158	—
62	4.7	2.21	3.0	0.42	2.85	780	0.20
57	4.8	2.0	0.037	—	—	—	—
72	4.8	2.0	1.0	0.40	2.10	1032	—
58	5.2	2.0	0.25	—	—	—	—
73	5.4	2.0	1.0	0.38	3.42	630	—
59	5.5	2.0	0.045	—	—	—	—
71	5.5	2.0	1.0	0.35	1.25	1620	0.12
79	6.0	2.0	1.0	0.34	1.26	1620	0.10

* Grain size achieved by grain growth process.

NOTE: Specimens that have no values given for $\dot{\epsilon}_{min}$, and ϵ at $\dot{\epsilon}_{min}$ were not strained sufficiently to experience a strain rate minimum.

PRESENTATION OF RESULTS

Specimen characteristics

Table 1 gives a list of the specimens tested, the initial applied stress level, the maximum axial strain before removal of the load, and the axial strain at which the minimum strain rate occurred.

Table 2a shows the specimen grain sizes as determined by the intercept method and two methods based on measurements of grains per unit area. As noted earlier, the results given in the third column, found using eq 19, are used in all subsequent work to characterize the material. These values tend to be significantly larger (52.5% on average) than those found with the often used intercept method.

Table 2b gives a comparison of the three methods of grain size estimation based on thin sections of untested material. The seed size refers to the sieve size range of the ice crystals used to form the specimen. Note that the intercept method yields grain size estimates that are smaller than the original seed grains. As discussed earlier, the method used in this work (d_3) gives estimates that are slightly larger than the seed grains, but these estimates are reasonable because the average seed grain diameter is expected to increase as the grain grows into the adjacent pore space during freezing.

Microcrack measurements

As described above, post-test observations yield the number and size of cracks in a given volume of material. When the crack density was very low, a large volume of material was sampled, and cracks were measured and counted directly from the thin section. Up to three thick sections were evaluated from each specimen. These data made it possible to estimate the crack density of the entire specimen.

Since moderate to extensive cracking levels required photographs for accurate interpretation, two or three sections of each specimen were photographed as described earlier. Generally, half a longitudinal thick section was photographed. Assuming radial symmetry in the crack distribution, these results were used to estimate the crack density in the central region of the specimen. The estimates of crack density did not include the ice near the ends of the specimen because the triaxial stress state induced by the end caps generally resulted in a lower crack density in these regions. Thus, the crack densities reported are assumed to be representative of the material under a uniaxial stress state.

Table 2. Grain size estimates and seed grain sizes.

a. Grain size estimates for tested specimens.*

Sample	d_1 *(mm)*	d_2 *(mm)*	d_3 *(mm)*
43	1.3	1.5	1.8
44	2.3	2.5	3.3
47	1.7	2.1	2.6
49	2.4	2.8	3.5
55	—	—	(1.8)
56	2.4	3.4	4.2
57	3.6	3.9	4.8
58	4.7	4.2	5.2
59	4.2	4.2	5.5
60	1.7	2.4	2.9
61	1.9	2.8	3.4
62	3.6	4.6	4.7
63	2.0	2.6	3.2
64	2.0	2.7	3.3
65	1.7	2.3	2.8
69	1.2	1.3	1.5
70	1.1	1.5	1.8
71	3.6	4.5	5.5
72	3.4	4.2	4.8
73	4.4	4.4	5.4
74	1.9	2.6	3.2
75	2.0	2.6	3.2
76	2.1	2.8	3.5
77	2.1	2.6	3.2
78	2.4	2.8	3.5
79	3.7	4.8	6.0

b. Seed grain sizes and resulting grain size measurements on untested ice.

Seed grain size (mm)	d_1 *(mm)*	d_2 *(mm)*	d_3 *(mm)*
2.80–3.35	2.5	3.1	3.8
4.0–4.76	3.6	4.1	5.0

* d_1: intercept method.
d_2: average area method.
d_3: uniform sphere assumption (eq 19).

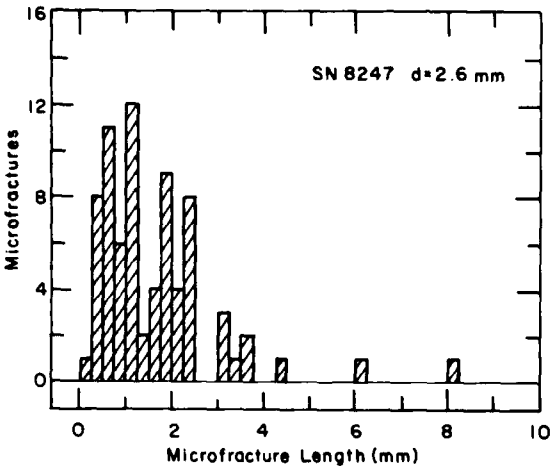

Figure 9. Typical crack length histogram.

Table 3. Crack location.

Specimen	d *(mm)*	*% GB cracks*	*% XT cracks*
49	3.5	58	42
56	4.2	41	59
65	2.8	57	43
71	5.5	54	46
72	4.8	60	40
73	5.4	47	53
Average		53 ±7	47 ±7

Crack lengths

Crack length measurements were a direct result of the post test analysis. Figure 9 shows a typical crack length histogram. Appendix A contains all the crack length data presented in the form of histograms. The average grain diameter is indicated for each specimen. In some cases where a more detailed examination of the cracking was carried out, transgranular and grain boundary crack histograms are shown separately. Table 3 gives the mean values of grain boundary and transcrystalline crack lengths obtained from these observations.

Figure 10 shows the average crack length plotted against the grain diameter for all cracks, regardless of location. This figure also shows plots of the least-squares best-fit curve for all the points shown along with the theoretical curve to be discussed later. The bars associated with each point indicate a bandwidth of ± one standard deviation.

Crack density

Figure 11 shows typical mosaics of the thick-section photographs. Each was formed from five enlarged photographs. Thin sections were generally used to quantify the cracking activity for severely cracked specimens (Fig. 11a), since the extensive network of overlapping cracks made interpretation of the thick section photographs difficult.

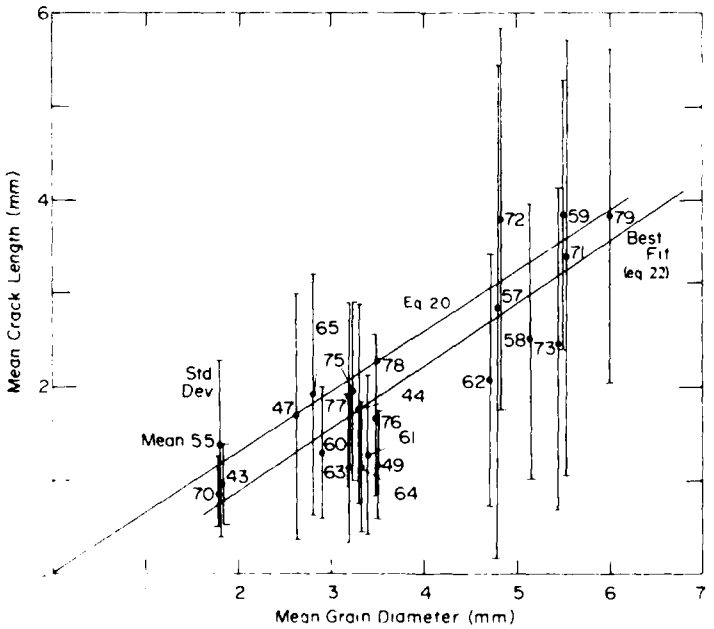

Figure 10. Mean crack length vs mean grain diameter.

a. A highly cracked specimen.

b. A moderately cracked specimen.

Figure 11. Mosaics formed from enlarged thick section photographs. Cracks show as black lines of varying thickness under back lighting.

The crack density data, expressed as cracks per unit volume, given in Table 4 represent averages of several thick section observations in most cases. Table 4 also gives crack densities in terms of cracks per grain. These values come about by dividing the observed number of cracks by the estimated number of grains in the sections under consideration. The calculation of the number of grains is based upon the grain sizes given in column 3 of Table 2a. Figure 12a gives plots of crack density, in terms of cracks per unit volume, versus grain size for several axial strain levels. Figure 12b gives the same data plotted in terms of cracks per grain. Note that at a constant initial stress of 2.0 MPa crack densities range from zero to nearly one crack per grain as grain size increases from 1.5 to 5.7 mm.

Crack density also increases with specimen strain for all but the smallest grain sizes. Figure 13 shows this dependency for several grain sizes.

In some instances cracking in the large-grained specimens was so extensive that interpretation using thick section photographs was very difficult. In these cases, thin sections were prepared and the number of cracks per grain was measured directly. The validity of this procedure was checked by

Table 4. Results of microfracture observations.

Specimen	d (mm)	Mean crack size (mm)	Standard deviation (mm)	Mean d	Crack density (cracks/m³)	Crack density (cracks/grain)
69	1.5	no cracks	—	—	—	—
70	1.8	0.83	0.43	0.46	6.8×10^{3}	2×10^{-3}
43	1.8	0.95	0.40	0.53	6.84×10^{3}	2.09×10^{-3}
55	(1.8)	1.39	0.89	0.77	4.83×10^{3}	1.47×10^{-3}
47	2.6	1.68	1.30	0.65	1.57×10^{4}	1.44×10^{-2}
65*	2.8	1.95	1.32	0.70	3.90×10^{7}	4.48×10^{-2}
60	2.9	1.28	0.70	0.44	1.03×10^{7}	0.13
77	3.2	1.92	0.99	0.60	6.16×10^{6}	0.10
63	3.2	1.29	0.90	0.40	1.53×10^{6}	2.58×10^{-2}
74	3.2	1.87	1.28	0.58	8.05×10^{6}	0.27
75	3.2	1.95	0.96	0.61	4.83×10^{6}	8.53×10^{-2}
64	3.3	1.14	0.70	0.35	2.38×10^{6}	4.36×10^{-2}
44	3.3	1.77	1.14	0.54	6.71×10^{6}	0.125
61	3.4	1.26	0.86	0.37	1.76×10^{6}	3.59×10^{-2}
76	3.5	1.66	0.89	0.47	4.50×10^{6}	0.10
78	3.5	2.28	2.94	0.65	5.30×10^{6}	0.12
49*	3.5	1.18	0.60	0.34	1.95×10^{7}	0.434
56*	4.2	1.15	0.61	0.27	1.30×10^{7}	0.523
62	4.7	2.09	1.36	0.44	4.26×10^{7}	2.53
57	4.8	2.85	2.66	0.59	4.03×10^{6}	0.23
72	4.8	3.8	2.05	0.79	1.76×10^{7}	1.03
58	5.2	2.51	1.48	0.48	4.20×10^{6}	0.30
73	5.4	2.45	1.56	0.45	1.83×10^{7}	0.80
59	5.5	3.85	1.45	0.70	3.18×10^{7}	2.27×10^{-2}
71	5.5	3.38	2.33	0.61	1.28×10^{7}	1.13
79	6.0	3.83	1.78	0.64	—	—

* Grain size achieved by grain growth process.

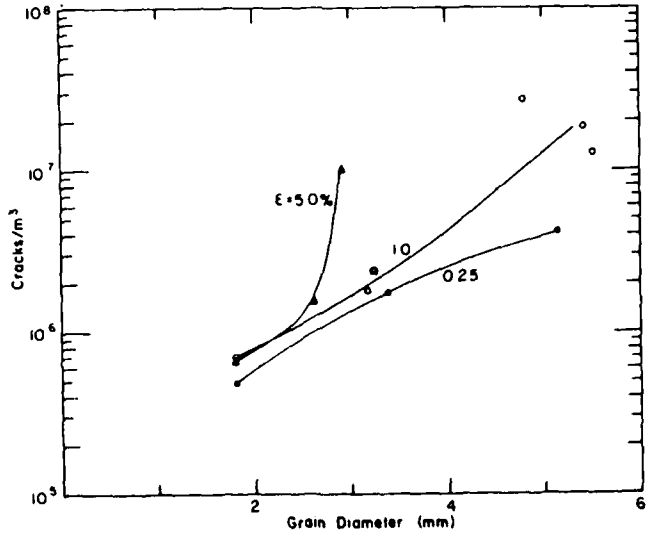

a. Number of cracks per cubic meter.

Figure 12. Crack density vs grain diameter. Axial strain levels are indicated.

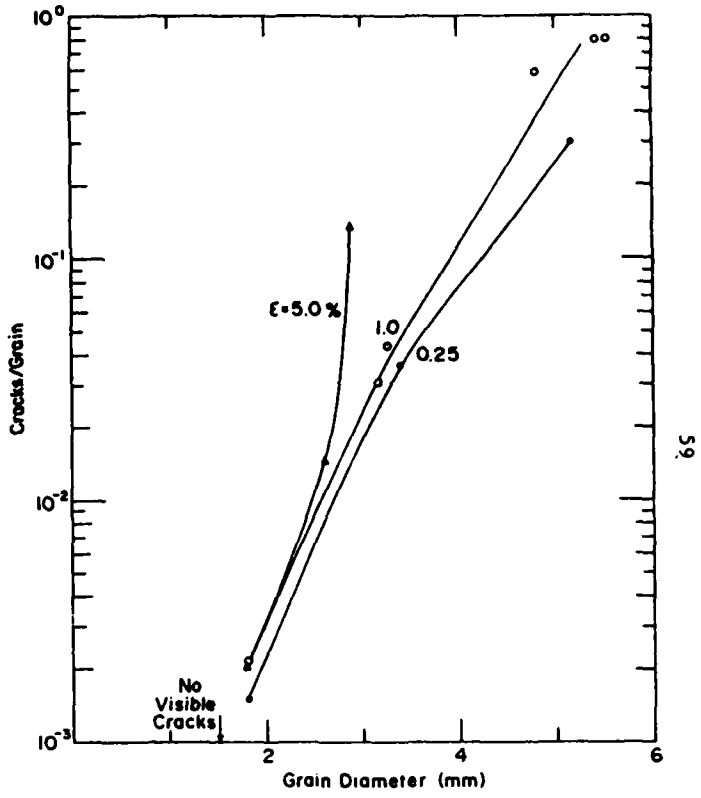

b. Number of cracks per grain.

Figure 12 (cont'd). Crack density vs grain diameter. Axial strain levels are indicated.

comparing the results with those of the usual cracks-per-unit-volume method discussed earlier. For specimen 71, the thick section analysis gave a crack density of 1.13 cracks per grain and the thin section analysis gave 0.92 crack per grain, indicating a reasonable agreement for the existing conditions.

Additionally, some observations were made from thick section photographs taken parallel to the stress axis. These provided information on the shape of the cracks and their orientation to the stress axis.

Creep behavior

Figure 14 shows some representative strain-time plots for tests at 2.0 MPa. Figures 15a-c show creep rate vs axial strain for all tests conducted at 2.0-MPa axial stress. Figures 15d-f show similar plots of the results of tests subjected to the higher stress levels (2.4, 2.6 and 2.8 MPa). The strain rate minima show up clearly when the data are plotted in this manner. Note that the scale of the strain axes varies to accommodate the range of strain found in the different tests.

Most specimens tested to sufficiently high strains exhibit typical creep behavior. The larger grain-sized material generally showed a rapidly decreasing primary creep rate, a brief minimum and a tertiary phase in which the creep rate tended to a constant at higher strains.

The smaller-grained material often showed a brief period of increasing creep rate at very low strains. The primary creep rate reached a maximum in the range of 10^{-3} to 2×10^{-3} strain and then decreased, developing a relatively broad minimum near 10^{-2} axial strain.

Several specimens were tested at stresses of 2.4, 2.6 and 2.8 MPa in order to examine the effect of axial stress on the cracking activity over a limited range. Creep data for these tests are plotted in Figures 15d and 15e. No strong trends emerge from the results of these tests. Results given in Table 4 show that no significant changes occur in the normalized crack size, indicating that the stress level

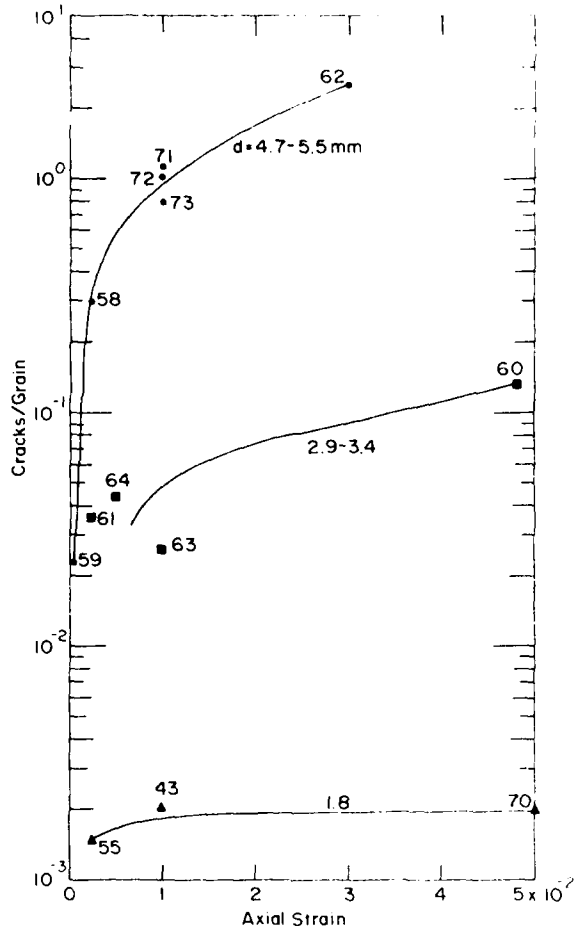

Figure 13. Crack density vs axial strain for several ranges in grain size.

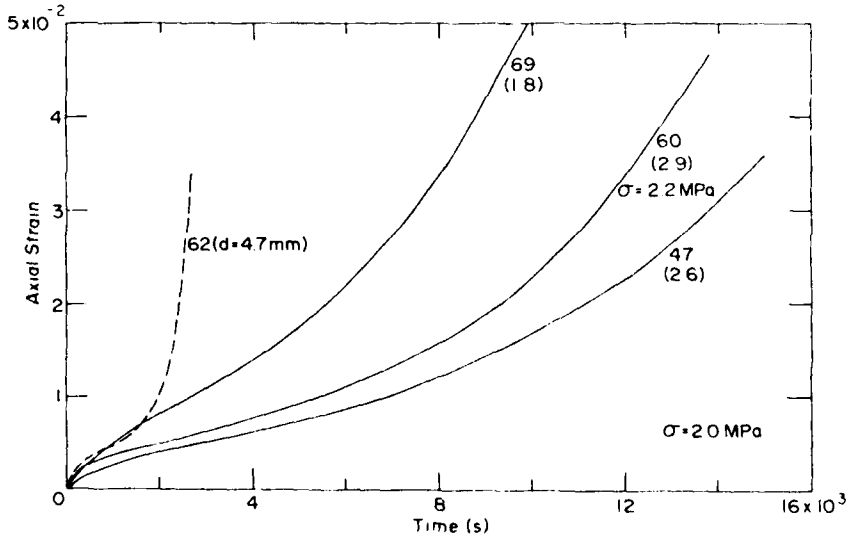

Figure 14. Strain-time plots for several tests, σ = 2.0 MPa.

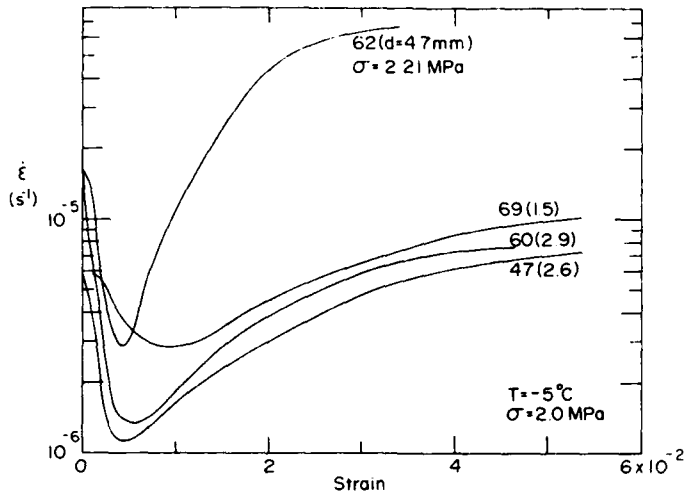

a. Specimens tested to large strains.

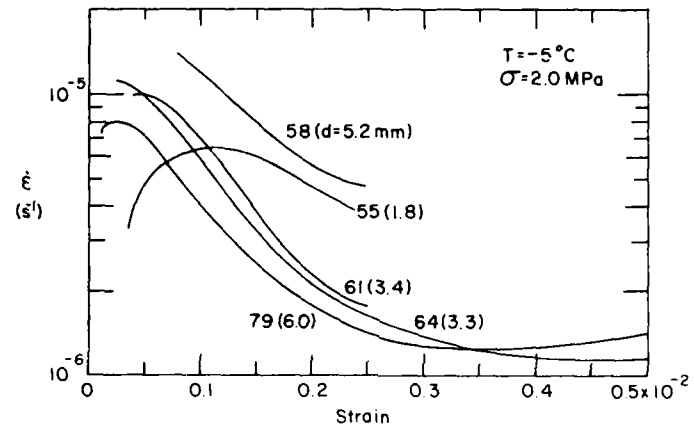

b. Some specimens tested to strains of 0.25×10^{-2} and 0.5×10^{-2}.

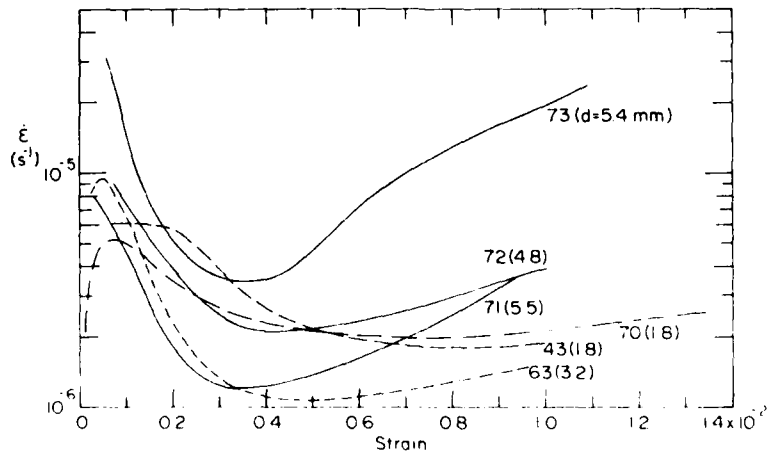

c. Specimens tested to strains of approximately 10^{-2}.

Figure 15. Creep curves for all tests.

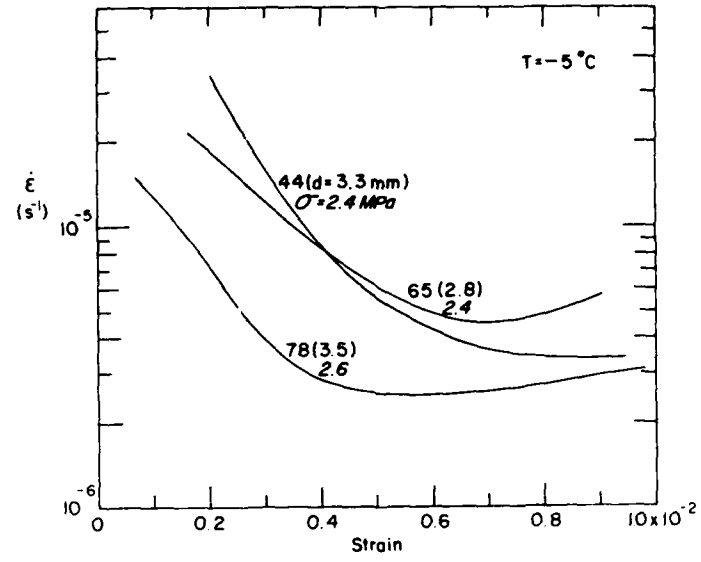

d. Some specimens strained to approximately 10^{-2} under various stresses.

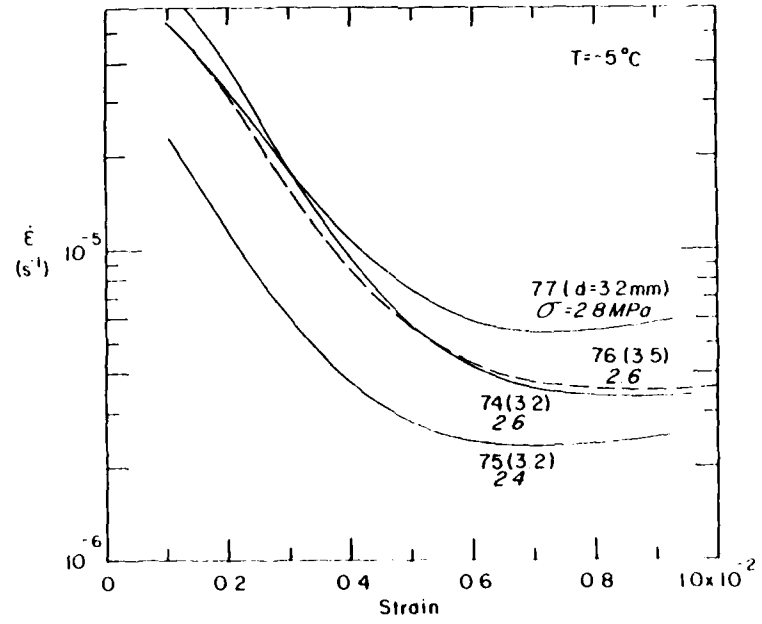

e. Additional specimens tested to strains of approximately 10^{-2} under various stresses.

Figure 15 (cont'd).

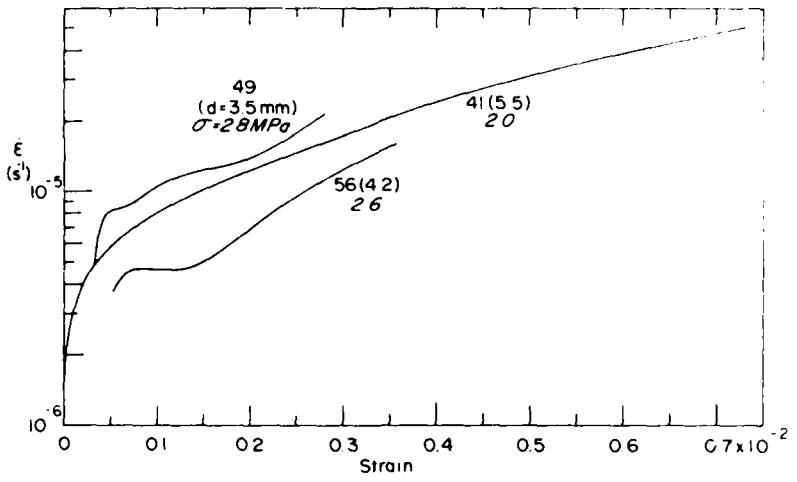

f. Specimens experiencing grain growth prior to testing.

Figure 15 (cont'd). Creep curves for all tests.

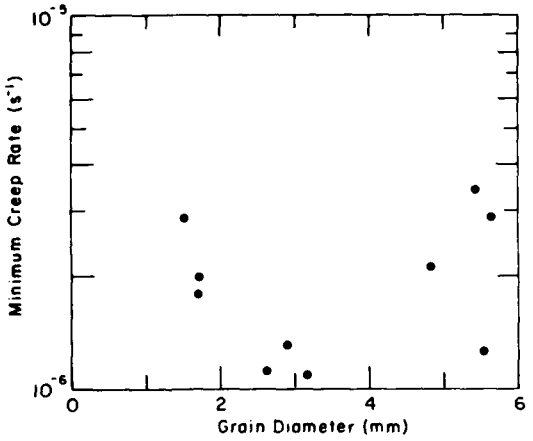

Figure 16. Minimum creep rate vs grain diameter, σ = 2 MPa.

does not affect the crack size - grain size relationship over this range.

Although there is scatter in the creep results, the minimum strain rate increases with increasing stress. Inspection of the results given in Table 4 indicates that the number of cracks per unit volume generally increases with stress as well. The maximum fracture rate with respect to time has a mild tendency to occur at lower strains as stress increases.

Figure 15f shows the creep curves of three specimens for which a relatively large grain size was achieved through a grain growth process. These specimens remained at a temperature of -2 °C for a number of weeks and consequently experienced considerable grain growth. Upon testing, they exhibited significantly different creep characteristics from the other specimens, developing no decelerating primary creep phase. This phenomenon is discussed in the section entitled *The Effect of Grain Growth.*

Table 1 gives the minimum creep rates along with other information. The creep rate minima are plotted in Figure 16 as a function of grain size.

Table 1 gives the strain at which the creep rate minimum $\dot{\epsilon}_{min}$ occurred. Figure 17 shows the strain at $\dot{\epsilon}_{min}$ as a function of grain size for these tests. Note the sharp decrease in strain level with increasing grain size, indicating the loss of ductility with increasing grain size.

Crack healing

Observations were made on two thick sections to ascertain the extent to which crack healing might influence the crack length observations. Figures 18 and 19 show two sequences of time lapse photographs of the crack healing process. The sections were stored at -5 °C and photographed periodically. Figure 18 shows an approximately 3-mm crack face on. The time after testing for each frame is given in the figure. Note the prominent surface relief of the crack face. Instead of a smooth planar surface, the crack face appears to be composed of many facets as indicated by the network of shadow lines. These features fade rapidly as the crack heals. The crack surface becomes smooth and the void is gradually transformed into a "bubble" having the shape of an oblate spheroid. Fig-

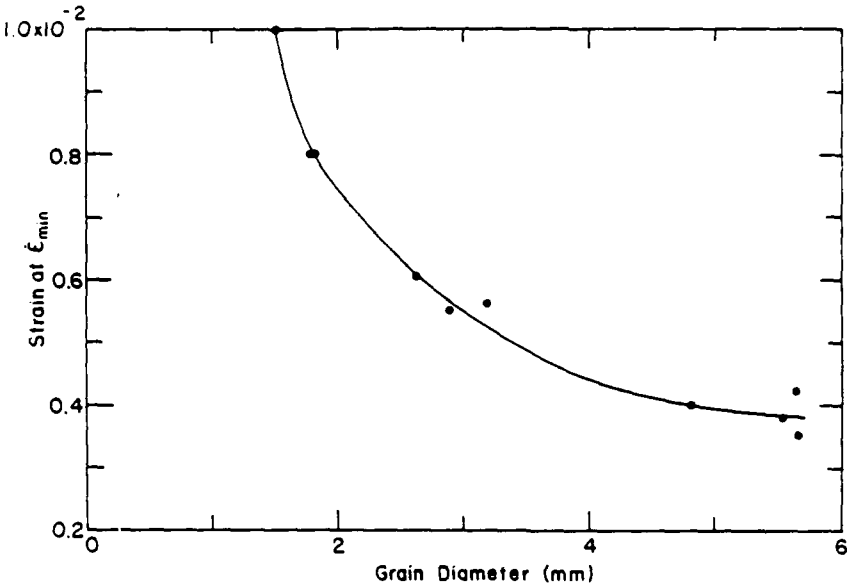

Figure 17. Strain at minimum creep rate vs grain diameter for 10 specimens.

ure 19 shows several cracks edge-on. The time sequence is the same as for Figure 18. The largest crack did not heal appreciably. The reason is that this void, unlike the others studied, was exposed to the atmosphere and was thus filled with air. As discussed in greater detail below, this changes the rate of the healing process significantly. Figure 20 shows the measured crack lengths as a function of time.

Slip plane length distribution

Initially, several methods of obtaining a distribution for ℓ, the length of slip plane, based on ideal grain geometries were considered. These proved somewhat unrealistic in light of the differences between, say, an idealized circular or hexagonal cross section and the variety of shapes actually observed in the material (see thin-section photographs, for example). In order to obtain a more realistic sampling of slip line lengths, the following method was devised. A straight edge was placed on a thin-section photograph and the distance between the grain boundaries thus intersected was recorded as the slip plane length. This was done several times on each photograph and for photographs from five specimens of varying grain size. In all, 419 measurements were taken. The values from each specimen were normalized to the specimen grain diameter, allowing all points to be merged. Nearly 10% of the values were greater than 1.0, indicating that several of the potential slip planes encountered were larger than the average grain size. This is to be expected since the grains are not exactly uniform in size. The mean and standard deviation of the normalized slip plane lengths are 0.6 and 0.3. Figure 21 shows the distribution of slip plane lengths. Note that the maximum length is $1.5d$. The mean value of $0.6d$ is used throughout this work when an "average" slip plane length is required.

Acoustic emission observations

Figure 22 shows typical AE results. Figure 22a gives accumulated events versus axial strain. The events are normalized to unit volume. The curve exhibits the same shape seen in other work (i.e. St. Lawrence and Cole 1982) but given the filtering process used in the present work, the curve is indicative of the actual number of fractures occurring per unit volume. Figure 22b shows the derivative of the curve in Figure 22a. Note that most of the fracturing activity occurs at very low strains. Table 5 summarizes the AE data; it contains only results from specimens for which adequate AE data were obtained. In certain cases technical problems occurred in the recording of the AE data, which prevented subsequent analysis. In other cases apparently inadequate specimen-transducer contact caused the results to be of questionable validity.

The onset of fracturing, as indicated by the AE results, occurred at an average axial strain of 4.7×10^{-4} with a standard deviation of 4.3×10^{-4}. The maximum fracturing rate with respect to strain, $[dAE/d\epsilon]_{max}$, occurred at 1.95×10^{-3} axial strain with a standard deviation of 9.6×10^{-4}. The maximum fracturing rate with respect to time,

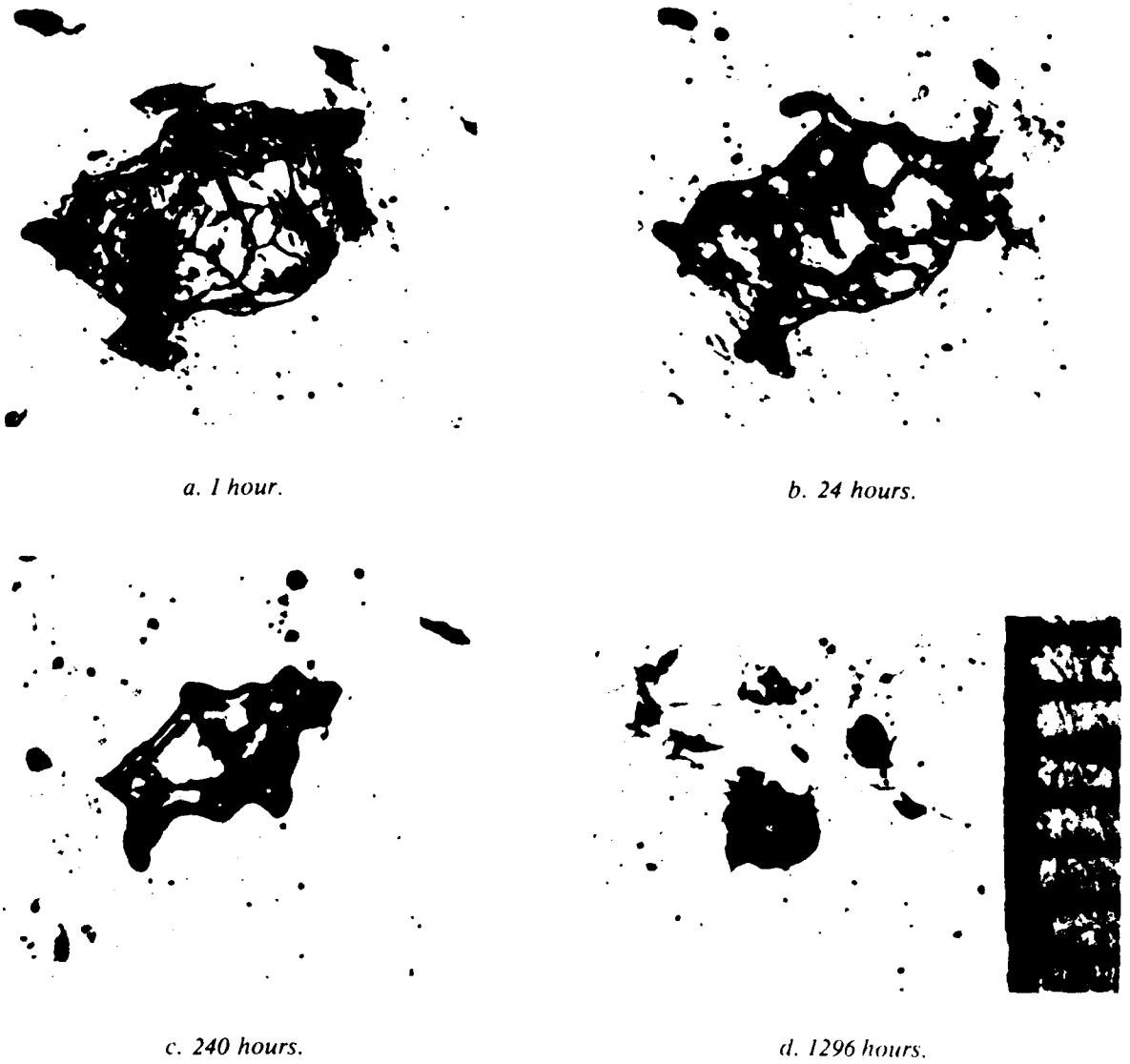

a. 1 hour. *b. 24 hours.*

c. 240 hours. *d. 1296 hours.*

Figure 18. Time-lapse photographs of crack healing, face view.

$[dAE/dt]_{max}$, occurred at an axial strain of 1.75×10^{-3} with a standard deviation of 8.8×10^{-4}. These maximum rate calculations omit specimen 59, which did not experience sufficiently high strains to exhibit a plausible maximum. There appears to be no systematic relationship between the strain at the fracturing onset and grain size.

Figure 23 shows the effect of grain size on the time to the maximum fracturing rates with respect to strain and time for the 2.0-MPa tests. The time to the rate maxima shows a strong dependency on grain size, decreasing roughly an order of magnitude as grain size increases from 1.8 to 5.5 mm.

Table 5 also gives the AE amplitude filter threshold and the average amplitude of the filtered events. The mean of the filtering threshold for all the tests is 83.7 dB with a standard deviation of 4.7 dB.

Grain orientation

A number of grain orientation measurements were made to discern any trends in the orientation of grains having internal cracks. Two thin sections prepared from specimen 79 were examined in detail. The thin sections contained numerous grain boundary and transgranular cracks. The *c*-axis

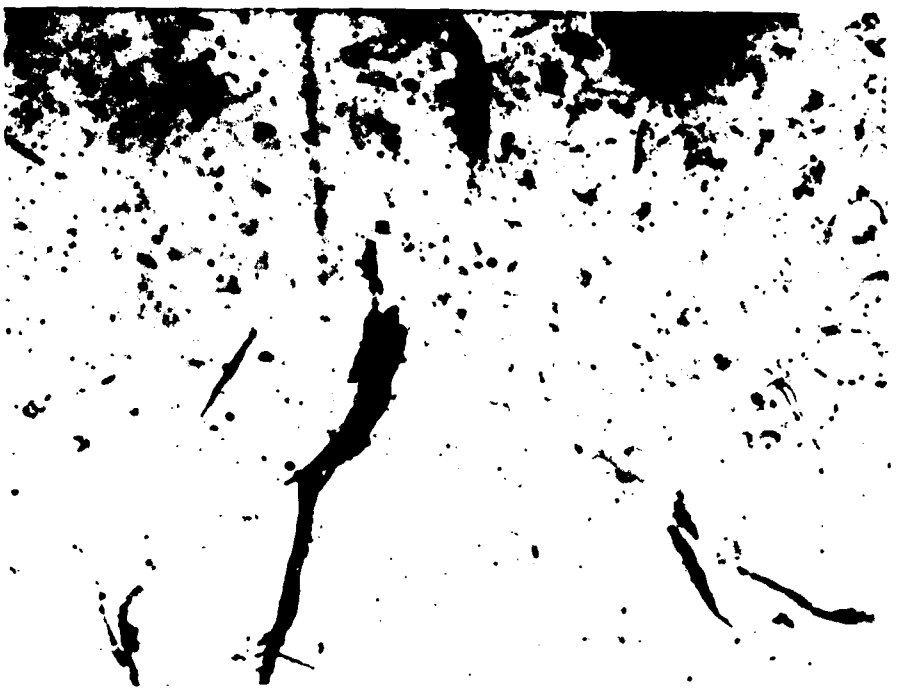

a. 1 hour.

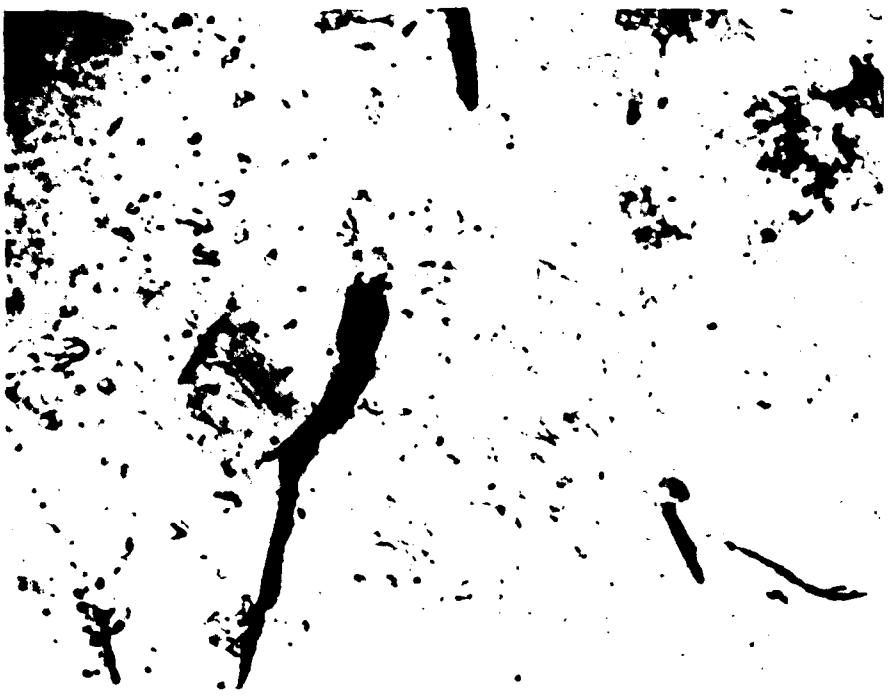

b. 24 hours.

Figure 19. Time-lapse photographs of crack healing, edge view.

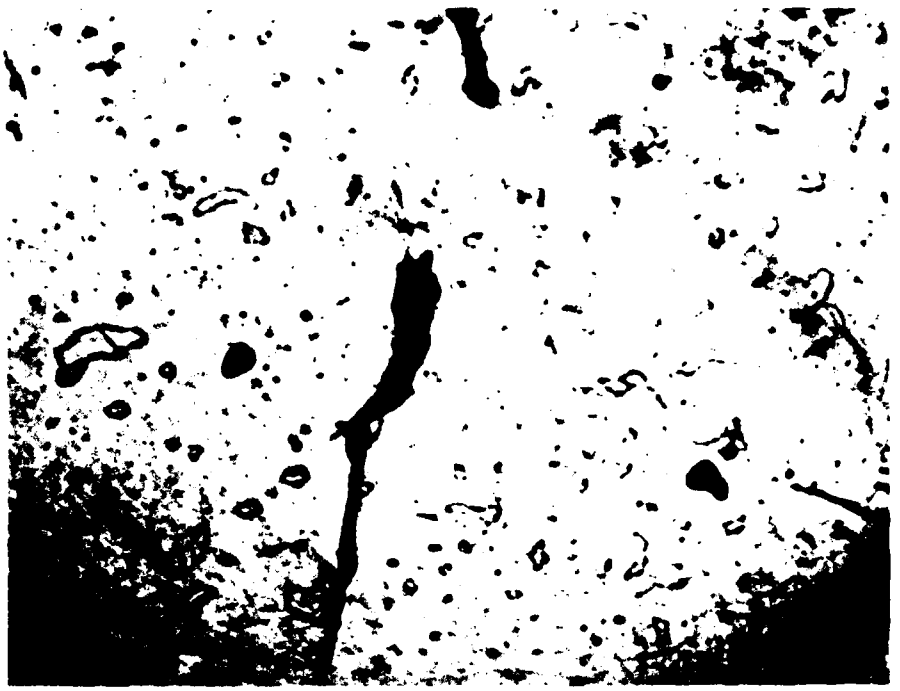

c. 240 hours.

d. 1296 hours.

Figure 19 (cont'd). Time-lapse photographs of crack healing, edge view.

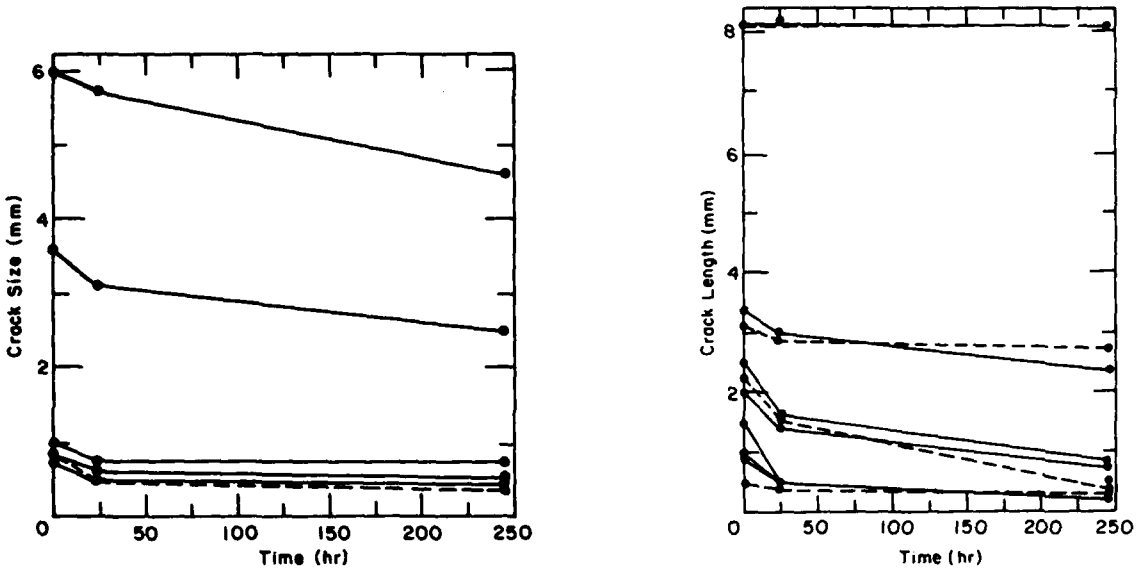

a. From face-view photograph.

b. From edge-view photograph.

Figure 20. Crack length vs time.

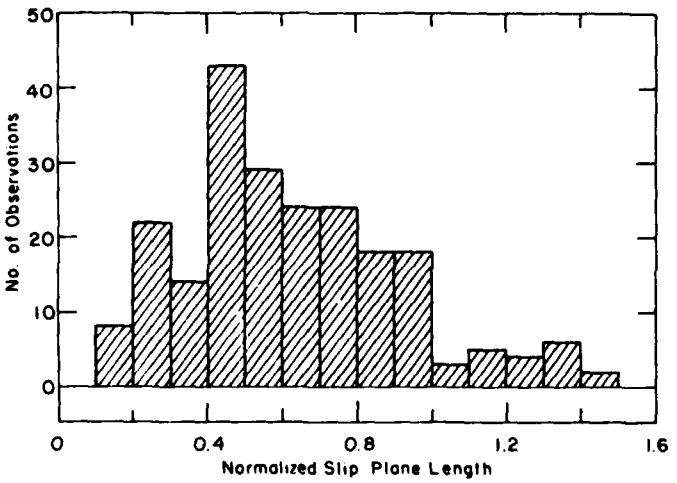

Figure 21. Slip plane length distribution.

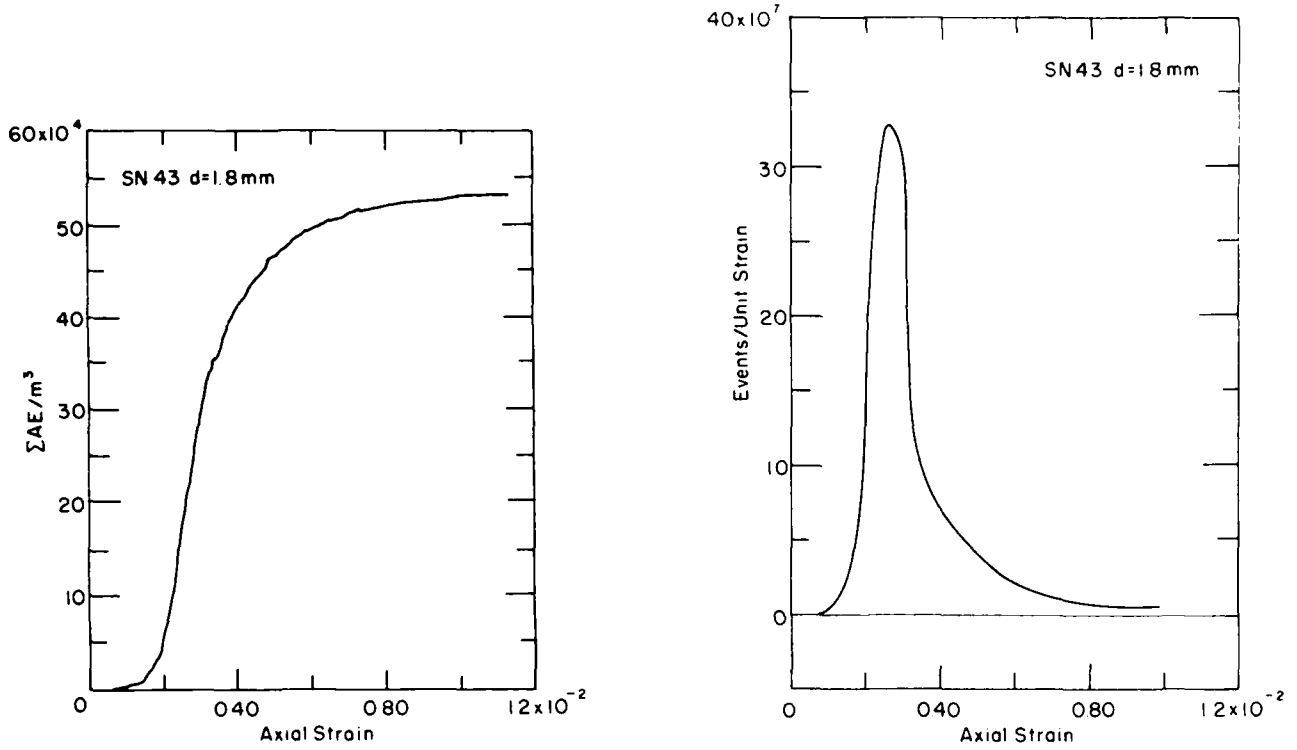

a. Accumulated acoustic events per cubic meter vs axial strain.

b. Acoustic events per unit strain vs axial strain.

Figure 22. Typical acoustic emission data.

Table 5. Results of acoustic emission observations.

Specimen	AE filter threshold (dB)	Average amplitude (dB)	Std. dev. (dB)	First event ϵ ($\times 10^{-4}$)	First event t (s)	AE rate maximum (with respect to strain) $[dAE/d\epsilon]_{max}$	AE rate maximum (with respect to strain) ϵ ($\times 10^{-2}$)	AE rate maximum (with respect to strain) t (s)	AE rate maximum (with respect to time) $[dAE/dt]_{max}$ (s^{-1})	AE rate maximum (with respect to time) ϵ ($\times 10^{-2}$)	AE rate maximum (with respect to time) t (s)
43	78.5	82.2	2.7	7.07	16.0	3.26×10^{8}	0.252	330	1.58×10^{3}	0.252	330
44	83.9	87.9	3.2	9.6	15.0	1.85×10^{9}	0.329	195	2.30×10^{4}	0.225	105
47	—	—	—	0.14	16.7	6.57×10^{8}	0.124	300	2.82×10^{3}	0.088	210
49	76.6	86.2	4.1	0.10	0.6	4.03×10^{9}	0.240	60	—	—	
55	75.5	83.7	3.9	2.69	15.3	5.89×10^{8}	0.237	420	2.26×10^{3}	0.237	420
56	85.7	87.8	1.4	—	1.0	1.16×10^{10}	0.312	150	5.45×10^{4}	0.312	150
58	88.0	90.0	1.3	3.6	9.4	1.39×10^{9}	0.104	51	1.41×10^{4}	0.104	51
59*	87.5	89.8	1.6	1.15	7.8	9.33×10^{9}	0.0417	39	8.33×10^{3}	—	—
63	81.6	86.1	2.6	0.60	3.9	9.38×10^{8}	0.125	150	4.59×10^{3}	0.125	150
65	88.7	90.0	0.94	at start	—	8.05×10^{8}	0.264	105	1.16×10^{4}	0.264	105
70	74.8	81.8	4.3	0.24	5.3	2.24×10^{8}	0.16	380	9.30×10^{2}	0.129	300
73	86.8	89.2	1.4	9.8	7.1	1.85×10^{9}	0.19	150	1.12×10^{4}	0.152	90
74	87.3	87.3	2.7	9.6	2.1	7.23×10^{9}	0.30	60	8.61×10^{4}	0.30	60
75	87.3	89.2	1.2	5.9	0.6	3.27×10^{9}	0.209	90	1.95×10^{4}	0.179	60
76	86.2	88.1	1.3	1.15	16.5	1.01×10^{10}	0.0147	60	2.41×10^{4}	0.0147	60
77	85.6	87.4	1.3	10.4	16.5	1.28×10^{9}	0.301	90	2.96×10^{3}	(0.16)	(30)
78	85.3	87.6	1.4	3.0	18.3	1.65×10^{9}	0.116	90	1.91×10^{4}	0.077	60

* Specimen not tested to sufficiently high strain to develop an obvious maximum AE rate.

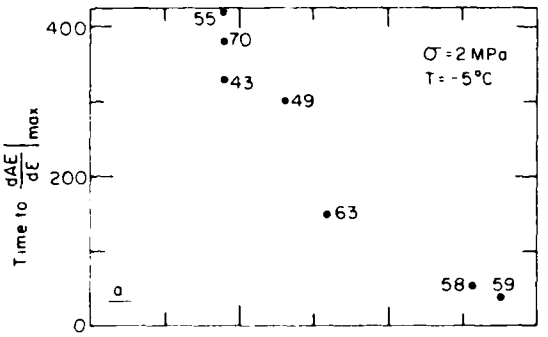

a. Time to $[dAE/d\epsilon]_{max}$ vs grain size.

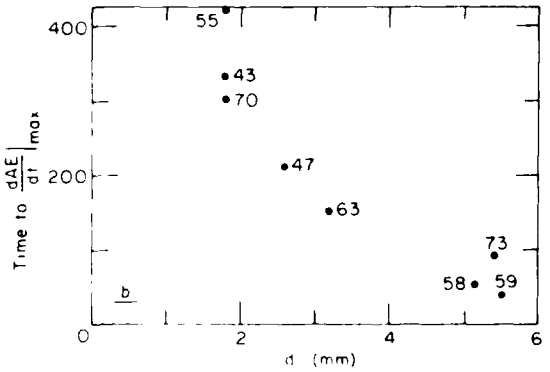

b. Time to $[dAE/dt]_{max}$ vs grain size.

Figure 23. Acoustic emission rate data.

orientations of selected clusters of grains were determined using a universal stage according to methods given by Langway (1958), and using a correction factor of 1.04 on the equatorial measurements rather than the tabulated values (see Kamb 1962). Appendix B gives the results of these measurements.

The results of measurements on all grains, both those containing cracks and the adjacent uncracked grains, reflect the random orientation of the test material. No pattern of preferred orientation of these grains emerges. A fabric diagram for only the grains containing cracks also yields no discernible pattern.

An examination of the relative orientation of two grains having a crack along their common grain boundary revealed that the angle between the respective *c*-axes ranges from 33° to 85°, with a mean of 63.3° and a standard deviation of 19°.

The above results are not unexpected, however, since it is the grains that contain the active slip systems, and not the cracked grains, where one would expect to find a preferred orientation. As noted in an earlier section, the grains most likely to slip and thus cause crack nucleation will tend to have orientations that maximize the shear stress on their basal planes. Unfortunately, it was not possible to determine which grains were important in forming the observed cracks. In all probability, the grains that generated the stress concentration were not even in the thin section.

These results also indicate that the cracks formed on planes other than the basal in grains containing transgranular cracks. Some grains were observed to have cracks running roughly parallel to the *c*-axis.

ANALYSIS AND DISCUSSION

As the previous section shows, the results of the testing program provide information on a considerable range of topics relative to the response of ice to uniaxial compressive loading. These topics, which are discussed in this section, may be briefly summarized as follows.

1) *Crack length.* The average crack length scales linearly with the average grain size.

2) *Crack density.* The number of cracks per unit volume increases with grain size for the stated conditions.

3) *Onset of cracking.* The test material showed a transition from ductile flow with no cracking to flow with a considerable degree of cracking as the grain size increased from 1.5 to 5.7 mm.

4) *Creep behavior.* Grain size affected creep behavior significantly. As grain size increased, primary and tertiary creep rates increased and the strain at the minimum creep rate decreased significantly.

5) *Crack healing.* Observations indicate that isolated, vapor-filled cracks undergo a fairly rapid healing process which eventually transforms them into a bubble-like cavity. Air-filled cracks undergo healing at a significantly slower rate.

6) *Stress effects.* Test results at somewhat higher stresses indicate that the crack density increased with stress, but that the size of the forming cracks was not affected by the stress level.

7) *Crack location and grain orientation.* Cracks formed either at grain boundaries or across grains with nearly equal probability, and the grains that developed cracks exhibited no preferred orientation to the stress axis.

8) *Acoustic emission activity.* All specimens emitted considerable acoustic activity. Visible cracks generated the highest amplitude events and

the observations permitted some progress toward establishing an event amplitude level associated with the formation of a visible microcrack.

This section deals with the above points and addresses the effect of the measurement techniques on the results as well as the level of uncertainty in the results.

Thick section observations

The estimation of the size and number of cracks in the thick sections proved to be a very tedious process. Specimens with a relatively high crack density were difficult to analyze from the photographs alone (see, for example Fig. 11a). In order to improve accuracy, it was sometimes necessary to record the number of cracks in each sector of the thick section at the time the photograph was taken, as well as note some general observations about the network of cracks. This additional information greatly improved the reliability of the measurements.

Since an observer's acuity in this type of task is likely to improve with experience, all the crack counts and measurements were carried out twice. In some cases (most notably specimens 49 and 55), the photographs were of relatively poor quality and thus these results should be treated with some caution.

Most specimens having low or intermediate crack densities (less than approximately 0.5 crack per grain) displayed relatively unambiguous networks of cracks when photographed. The cracks were isolated and were thus easily identified and measured. The photograph in Figure 11b shows a typical sector from the thick section of specimen 44. As noted earlier, highly cracked specimens were evaluated by using thin sections. Additionally, a careful examination of the size and number of cracks which would appear ambiguous in the thick section photographs provided information which helped improve the reliability of the results.

As noted above, thick sections taken parallel to the axis of stress were not suitable for crack density measurements since it was difficult to identify individual cracks in that plane of observation. Figure 24 shows a photograph of a typical tested spec-

Figure 24. Thick section photograph taken parallel to the axis of applied stress.

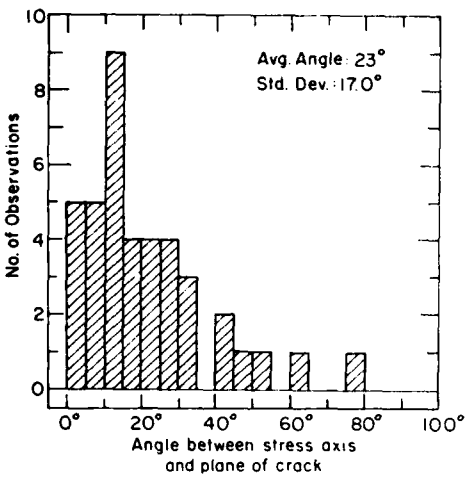

Figure 25. Distribution of the angle between the axis of compressive stress and the plane of the observed crack (40 observations).

imen. It is a thick section of material near the center of the specimen and it shows several cracks face-on or nearly so. When viewed from this angle, the cracks near the surface mask those deeper in the section, making an accurate count nearly impossible. However, this type of photograph is useful in that it shows the general shape of the cracks and it also provides a means of estimating the orientation of the plane in which the crack forms relative to the axis of applied stress.

Reliable measurements of this angle can be made only on cracks that appear edge-on in the photograph. Consequently, relatively few measurements were available since only several representative photographs of these vertically oriented thick sections were taken. Figure 25 shows the results of 40 observations in the form of a histogram. Note that the cracks tend to cluster about the vertical plane. The average angle is 23° with a standard deviation of 17.5°. Ninety percent of the observations fall within 45° of the stress axis.

Interestingly, a few cracks formed at a relatively large angle to the stress axis and one crack formed nearly perpendicular to it.

The grain size vs crack size relationship

This section examines the results of the crack length observations and addresses the errors introduced by the observational method and crack healing. Quantification of the sources of error provides a means of studying their effect on the results. Initially, a theoretical grain size vs crack size relationship is developed; later this relationship is compared to the experimental results.

The relationship between grain size and nucleated crack size

This section develops a relationship between grain size and nucleated crack size by using the concepts of elastic strain energy and surface energy. It is similar to the approach of Gold (1966) except that the strain energy term considers the pileup as a superdislocation and no flaw exists until the instant of nucleation. The method relies on the assumption that all the strain energy associated with the pileup goes to form new surface area when the crack forms. There is also some inherent inaccuracy because the expression used for strain energy was developed for the isotropic elastic case. Additionally, it is recognized that the results of such an analysis are a strong function of the values assumed for various geometric parameters such as obstacle spacing and the width of the slip plane. The values used here are in agreement with those found in the literature (e.g. Gold 1966) and no attempt has been made to obtain a range of values or a distribution to represent such quantities, with the exception of the slip plane length.

The calculations are based on a grain diameter of 2 mm. A slip plane length of $\ell = 0.6d = 1.2$ mm is used as a representative value. This comes from using the average value of the normalized slip plane length distribution, which was discussed in a previous section. Only basal slip is considered in this treatment. It is also assumed that the dislocation pileup extends across a grain on the slip plane so the pileup length is equivalent to the slip plane length.

Using eq 12 with

$\gamma = 0.109$ J m^{-2} (average surface energy from Hobbs 1974)
$\mu = 3.5$ GPa (Hobbs 1974)
$\ell = 1.2\times10^{-3}$ m
$\phi = 70.50°$
$\upsilon = 0.33$

the resulting nucleation stress is

$$\sigma_n = 1.05 \text{ MPa}.$$

When eq 13 is used with $b = 4.52\times10^{-10}$ m, the number of dislocations causing nucleation is

$$n \approx 1200.$$

Now the elastic strain energy of n dislocations in a pileup is given by Hirth and Lothe (1968) as

$$W = \frac{L\,\mu(nb)^2}{4\pi(1-\upsilon)} \ln \frac{4R}{\ell} \qquad (21a)$$

where ℓ = length of dislocation pileup (slip plane length)
L = length of dislocation line
R = half obstacle spacing.

Assuming that $L = d$, i.e. the slip line extends across the grain, that $\ell = 0.6d$ (the average of the slip plane length distribution) and that $R = 0.5d$, the energy of the pileup is found to be

$$W = 2.9 \times 10^{-7} \text{ J}.$$

To a first approximation, if the crack is assumed to be circular, it will have area $A = \pi y_c'^2/4$ where y_c' is the calculated crack size. The nucleated crack has $2A$ of new surface area. The energy required to generate this area is $\gamma(2A)$. If the elastic energy of the pileup is equated to the energy required for generating surface area,

$$W = \gamma(2A) \tag{21b}$$

it is seen that

$$A = (W/2\gamma) = 1.33 \times 10^{-6} \text{ m}^2$$

or

$$y_c' = 1.30 \times 10^{-3} \text{ m}.$$

Thus, a crack size of 1.30 mm results on average for 2.0 mm grain size material when it is subjected to sufficient stress to nucleate cracks. The ratio of crack size to grain size in this case is 0.65. A plot of this relationship (see Fig. 10) indicates the linear relationship between grain size and nucleated crack size.

Since in the above analysis the crack size goes to zero as grain size goes to zero, and the ratio of 0.65 may be interpreted as the slope of the relationship between the two variables, the theoretical relation between crack size and grain size may be written as

$$y_c' = 0.65d. \tag{22}$$

where y_c' is crack size (mm) and d = grain diameter.

Note that the above treatment assumes crack formation at all grain sizes. Since this is clearly not the case, a crack nucleation criterion must be applied to determine the threshold grain size for nucleation, and thus establish a lower limit to eq 22.

Note that the crack nucleation theory examined in an earlier section (eq 12) provides a means to establish this threshold grain size for crack nucleation.

Observed crack length and sources of error

As noted earlier, Figure 10 shows the result of the crack size measurements for all tests along with the best fit line using the linear regression technique. The equation for this line ($r^2 = 0.75$) is

$$y_c = -0.44 + 0.67d. \tag{23}$$

Equation 22, the theoretical prediction, is also plotted in Figure 10. Note that the test results exhibit the linearity predicted by the model. Interestingly, the theory predicts nearly the same slope found in the regression equation, but the curve is shifted to somewhat higher crack sizes throughout the range of grain size.

The overprediction of the model probably stems in part from its simplicity. It is likely that energy is expended in overcoming the compressive background stress in addition to creating new surface area. This would tend to decrease the resulting crack size prediction. Additionally, failure of the crack formation event to dissipate all the available strain energy could contribute to the observed disparity. In fact, this circumstance would help explain the difference in x-intercept between the theoretical and actual results. In this case, equation 21b would take the form

$$W = \gamma(2A) + W_R \tag{24}$$

where W_R is the residual strain energy after formation of the crack. The net effect would be a decrease in crack size for a given grain size and a shift in the x-intercept from the origin to some small grain size.

Although this potential source of error in the modeling will not be addressed further, two sources of error in the crack length measuring process require special attention, namely the effects of crack healing and the method of crack length measurement on the observed crack lengths.

Crack healing. When a crack forms, it immediately begins to heal. This is a result of the thermodynamic instability associated with the crack geometry. The edges of the cracks have an extremely small radius of curvature and the crack faces have a relatively large radius of curvature. When the crack remains isolated from the atmosphere after its formation, it quickly fills with water vapor in an attempt to reach equilibrium. However, the large differences in surface curvature within the crack must be eliminated before equilibrium can be achieved.

Equilibrium results when there is no pressure difference between the ice and vapor phases at all

points on the interface. This is clearly not the case in a newly formed crack. The variations in the radius of curvature result in variations in the pressure difference between the two phases along the crack surface (see Colbeck 1980). The pressure difference variation drives a flow process whereby material is transported from regions of low curvature to regions of high curvature. This process gradually brings the void into a nominally spherical shape with a relatively constant radius of curvature. The rate of the process decreases as the difference in curvature decreases.

In the present case of an isolated crack, the void contains only water vapor. The transport mechanism is viscous flow in the vapor phase, which is fast relative to a diffusion process. The process that the ice undergoes is sublimation in the true sense of the word, in that it consists of both evaporation from and then condensation back to the solid phase.

If the crack and the surrounding ice are viewed as a closed system with no imposed temperature gradient, heat must flow from the surface of the crack receiving material to the surface losing material in order for the sublimation process to proceed. Colbeck (1986) points out that this heat flow is in fact the rate-limiting factor in the healing process of vapor-filled cracks.

Now, if the crack interior contains air, either from being opened to the atmosphere or from intersecting a gas bubble upon nucleation, the healing rate is slowed considerably because the transport mechanism changes from viscous flow to diffusional flow, an inherently slower process. The rate limiting factor is not heat flow, but rather the diffusional process by which water vapor travels from the source surface to the sink surface. Thus, the presence of another gas in the void results in a significant retardation of the sublimation process. Consequently, the healing rate of a gas-filled crack is much slower than that of a crack containing only water vapor (see Colbeck 1986 for an in-depth treatment of this topic). The large crack in the center of the photographs in Figures 19a-d was filled with air during the sectioning process and displayed virtually no healing during the observation period (see top curve in Fig. 20b).

The question at hand is whether this crack-healing process occurs fast enough to significantly influence the crack length measurements taken up to several hours after their formation. To obtain the answer to this question, a set of measurements were made as discussed earlier (refer to Fig. 20a,b).

Since most of the cracks observed in these experiments are isolated within the specimens, it appears that the fast healing rates associated with the vapor diffusion mechanism should be considered. Considering the crack size vs time data, the initial healing rate is evidently not a strong function of initial crack size. Over the first 24-hr period of observation, the crack length reduction does not vary systematically with the original crack length, but shows considerable scatter for cracks of similar initial length. This scatter is probably due to variations in the distance between faces (the width) of the individual cracks. A "wide" crack, i.e. one with a relatively large distance between opposite faces, requires transport of a greater volume of material to reduce its length a given amount than a narrow or sharp crack. If the vapor transport mechanism is assumed to operate at nominally the same rate for both wide and narrow cracks, the wider cracks would require more time to heal a given amount.

Since crack length measurements were generally taken less than 4 hr after testing, estimation of the maximum amount of healing likely to occur during this time interval is of interest. Some healing could have occurred during the tests, and thus the average amount of healing after 5 hr should provide a very conservative upper bound to the crack length reduction.

The data indicate that, on the average, the measured crack length decreases by approximately 10% of the original length in the first 5 hr after testing. However, as noted above, the absolute reduction in length due to healing appears to be relatively independent of initial crack length, especially at low elapsed times. This implies that the crack lengths observed at a fixed time after formation require the addition of a constant as the appropriate means to correct for the effects of the healing process. The average amount of healing in the first 5 hr after formation was 0.08 mm and this value is used as the healing correction factor. Again, there are large variations in the amount of healing of individual cracks and cracks which are not isolated from the atmosphere will have a negligible healing rate over this time interval.

Since the crack healing phenomenon is a peripheral aspect of this work, the complexities of the healing process prevent an in-depth examination at the present time. There are many questions to be answered in this connection: the effect on healing of crack location (i.e. grain boundary or intracrystalline), the point in the healing process at which the crack becomes insignificant as a cause of stress concentration, and the manner in which crack size and shape affect the healing process.

Crack orientation and measured length. In general, the reported crack lengths are the longest di-

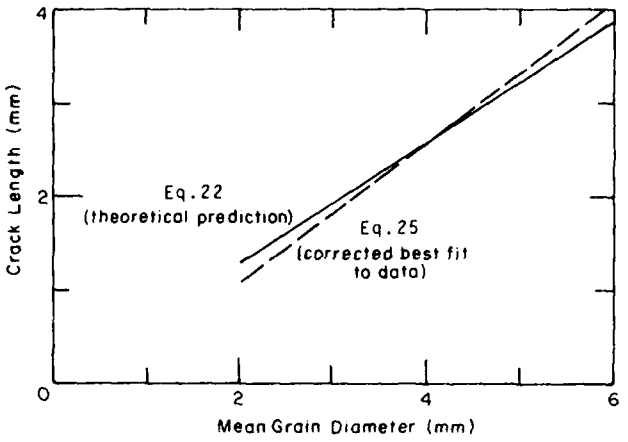

Figure 26. Theoretical prediction and observed relationship (after error corrections) for the average crack size/ grain size relationship.

mensions of the cracks projected on a plane perpendicular to the long axis of the specimen. Error can result if this projection does not adequately reflect the true maximum crack length. To assess this error, 60 cracks were evaluated from thick sections taken parallel to the long axis of the specimen. For each crack, the ratio of the maximum dimension to the dimension projected on a horizontal plane (which corresponds to the measurements taken in the crack length analysis) was computed. The minimum value of this ratio is one. The ratio increases as the true maximum becomes larger than the maximum projected length. The average of the ratio was 1.12 with a standard deviation of 0.19, indicating that the true crack lengths average 12% greater than the values actually measured.

Effect of error on the observations

The influence of the healing process and the method of crack length measurement may be incorporated into the results by applying the appropriate corrections to the regression equation (eq 23) which represents the test data.

Using the conservative estimate of 5 hr for the elapsed time between crack formation and measurement, the crack healing data indicate that, on average, a crack heals 0.08 mm in this period. The regression equation may then be corrected by adding the healing correction and multiplying the result by the factor 1.12. The factor 1.12 corrects for the 12% difference between the projected crack length actually observed and the true maximum length. Thus

$$y_c^* = (y_c + 0.08)\ 1.12$$

where y_c^* is the corrected crack length and y_c is the observed crack length. Substituting the expression for y_c from eq 23,

$$y_c^* = (-\ 0.44 + 0.67d + 0.08)\ 1.12$$

or

$$y_c^* = -\ 0.4 + 0.75d. \qquad (25)$$

Figure 26 shows the predicted relationship (eq 22) plotted along with eq 25, which is the observed relationship after error corrections.

Although the corrected curve has a somewhat steeper slope than the theoretical prediction, as well as a nonzero y-intercept, the agreement over the indicated range in grain size is very good.

As a final note in this regard, the crack length histograms presented (i.e. App. A) consist only of the uncorrected observations. The effect of applying the corrections to these data would be a shift to larger crack lengths and a slight increase in the range or spread of the data.

Crack nucleation condition

The results show that under the prevailing test conditions, cracks begin to nucleate at grain sizes between 1.5 and 1.8 mm. Recall that the 1.5-mm grain-sized specimen exhibited no cracking and very slight cracking was observed in the 1.8-mm grained specimen (see Table 1). Thus the threshold grain size for crack nucleation lies in this range of grain sizes.

Given this information, then, the validity of the crack nucleation condition (eq 12) may be tested by solving for the slip plane length and substituting appropriate values for the various elements of the relationship. If eq 12 adequately represents the mechanism of crack nucleation, the resulting critical slip plane length for crack nucleation should coincide reasonably well with the observed critical grain size for crack nucleation. The development of this correspondence between slip plane length and grain size, as noted earlier, relies on the assumption that shear strain propagates via slip planes that extend completely across the grains.

The following expression is obtained by solving eq 12 for the critical slip plane length, ℓ:

$$\ell = \frac{\pi\gamma\mu}{2(1-\upsilon)\sigma_E^2} \cdot \frac{1}{F(\phi)} \cdot \tag{26}$$

Values for γ, μ and υ given earlier are used. However, the values for σ_E, the effective shear stress required for crack nucleation, and $F(\phi)$, the geometrical parameter, require some discussion.

Under the prevailing test conditions, the maximum resolved shear stress σ_{MRSS}, which occurs on the most favorably oriented slip plane, is the axial stress σ_A multiplied by the maximum Schmid factor m or

$$\sigma_{MRSS} = \sigma_A \cdot m.$$

Since σ_A = 2.0 MPa and the highest value of m is 0.5,

$$\sigma_{MRSS} = 1.0 \text{ MPa}.$$

Now the maximum effective shear stress σ_{MESS} is the maximum resolved shear stress less the frictional stress component σ_0, or

$$\sigma_{MESS} = \sigma_{MRSS} - \sigma_0.$$

σ_0 represents the lattice resistance to dislocation movement in terms of shear stress. The only source for a value of σ_0 for ice prepared in the same manner as in this work, and at the same test temperature of -5°C, is Lim (1983). He reported a value of 0.56 MPa for the frictional component of stress, in terms of axial stress, for polycrystalline ice tested in tension under an average strain rate of 9.4×10^{-7} s^{-1}. Since the present work deals with shear stress, the value of 0.56 MPa has been multiplied by 0.5 and rounded to one significant figure, yielding a value of σ_0 = 0.3 MPa for the shear stress required to overcome lattice resistance to dislocation movement. The direction of applied stress is assumed to exert no influence on the frictional stress value.

Thus, the value of the maximum effective shear stress σ_E to be used in eq 24 is

$$\sigma_E = \sigma_{MRSS} - \sigma_0$$

$$= 1.0 \text{ MPa} - 0.3 \text{ MPa}$$

or σ_E = 0.7 MPa.

The function

$$F(\phi) = (5 + 2\cos\phi - 3\cos^2\phi)/4$$

given by Smith and Barnby (1967) provides a means of making the nucleation stress σ_E sensitive to the slip plane/crack plane geometry. In his treatment, Stroh (1957), as noted above, calculated the optimum value of ϕ to be 70.5° based on the normal stress distribution associated with the pileup. His results show this point to be relatively well defined. That is, the probability of developing a crack at a larger or smaller angle ϕ decreases sharply as the angle deviates from 70.5°.

By considering shear stress, Smith and Barnby (1967) showed that, while the optimal value of 70.5° was correct, the angle ϕ can vary from 0° to somewhat over 90° with relatively little change in the stress required for crack nucleation. This result has the net effect of making the stress required for nucleation of a crack less sensitive to local geometric factors.

Considering the likely range in ϕ to be 0° to 90°, the minimum and maximum values of $F(\phi)$ are 1.0 and 1.34. These values occur at ϕ = 0° and 70.5°.

It is now possible to calculate a range in slip plane lengths over which crack nucleation is possible given the prevailing test conditions. Equation 26 yields the following values:

$$F(\phi) = 1.00, \qquad \ell = 1.8 \text{ mm}$$

$$F(\phi) = 1.34, \qquad \ell = 1.4 \text{ mm}.$$

This range in slip plane length agrees well with the range in grain size (1.5 to 1.8 mm) over which the transition from no cracking to cracking was observed. Thus, given the assumptions mentioned above, the nucleation criterion (eq 12) appears to model the observed ice behavior reasonably well.

The fact that ice has a relatively low coefficient of self-diffusion D_v is undoubtedly a major factor

in the agreement between theory and observation in this case. D_v for ice at -10°C (corresponding to a homologous temperature of 0.96) is on the order of 10^{-13} m^2 s^{-1} (Hobbs 1974) while a typical value for a metal is on the order of 10^{-12} m^2 s^{-1} (Shewmon 1969). The lower capability for the diffusion of vacancies in ice enhances the material's ability to build and sustain the stress concentrations necessary for the nucleation of cracks at high homologous temperatures. In contrast, at high homologous temperatures in metals, the high degree of vacancy diffusion inhibits pileup formation and thus precludes the development of stress concentrations necessary for crack nucleation.

Crack density and specimen strain

It is useful to examine the cracking activity as a function of strain. The results given in Figure 13 are in qualitative agreement with the work of others who have made direct observations of internal cracks in ice (Gold 1970a, Zaretsky et al. 1979).

Typically, cracks begin to form after a small amount of strain has occurred. The acoustic emission results given later indicate the strain level for the onset of visible cracking is 4.7×10^{-4} on average. Interestingly, this strain level agrees well with Gold's (1970a) observations on columnar-grained ice at -9.5°C. He found this strain level to be relatively independent of stress provided it was sufficient to cause cracking.

The results show that the manner in which cracks accumulate with strain depends upon the grain size (refer again to Fig. 13). For the small-grained material, most all the cracking occurs in the first 10^{-2} strain. Additional straining results in a negligible increase in the number of cracks. However, at the intermediate grain sizes (approximately 3 mm), the cracking continues, but at a much reduced rate as straining proceeds beyond 10^{-2}. Finally, the largest-grained material exhibits a very high initial rate of cracking at strains below 10^{-2} and then continues to generate cracks at a significant rate. At total strains of less than 3×10^{-2}, these specimens are so completely saturated with cracks that they appear opaque. The crack density can be estimated only from thin sections for these specimens.

These results, brought about only by an increase in grain size, are in good agreement with the trends observed by St. Lawrence and Cole (1982). These resulted from an increase in applied stress, while grain size remained constant at 1.2 mm (estimated by the intercept method) and the test temperature was -5°C. In that work, an increase in stress brought about an increase in cracking activity as indicated by acoustic emissions monitoring. A brief comparison of the influence of stress and of grain size on cracking shows that the increase in grain size in the present work has an effect on the cracking activity that is very similar to the effect of an increase in axial stress. This is not surprising, however, since it is well recognized that an increase in either stress or grain size generally reduces ductility.

Creep behavior

Grain size effects

The character of the creep behavior seen in Figures 15a-c is similar to that found in other work for the finer-grained material at similar stress levels (Mellor and Cole 1982, Jacka 1984).

The effect of grain size on the creep curve can be seen by comparing specimens 62 and 69 in Figure 15a. An increase in grain size from 1.5 to 4.7 mm causes a drop in the strain at the minimum creep rate from 10^{-2} to 4.2×10^{-3}. There is a tendency for the larger-grained material to exhibit both a faster drop in the primary creep rates and a faster increase in the tertiary rates than the fine-grained material.

Some of the tests (see Fig. 15a, specimens 47, 60 and 62) exhibited a trend toward higher primary creep rates with larger grain size. Duval and LeGac (1980) observed this trend in creep tests on polycrystalline ice at a temperature of -7°C and a creep stress of approximately 0.5 MPa. The same workers also noted that grain size exerted no apparent influence on the "steady state" creep rate of their test material. The results of Duval and LeGac (1980) are at variance with results reported by Baker (1978), who observed a significant effect of grain size on the steady-state creep rate of laboratory-prepared ice. Baker found the creep rates exhibited a minimum at a grain size of 1.0 mm for tests performed at temperatures of -7 to -10°C and at a creep stress of approximately 0.56 MPa. He attributed the observed reversal of the influence of grain size (from strengthening to weakening the material) to a change in the main deformation mechanisms. He reasoned that the grain boundary weakening resulted from diffusional processes operative for the small-grained material and that the strengthening resulted from the operation of the dislocation-controlled creep mechanism.

Unpublished work referenced by Jacka and Maccagnan (1984) indicates no significant grain size effect on the minimum creep rate of laboratory-prepared ice over the grain size range of 0.8 to 3.4 mm, at temperatures of -7 and -10°C

and under creep stresses of 0.3 and 0.26 MPa octahedral (0.64 and 0.55 MPa normal). These experimental conditions cover the range of Baker's (1978) tests, but the grain size effect observed by Baker is absent. Thus, the work by Baker (1978) remains unsubstantiated. The reason for the disagreement on grain size effects, however, is not clear. Historically, a main difficulty in the field of ice mechanics lies in the effect of the specimen preparation procedure on the mechanical properties of the material. Since there is no standard method for specimen preparation, workers generally begin with a commonly used approach such as packing a mold with sieved ice grains, evacuating and flooding the mold with degassed water and then freezing the resulting ice-water mixture. However, details of the procedure, such as the source of the seed grains, the size range of the seed grains, the rate and direction of freezing final specimen porosity, and the chemical purity of the melt, often go unreported. These factors can influence the mechanical behavior of the material under certain conditions, and when data from different sources are compared, possible specimen differences must always be considered. In addition, when grain size is varied, questions regarding the influence of specimen size generally arise as well. For example, Baker's (1978) specimens were 19.7 mm in diameter and his grain diameter ranged from 0.62 to 2.11 mm. Duval and LeGac (1980) used specimens of 80-mm diameter and their grain size range was 1.07 to 9.8 mm. Thus, although stress and temperature were the same for both sets of data, the sample sizes, and hence the number of grains across a sample diameter for a given grain size, vary greatly.

Unfortunately, the works cited above are not strictly germane to the present study because of the significant difference in creep stress levels. The higher stress level generally results in material behavior in the dislocation glide with cracking regime rather than a diffusion controlled regime. Also, the grain size range of the present work induces a significant change in the material's response to stress by causing the onset of internal fracturing. Thus the grain size effect found here is only relevant when considering the onset of internal cracking. A study of grain size effects near the ductile-to-brittle transition offers an inherent advantage since the effect of the grain size variations is evidenced by visible cracking. Thus, a grain size effect, and the associated shift in deformational mechanism, can be verified visually. This is a preferable situation to the case cited above, where stress-strain rate data were the only evidence of an apparent deformational mechanism change, and no independent means of verification was available.

In Figure 16, which shows minimum creep rate $\dot{\epsilon}_{min}$ vs the average grain size, there appears to be a subtle trend for the lowest values of minimum creep rate to occur near a grain size of 3.0 mm. The creep rates at the largest grain sizes exhibit a fairly large degree of scatter, however, making it difficult to discern a trend beyond the 3-mm grain size.

It is interesting to note that the more clearly defined drop in $\dot{\epsilon}_{min}$ for grain sizes between 1.5 and 3 mm coincides with the transition from the threshold of cracking to a significant degree of cracking. Over this same range in grain size, the strain at $\dot{\epsilon}_{min}$ undergoes a significant drop from 10^{-2} to approximately 5.5×10^{-3}. Thus, the material appears to lose ductility as a result of the grain size increase. A good deal more testing will be needed to clarify the trends in these creep results.

It is possible that the behavior seen in Figure 16 is merely the result of random variations in the balance between competing deformational mechanisms. This is an inherent problem at the transition point between two distinct regimes of material behavior.

Another possibility for the apparent grain size effect for the larger grain sizes relates to specimen size effects. When grain size varies as in the present work, the number of grains in a specimen of fixed dimensions varies greatly, as does the number of grains across the diameter. In fact, a few of the larger-grained specimens tested are somewhat over the acceptable limit of 10 to 12 grains across the diameter. (Note, however, that when using the results of the intercept method of grain size estimation, all specimens appear to be within the limit of 10 grains across the diameter.) Jones and Chew (1983) recommended having at least 12 grains across the diameter to avoid specimen size effects. Their results indicated a noticeable increase in uniaxial compressive strength when the number of grains across the specimen dropped to eight. In these tests, grain size was held constant at 1.0 mm and the specimen size was changed to achieve the range in the number of grains per diameter. There is still some uncertainty as to specimen size effects in the testing of ice and it is possible that the present testing methods do not completely isolate grain size effects from possible specimen size effects. A considerable amount of work will be needed, however, to clarify the roles of grain size and specimen size in the mechanical testing of ice.

Potential difficulties in this regard are recognized, but since it is not of primary concern in the present work, this matter will not be dealt with further.

The effect of grain growth

An interesting aspect of material behavior came to light regarding the effect of time/temperature history on the creep response of the ice. Specimen grain size is generally controlled by the seed grain size and a given sample is tested soon after molding to avoid grain growth effects. However, a large average grain size can be achieved by suitably aging a smaller grain-sized specimen. The question naturally arises as to whether specimens of equal grain size display similar mechanical behavior regardless of the method used to achieve the grain size. Figure 15f shows data which address this point. The grain sizes of specimens 41, 49 and 56 in Figure 15f were achieved by allowing grain growth to occur for some time after molding. The seed grains for these specimens were in the 0.59–0.83 mm range. The grain size in all other tests resulted directly from the seed grain size and no significant grain growth occurred before testing. The difference in the creep behavior between the two groups of specimens is striking. Specimens 41 and 49 do not exhibit minimum strain rates as such, and 56 merely develops a subtle trend near 10^{-3} strain somewhat indicative of a minimum strain rate. The common trend here is the absence of the decreasing strain rate usually found in primary creep. Additionally, these specimens always show an extreme degree of internal cracking.

The reasons for the anomalous behavior of the grain-growth specimens are unclear. It is unlikely that a preferred orientation developed during grain growth under these conditions when the grains were originally randomly oriented.* A possible explanation may be related to the dislocation density of the material just prior to testing. The grain-growth specimens, after being aged for several weeks at a relatively warm temperature (i.e. -2°C), presumably had a significantly lower dislocation density than the specimens that were tested shortly after molding. This difference in dislocation density can cause a corresponding difference in the value of the stress needed to start dislocation motion in the two types of specimens. Armstrong et al. (1962) showed that the frictional stress term σ_0 increases as a material undergoes the increase in dislocation density associated with work hardening. If this is the case, the grain-

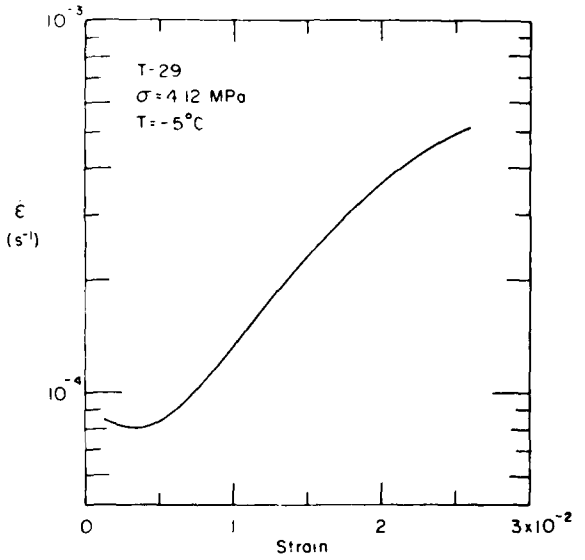

Figure 27. Creep curve for a fine-grained specimen under high load (σ = 4.12 MPa).

grow th specimens will experience higher effective shear stresses than the other specimens. This in turn leads to higher internal stress concentrations and hence the greater degree of cracking. Apparently, this greater degree of damage through cracking is associated with a reduction in the strain at the minimum creep rate or, in some cases, the absence of a discernible minimum creep rate. It is expected that this behavior would result if the applied stress, in a test on material having a greater initial dislocation density, was sufficiently high to give the same level of effective shear stress. Some evidence exists in support of this, namely fine-grained ice without any grain growth was found to experience only a brief strain rate minimum at 3.4×10^{-3} strain under a stress of 4.12 MPa (see Fig. 27). A severe amount of cracking accompanied this behavior. Specimens subjected to slightly lower stresses, however (i.e. 3.7 MPa), exhibit typical creep behavior (see, for example, Mellor and Cole 1982) and strains at $\dot{\epsilon}_{min}$ are near 10^{-2}. Presumably, the strain rate minimum would disappear completely under some further increase in stress. Thus, there is an indication that, at some level of effective shear stress, ice essentially fails upon loading and does not develop the strain rate trends typical of creep behavior.

An additional factor complicating an assessment of the observed behavior is that the specimens experiencing grain growth are likely to have a rather broad range in grain sizes because the larger grains grow at the expense of the smaller

*A.J. Gow, pers. comm. 1983.

a. Thin section of an untested specimen showing an extreme example of the grain growth process.

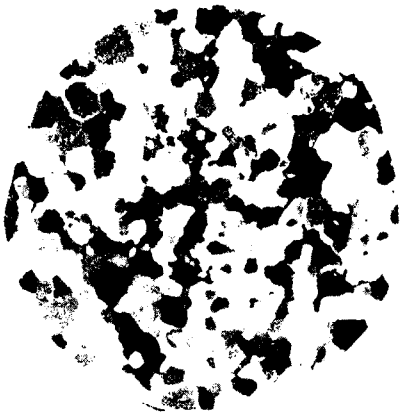

b. Thin section of specimen 49 after testing. Note the range in grain size resulting from the grain growth process.

Figure 28. The effect of grain growth on grain size.

grains. Figure 28a shows an extreme example of this. It shows an untested specimen held at -2°C for approximately three months before the section was taken. It exhibits abnormal grain growth as well as an extremely broad range in apparent grain diameters. Figure 28b shows a thin section of specimen 49 after testing under 2.8 MPa to a strain of 2.5×10^{-3}. Note that some grains have grown considerably while clusters of fine grains (near the center of the photograph), apparently from the original structure, still persist. It is difficult to determine which characteristics of such a structure control the deformational processes.

Due to the uncertainties involved and the limited amount of data available, it was decided not to pursue the effect of grain growth on mechanical behavior in the present work. Once the above-mentioned deviations were encountered, specimens were tested only as molded, not allowing significant grain growth to occur.

Normalized crack length

It is useful to normalize the crack length data given in Appendix A to the grain size of each specimen. This allows a broad comparison of the results and sheds light on the relationship between the crack size distribution and the grain size. Figure 29 shows a histogram of some 2246 observations made from the thick sections. These data have been normalized to grain size. The mean is 0.5 and the standard deviation is 0.39. Table 4 gives the values of the normalized mean crack length for all specimens (CL/d). Although these values display a certain amount of scatter, they are reasonably well grouped about the mean. Interestingly, the distribution of the merged normalized data retains essentially the same shape as the raw crack size data of the individual specimens in Appendix A. Given the above observations, it appears likely that a generalized distribution, such as that in Figure 29, in terms of normalized crack length, may be used to estimate the actual crack size distribution for any given grain size.

The main difficulty in this connection lies in assessing the maximum crack length. There is considerable scatter in the largest normalized crack length values for the specimens tested. Figure 30 shows the maximum normalized crack length as a function of grain size for all tests. They range from 0.83 to 3.10 and do not appear to correlate with either grain size or axial strain level. Perhaps fortuitously, the maximum crack size of $3.1d$ agrees with the observations made by McMahon and Cohen (1965) cited earlier. The average of the maximum normalized crack lengths is 1.70 with a standard deviation of 0.66. Additionally, the raw data indicate that 8.8% of the observed cracks are greater in length than the average grain size.

A Beta-distribution fit to all the data indicates that the probability of encountering a crack equal to or larger than $1.6d$ is 1% and the probability of encountering a crack equal to or larger than $2.0d$ is 0.1%. In other words, it is relatively rare to encounter a crack larger than the average maximum

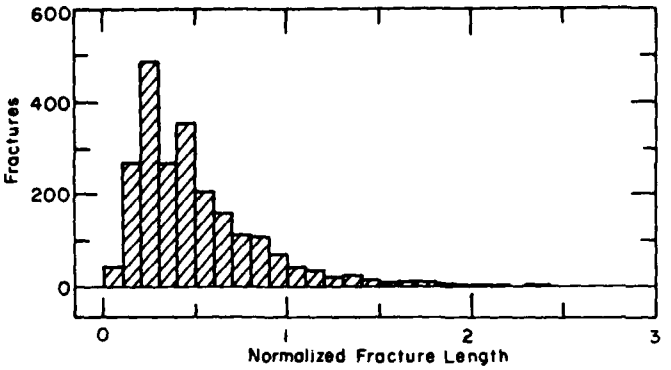

Figure 29. Normalized fracture length distribution for all tests.

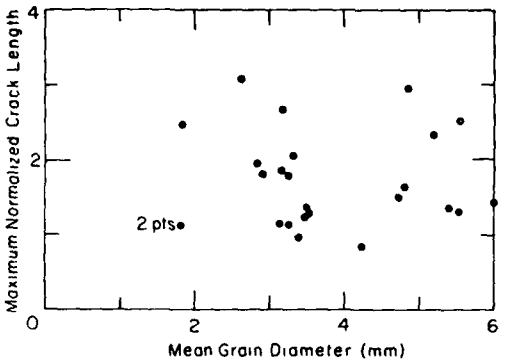

Figure 30. Maximum normalized crack length vs grain diameter for all tests.

value. In fact, all observed cracks with normalized values greater than 2.2 occurred in either specimen 71 or 74. The reason for the unusually high values in these particular specimens is not apparent, but the likelihood of their existence must nonetheless be considered in applying these results.

An estimate of the actual crack size distribution of material with an arbitrary grain size d can be obtained from the normalized crack size distribution by substituting the term CL/d for the normalized crack size CL_N and then multiplying the coefficient by $1/d$ to maintain unit area of the probability density function.

Location of cracks

As mentioned above (see Table 3), thin sections of several highly cracked specimens were examined in detail in order to assess the location of the microfractures. The microfractures were categorized as either grain boundary or transcrystalline. In total, 573 observations were made and Figure 31 shows the results in the form of histograms. These data have been normalized to grain size.

All of these specimens were strained to 10^{-2} under the 2.0-MPa initial creep stress. There is no apparent systematic variation of crack location with grain size under these conditions.

The mean lengths of the normalized grain boundary and transcrystalline cracks were 0.37 and 0.35 respectively. The maximum values were 1.6 and 1.2 respectively. The fact that these measurements came from thin sections probably led to the lower mean and extreme values relative to results obtained from thick sections. It would be highly unlikely for the maximum crack dimension to lie in an arbitrarily selected thin section of 1 mm, while the probability of observing the complete length of a crack in a thick section (of 10 mm) is much greater. Thus, the absolute magnitude of the results in Figure 31 should be treated with some caution.

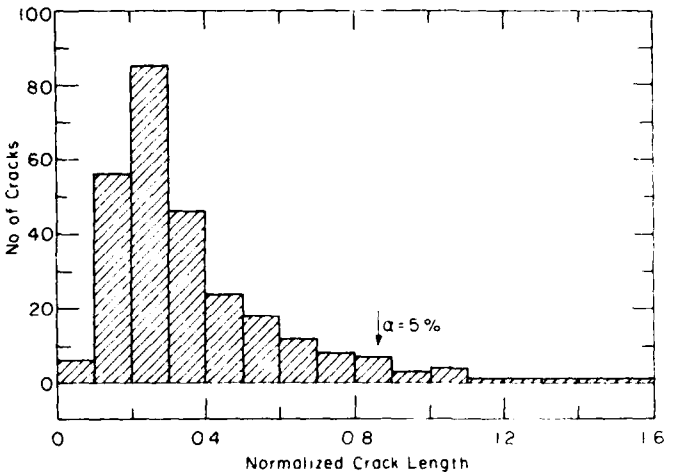

a. Normalized grain boundary crack size distribution.

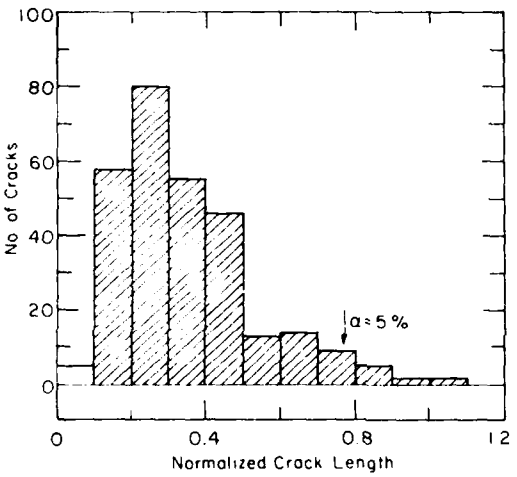

b. Normalized transcrystalline crack size distribution.

Figure 31. Normalized crack length histograms.

Acoustic emission activity

In the present work, the acoustic emission data serve as a vehicle to link the fracturing activity with time and thus specimen strain. The initial task concerns the development of a correspondence between an acoustic event and the nucleation of a discernible microfracture. The correspondence is based on the reasonable assumption that the recorded AE event amplitude is in proportion to the microfracture size, as noted in an earlier section.

The crack density measurements allow the estimation of the total number of visible cracks in a given specimen. The AE monitoring system is set to a sensitivity great enough to respond to acoustic activity of much lower amplitudes than that generated by the observable microfractures. Thus, in a given test, there are generally many more AE events recorded than cracks nucleated. Consequently, filtering the AE data was necessary in such a manner as to retain the appropriate number of events corresponding to the estimated total number of microfractures in the specimen. Events were filtered with respect to amplitude only. A computer program performed the filtering process in two modes: 1) given a threshold amplitude level, it determined the number of events having amplitudes greater than or equal to the threshold

using a simple sorting method, and 2) given a specific number of events, it determined the AE amplitude threshold that was passed the required number of times. The latter mode proved most useful in the present context. The program was entered with the estimated number of microfractures and an output file was in turn generated that contained only the AE events that passed the filtering process. The file contained the time of occurrence and the amplitude of each event.

In most tests, a remotely controlled solenoid imparted a trigger signal to the specimen at the moment the load application began. The AE system sensed this signal and its time of occurrence was taken as the zero or reference time for the test. The deformation readings also were "zeroed" to this time to ensure a common starting time for both the AE and deformation data. Due to the method of recording test information, two separate files were initially developed for each test. One consisted of AE data as a function of time and another was deformation as a function of time. Both files were interpolated to yield readings at the same time increments and merged to form a single file.

The resulting file contained sufficient information to determine, for specific time increments, the specimen strain, strain rate, stress, accumulated fractures, fracturing activity per unit time and per unit strain. The acoustic activity was normalized to unit volume in these calculations.

An eventual goal of the AE work is to firmly establish a correspondence between acoustic activity and fracturing activity. This relationship will allow a prediction of the size distribution of the fractures generating the observed acoustic activity. However, at this writing, this relationship is not yet sufficiently established to warrant a detailed analysis. For the present the filtered AE results may be reasonably taken to indicate the occurrence of visible cracks. The AE observations for each test are based on filtered data employing the filtering thresholds determined for each specimen.

The results allow the determination of the time and strain at the onset of fracturing as well as at the peak fracturing rate, as given in an earlier section.

With the exception of specimens 43, 49, 55 and 70, the amplitude thresholds fall within the range of 81.6 to 88.7 dB, with a mean and standard deviation of 86.2 dB and 2.0 dB. When all data are considered, the mean amplitude threshold is 83.7 dB with a standard deviation of 4.7 dB. It is not clear why the four specimens mentioned have significantly lower filtering thresholds, but there are several sources of error that could contribute to inaccuracies in the AE measurements:

1) inconsistencies in the characteristics of the specimen-transducer interface
2) signal attenuation
3) crack orientation effects
4) frequency effects.

A variable in the AE considerations for all tests is the consistency or repeatability of the characteristics of the specimen-transducer interface. Although a great effort was made to be as consistent as possible in the placement of the transducers, variations in the quality of the specimen/transducer interface can nonetheless occur. The measured amplitude of identical acoustic pulses decreases with poor specimen-transducer contact. Ideally, the system should be calibrated with an acoustic pulse, similar to that generated by a nucleating crack, just prior to each test. Thus, deficiencies could be detected beforehand and the transducer remounted to provide a satisfactory result. Unfortunately, such a method was not available during the course of this study, so some uncertainty is inherent in the AE results.

In fact, such uncertainty could be the major cause of variations in the filtering thresholds (see Table 5). This circumstance causes difficulty in the longer-range objective of establishing an overall amplitude threshold for visible fractures. However, it does not adversely affect the veracity of the results when specimens are considered individually. Thus, even though the thresholds may vary, the filtered AE events for a particular specimen correspond to the observed number of cracks for that specimen. Consequently, such quantities as the cracking rate and the strain level for the onset or peak rate of cracking are not directly influenced by small variations in the specimen-transducer interface quality.

Attenuation of the acoustic signal is significant for high frequencies and large distances in ice. However, in this study, the maximum travel distance from an event source to one of the transducers is approximately 50 mm. Bogorodskii and Gusev (1973) indicate that attenuation is on the order of 5 dB m^{-1} in ice. Thus, signal variations of much less than 1 dB are expected in the present work, and are thus not a significant factor in the results.

The orientation of the crack to the transducer face is likely to have an effect on the measured amplitude. The effect is, however, difficult to

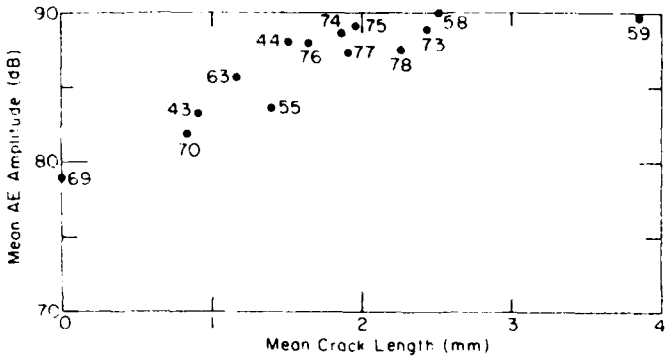

Figure 32. Mean AE amplitude vs mean crack length.

quantify. It is assumed that the orientation of the cracks to the transducer face is sufficiently random to preclude systematic effects of this variable.

This treatment does not address the effects of possible variations in the frequency content of the acoustic pulses. Since the mechanics of crack formation are expected to be the same for all crack sizes, little variation is expected. However, the possibility that the frequency spectra of the acoustic pulses may change with crack size should be kept in mind.

As pointed out in an earlier section, a microfracture is expected to generate an acoustic pulse in proportion to its size, with certain geometric considerations. Thus, the magnitude of the acoustic pulses passing the filter should correspond to the sizes of the observed microfractures. Figure 32 shows the average AE amplitude vs the average crack size for all the specimens for which suitable AE data were obtained. Included in this plot is a point from specimen 69, which evidenced no visible cracking. This amplitude of 79 dB was very rarely exceeded in the test and is assumed to represent the greatest AE amplitude produced by a subvisible crack.

These data indicate the tendency for the mean AE amplitude to increase with mean crack size. The scatter, however, is considerable and, as mentioned above, this scatter is probably due to variations in the quality of the specimen/transducer interface. The average crack size - average amplitude relationship could be strengthened by an increase in the relatively narrow range of 0.90 to 2.5 mm in the average crack size. Significantly larger specimens would be required to increase this range.

The onset of cracking, as indicated by the AE results, occurs at an axial strain of 4.7×10^{-4} with a standard deviation of 4.3×10^{-4}. Interestingly, this strain level is in good agreement with that given by Gold (1967) for the strain at the formation of grain-sized cracks in columnar-grained ice. The strain and time at the onset of cracking activity do not appear to vary systematically with grain size in these tests. Strain values for the cracking onset range from effectively zero to a maximum of 1.15×10^{-3}.

As Figure 23 shows, grain size exerts a strong influence on the time to the maximum cracking rate (as indicated by the maximum AE rate). Since the strain at $[dAE/d\epsilon]_{max}$ is not strongly affected by the grain size in these tests, it is evident that the average strain rate prior to the peak cracking rate must increase with grain size. Indeed, an inspection of the creep curves (Fig. 15c) shows, for a constant initial stress of 2.0 MPa, that the average strain rate prior to $[dAE/d\epsilon]_{max}$ increases by nearly a factor of four as grain size increases from 1.8 to 5.5 mm. There is a very moderate tendency for the strain at $[dAE/d\epsilon]_{max}$ to decrease with increasing grain size, further contributing to observed decrease in time to the maximum cracking rate. The average strain at $[dAE/d\epsilon]_{max}$ is 1.95×10^{-3} with a standard deviation of 9.6×10^{-4}. The average strain at $[dAE/dt]_{max}$ is 1.75×10^{-3} with a standard deviation of 8.8×10^{-4}.

In general, these results reinforce earlier findings regarding cracking in polycrystalline ice. A small amount of strain is required to initiate cracking, and once started, the rate of cracking reaches a peak during the primary creep stage, well before the minimum creep rate is reached.

The average strain at which $[dAE/dt]_{max}$ occurs coincides with the average strain at $\ddot{\epsilon}_{min}$, the inflection point found in the primary creep portion of a plot of $\dot{\epsilon}$ vs ϵ (see Fig. 15). (Both these values of average strain are very near 2×10^{-3}.) In the present deformational mechanism regime of plas-

tic flow with cracking, AE results generally show no distinct characteristic at either the occurrence of $\dot{\epsilon}_{min}$ in a creep test or σ_{max} in a strength test (see Cole and St. Lawrence 1984). However, it is expected that the maximum cracking rate should coincide with a fundamentally significant aspect of material behavior. Mellor and Cole (1982) were the first to distinguish the point of $\ddot{\epsilon}_{min}$ in ice creep data, and noted that it is the point of maximum deceleration in the primary creep curve. Thus, the AE results indicate that the material is apparently undergoing its greatest rate of strain hardening (i.e. creep rate is decreasing most rapidly).

Although this application of AE technology requires further development, the potential for its use is clear. Proper interpretation of AE data will preclude the time-consuming post-test analysis currently required for examining internal cracking activity. Much insight can be gained from detailed information on the characteristics of internal fractures in ice in terms of understanding deformation mechanisms and for verification of micromechanical models of material behavior.

SUMMARY AND CONCLUSIONS

This work presents the results of constant load creep tests performed at -5°C on polycrystalline ice. Some 26 tests were performed on specimens having equiaxed grains ranging from 1.5 to 6.0 mm. Most specimens experienced an initial stress of 2.0 MPa. Tests were terminated after axial strains ranging from 3.7×10^{-4} to 5×10^{-2}. Some specimens were tested at higher stress levels of 2.4, 2.6 and 2.8 MPa.

The results demonstrate the influence of grain size on the internal fracturing in ice. The stated increase in grain size brought about the onset of internal cracking as predicted by the nucleation equation of Smith and Barnby (1967). The material showed a loss in ductility as evidenced by a significant decrease in the strain at $\dot{\epsilon}_{min}$ and a dramatic increase in the number of internal cracks.

In all tests where internal cracking occurred, an extensive post-test analysis on the size and number of cracks in the ice was made. This analysis allowed the determination of the crack size distribution as well as the crack density in each specimen. A linear relationship between grain size and the average crack size distribution emerged from these data.

Peripheral aspects of the work addressed crack healing, the theoretical aspects of the grain size/crack size relationship, the grain size effect on the strain at $\dot{\epsilon}_{min}$, the relationship between grain size and slip plane length and the effect of grain size on creep behavior.

Acoustic emissions monitoring techniques were employed and the results were promising. Considerable progress was made toward determining the onset, total number and rate of formation of microcracks from AE data.

In view of the test conditions stated above, this work leads to the following conclusions:

1. Both the crack nucleation condition and the crack size/grain size relationship are well modeled using the concept of the dislocation pileup.

2. Cracks begin to nucleate in ice at grain sizes between 1.5 and 1.8 mm under a 2.0-MPa creep stress at -5°C.

3. The extent of internal microfracturing increases sharply as grain size increases from 1.8 to 6.0 mm.

4. The average microcrack dimension scales linearly with the mean grain size.

5. As grain size increases from 1.5 to 6.0 mm, the axial strain at the minimum creep rate falls from 10^{-2} to near 4×10^{-3}.

6. The minimum creep rate, while exhibiting some subtle trends, is not clearly affected by grain size.

7. The peak fracturing rate occurs at relatively low strains, well before $\dot{\epsilon}_{min}$ is reached, and the time to the peak fracturing rate decreases with increasing grain size.

8. Grain size apparently does not systematically affect the strain at the onset of cracking or the strain at the peak fracturing rate.

9. Based on a limited number of observations, grains that develop transgranular cracks do not appear to have a preferred orientation to the stress axis.

10. Crack healing processes significantly affect crack size. Water-vapor-filled cracks heal by a viscous flow mechanism at a significantly higher rate than air-filled cracks.

11. The crack lengths for all specimens, when normalized to grain size, tend to follow a common distribution.

SUGGESTIONS FOR FUTURE WORK

1. Experimental work must be carried out to explore specimen size effects on the mechanical behavior of polycrystalline ice. This should be done in conjunction with a grain size study in order to isolate grain size and specimen size effects.

2. Both strength and creep tests on specimens of varying grain size should be performed both above and below the threshold of cracking as indicated in this work. This would help clarify the trends suggested in the present data. Specifically, such results would show if grain size exerts an influence on the stress vs strain rate relationship to accompany its influence on the internal fracturing activity.

3. Continued efforts toward establishing a crack size vs AE amplitude relationship appear warranted. A useful relationship of this type would greatly reduce the amount of work required to analyze fracturing activity. The optical post-test analysis methods used in this work are too time-consuming and tedious to become part of a routine testing procedure. However, the AE technique, once sufficiently advanced, will lend itself to routine use.

4. A detailed study of crack orientation to the axis of applied stress, especially under uniaxial tension, would be useful. Given a sufficient number of observations, it is possible to establish a distribution of the angles between the crack plane and the stress axis. Knowledge of this distribution as well as its development during the course of straining will shed light on the failure process of ice in tension.

5. Cracking in specimens having grains significantly larger than those tested in this work should be examined. It is possible that subgrain structure might become a factor at large grain sizes and thus limit the applicability of the crack size vs grain size relationships found in the present work.

6. The effects of grain growth on the mechanical properties of ice should be examined systematically. It is possible the time-temperature history should be considered as a test variable along with structural parameters.

LITERATURE CITED

Agarwal, A.B.L., J.R. Frederick and D.K. Felbeck (1970) Detection of plastic microstrain in aluminum by acoustic emission. *Met. Trans.*, **1**: 1069-1071.

Armstrong, R.W. (1970) The influence of grain size on several mechanical properties of material. *Met. Trans.*, **1**: 1169-1176.

Armstrong, R.W., I. Gold, R.M. Douthwaite and N.J. Petch (1962) The plastic deformation of polycrystalline aggregates. *Philosophical Magazine*, **7**: 45-58.

Baker, R.W. (1978) The influence of ice crystal on creep. *Journal of Glaciology*, **21**(85): 485-497.

Baram, J. and M. Rosen (1981) Effect of grain size on the acoustic emission generated during plastic deformation of copper. *Material Science and Engineering*, **47**: 243-246.

Bogorodskii, V.V. and A.V. Gusev (1973) Attenuation of sound in ice in the frequency range 200-1100 kHz. *Sov. Phys. Acoust.*, **19**(2), Sept-Oct: 97-99.

Bullough, R. (1964) The cracked dislocation under tension. *Philosophical Magazine*, 8th series, **9**(102): 917-925.

Carter, D. (1970) Brittle fracture of snow ice. *Proceedings, IAHR Ice Symposium*, Reykjavik, pp. 1-8.

Colbeck, S.C. (1980) Thermodynamics of snow metamorphism due to variations in curvature. *Journal of Glaciology*, **26**(94): 291-301.

Colbeck, S.C. (1986) Theory of microfracture healing in ice. *Acta Met.*, **34**(*1*): 89-95.

Cole, D.M. (1979) Preparation of polycrystalline ice specimens for laboratory experiments. *Cold Regions Science and Technology*, **1**(2): 153-159.

Cole, D.M. (1984) The amplitude of acoustic emissions in ice. USA Cold Regions Research and Engineering Laboratory, CRREL Report (in prep.)

Cole, D.M. and W.F. St. Lawrence (1984) Acoustic emission from ice. In *Third International Symposium on Acoustic Emissions and Microseismic Activity in Geologic Structures and Materials* (H.R. Hardy, Jr. and F.W. Leighton, Ed.). Pennsylvania State University Press.

Cottrell, A.H. (1958) Theory of brittle fracture in steel and similar metals. *Transactions of the Metallurgical Society of AIME*, April, pp. 192-203.

Cousland, S.McK. and C.M. Scala (1981) Acoustic emission and microstructure in aluminum alloys 7075 and 7050. *Metallurgical Science*, **15**(11 and 12): 609-614.

Currier, J.H. (1983) The brittle to ductile transition in polycrystalline ice under tension. USA Cold Regions Research and Engineering Laboratory, CRREL Report 83-14.

Dieter, G.E. (1976) *Mechanical Metallurgy*. New York: McGraw-Hill.

Duval, P. and H. LeGac (1980) Does the permanent creep-rate of polycrystalline ice increase with crystal size? *Journal of Geophysics*, **25**(91).

Evans, A.G. (1982) Acoustic emission sources in brittle solids. In *Fundamentals of Acoustic Emissions* (K. Ono, Ed.), pp. 209-228.

Frederking, R. (1977) Plane-strain compressive strength of columnar-grained ice and granular-snow ice. *Journal of Glaciology*, **18**(80): 505-516.

Gandhi, C. and M.F. Ashby (1979) Fracture mechanism maps for materials which cleave: FCC, BCC and HCP metals and ceramics. *Acta Metallurgica,* **27**: 1565-1602.

Gold, L.W. (1960) The cracking activity in ice during creep. *Canadian Journal of Physics,* **38**(9): 1137-1148.

Gold, L.W. (1965a) The initial creep of columnar-grained ice. Part I. Observed behavior. *Canadian Journal of Physics,* **43**: 1414-1422.

Gold, L.W. (1965b) The initial creep of columnar-grained ice. Part II. Analysis. *Canadian Journal of Physics,* **43**: 1423-1434.

Gold, L.W. (1966) Elastic and strength properties of freshwater ice. *Proceedings, Ice Pressure Against Structures,* Laval University, Quebec, pp. 13-23.

Gold, L.W. (1967) Time to formation of first cracks in ice. *Proceedings, International Conference on Low Temperature Science, Sapporo, Japan.* Vol. 1, Part 1, pp. 359-370.

Gold, L.W. (1970a) Process of failure in ice. *Canadian Geotechnical Journal,* **7**: 405-413.

Gold, L.W. (1970b) Failure of ice. In *Proceedings, IAHR Ice Symposium, Reykjavik,* pp. 1-6.

Gold, L.W. (1972) The process of failure in columnar-grained ice. *Philosophical Magazine,* **26**(2): 311-328.

Gold, L.W. (1977) Engineering properties of freshwater ice. *Journal of Glaciology,* **19**(81): 197-212.

Goodman, D.J. (1977) Creep and fracture of ice and surface strain measurements on glaciers and sea ice. Ph.D. thesis, Christ's College, Cambridge.

Hirth, J.P. and J. Lothe (1968) *Theory of Dislocations.* New York: McGraw-Hill.

Hobbs, P.V. (1974) *Ice Physics.* Cambridge: Oxford University Press.

Jacka, T.H. (1984) The time and strain required for minimum ice strain rates. *Cold Regions Science and Technology,* **8**(3): 261-268.

Jacka, T.H. and M. Maccagnan (1984) Ice crystallographic and strain rate changes with strain in compression and extension. *Cold Regions Science and Technology,* **8**(3): 269-286.

Jones, S.J. and H.A.M. Chew (1983) Effect of sample and grain size on the compressive strength of ice. *Annals of Glaciology,* **4**: 129-132.

Kamb, W.B. (1962) Refraction corrections for universal-stage measurements. I. Uniaxial crystals. *American Mineralogist,* **47**: 227-245.

Khan, M.A., T. Shoji and T. Takahashi (1982) Acoustic emission from cleavage microcracking in alloy steels. *Metallurgical Science,* **16**: 118-126.

Langway, C.C. (1958) Ice fabric and the universal stage. USA Snow, Ice and Permafrost Research Establishment (SIPRE), Technical Report 62.

Li, J.C.M. and Y.T. Chou (1970) The role of dislocations in the flow stress grain size relationships. *Metallurgical Transactions,* **1**: 1145-1159.

Lim, P.N. (1983) The effects of temperature and grain size on the tensile strength of ice. M.S. thesis, Thayer School of Engineering, Dartmouth College, Hanover, N.H.

McMahon, C.J. and M. Cohen &1965) Initiation of cleavage in polycrystalline iron. *Acta Metallurgica,* **13**(June): 591-604.

Mellor, M. and D.M. Cole (1982) Deformation and failure of ice under constant stress or constant strain rate. *Cold Regions Science and Technology,* **5**: 201-219.

Mendiratta, M.G., S.M.L. Sastry and J.V. Smith (1976) Effect of grain size upon flow and fracture in a precipitation strengthened Ti-8 wt% Al-0.25 wt% Si alloy. *Journal of Material Science,* **11**: 1835-1842.

Ono, K., R. Landy and C. Ouchi (1978) On the amplitude distribution of burst emission due to MnS inclusions in HSLA steels. *Proceedings, Fourth Acoustic Emission Symposium, High Pressure Institute of Japan,* pp. 4-33 to 4-44.

Pollock, A.A. (1981) Acoustic emissions amplitude distributions. *International Advances in Nondestructive Testing,* **7**: 215-239.

St. Lawrence, W.F. and D.M. Cole (1982) Acoustic emissions from polycrystalline ice. *Cold Regions Science and Technology,* **5**: 183-199.

Schulson, E.M. (1979) An analysis of the brittle to ductile transition in polycrystalline ice under tension. *Cold Regions Science and Technology,* **1**: 87-91.

Scruby, C., H. Wadley and J.E. Sinclair (1981) The origin of acoustic emission during deformation of an aluminum-magnesium alloy. *Philosophical Magazine,* Series A, **44**(2): 249-274.

Shewmon, P.G. (1969) *Transformations in Metals.* New York: McGraw-Hill, p. 54.

Sinha, N.K. (1978) Observation of basal dislocations in ice by etching and replicating. *Journal of Glaciology,* **21**(85): 385-395.

Sinha, N.K. (1082) Acoustic emissions and microcracking in ice. *Proceedings of the 1982 Joint Conference on Experimental Mechanics, Oahu-Maui, Hawaii,* pp. 767-772.

Smith, E. and J.T. Barnby (1967) Crack nucleation in crystalline solids. *Metal Science Journal,* **1**: 56–64.

Stroh, A.N. (1954) The formation of cracks as a result of plastic flow. *Proceedings, Royal Society,* A223: 404–414.

Stroh, A.N. (1957) A theory of the fracture of metals. *Advances in Physics,* **6**: 418–465.

Terlinde, G. and G.L. Luetjering (1982) Influence of grain size and age hardening on dislocation pile-ups and tensile fracture for a Ti-Al alloy. *Metallurgical Transactions,* A, **13A**(July): 1283–1292.

Wadley, H.N.G., C.B. Scruby and G.S. Shrimpton (1981) Quantiative acoustic emission source characterization during low temperature cleavage and intergranular fracture. *Acta Metallurgica,* **29**: 399–414.

Wang, Y.S. (1979) Sea ice properties. Exxon Technical Seminar on Alaskan Beaufort Sea Gravel Island Design. Exxon, Houston, Texas.

Zaretsky, Y.K., A.M. Fish, V.P. Gavrilo and A.V. Gusev (1976) Short-term ice creep and microcrack formation. USA Cold Regions Research and Engineering Laboratory, Draft Translation 539, pp. 196–202.

Zaretsky, Y.K., B.D. Chumichev and V.I. Solmatin (1979) Ice behavior under load. *Engineering Geology,* **13**: 299–309.

Zener, C. (1948) *Fracturing of Metals.* American Society of Metals.

APPENDIX A: CRACK LENGTH HISTOGRAMS

This appendix contains microfracture length histograms for the specimens tested. In some cases the observations were broken down to indicate crack location (i.e. grain boundary). The following list describes the notation used for this purpose.

1. A four-digit sample number (SN) indicates that all crack length observations taken from thick sections of the sample are included.

2. The suffix GB indicates that the histogram includes only grain boundary crack observations taken from thin sections.

3. The suffix XT indicates that the histogram contains only transcrystalline or intracrystalline crack observations taken from thin sections (cracks of mixed character were categorized according to their dominant characteristics).

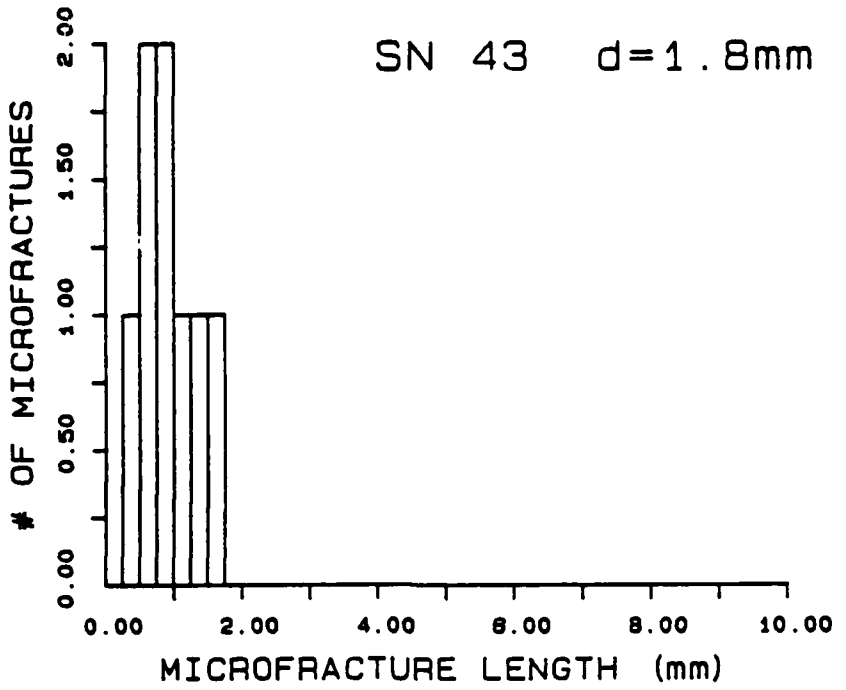

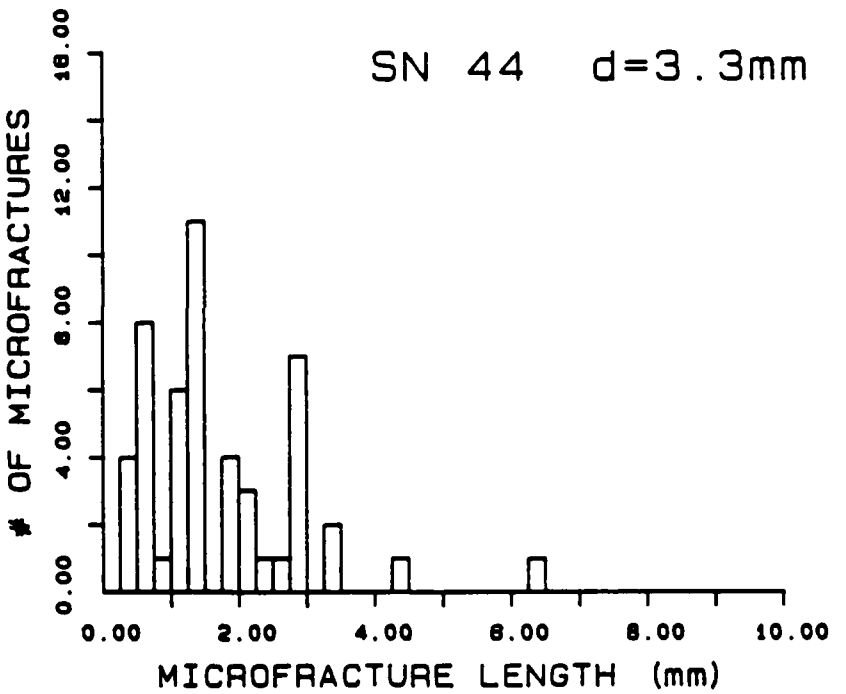

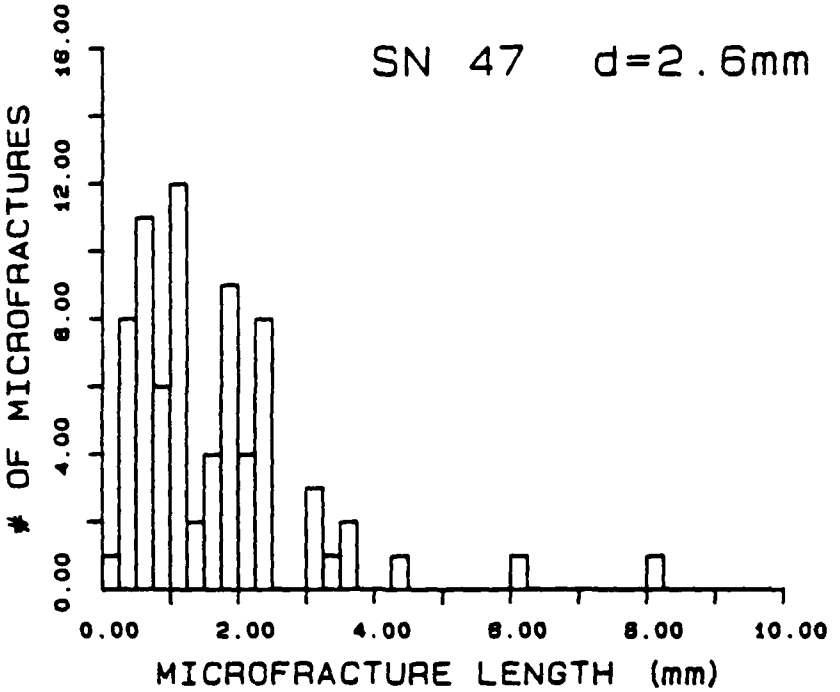
SN 47 d=2.6mm
OF MICROFRACTURES
0.00
4.00
8.00
12.00
16.00
0.00
2.00
4.00
6.00
8.00
10.00
MICROFRACTURE LENGTH (mm)

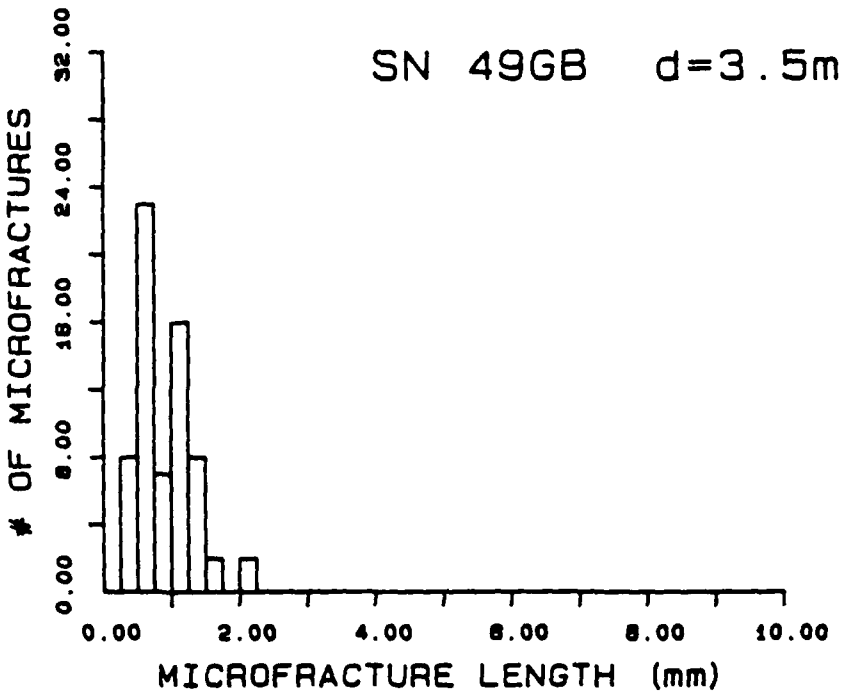
SN 49GB d=3.5mm
OF MICROFRACTURES
0.00
8.00
16.00
24.00
32.00
0.00
2.00
4.00
6.00
8.00
10.00
MICROFRACTURE LENGTH (mm)

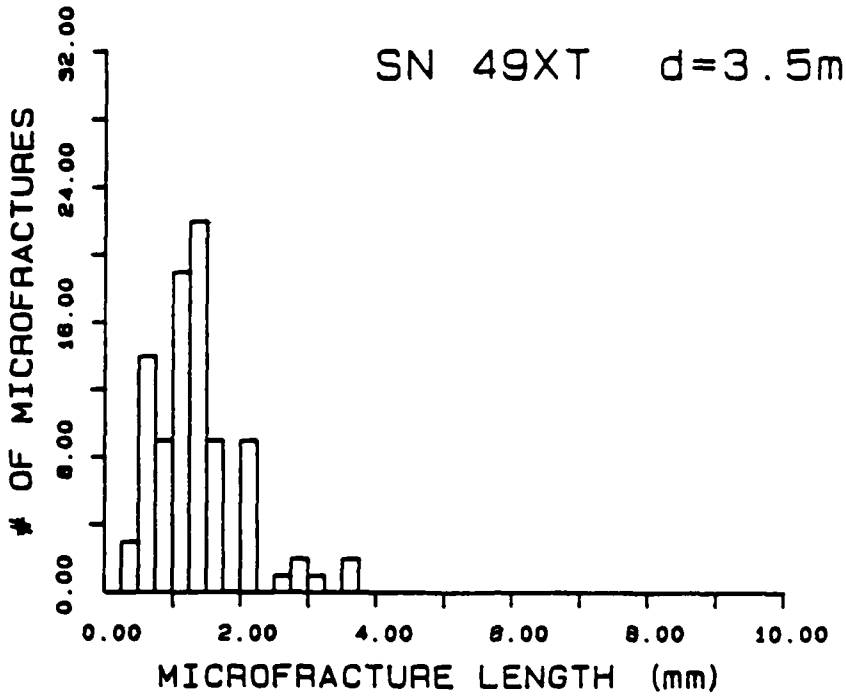
SN 49XT d=3.5mm
OF MICROFRACTURES
0.00
8.00
16.00
24.00
32.00
0.00
2.00
4.00
6.00
8.00
10.00
MICROFRACTURE LENGTH (mm)

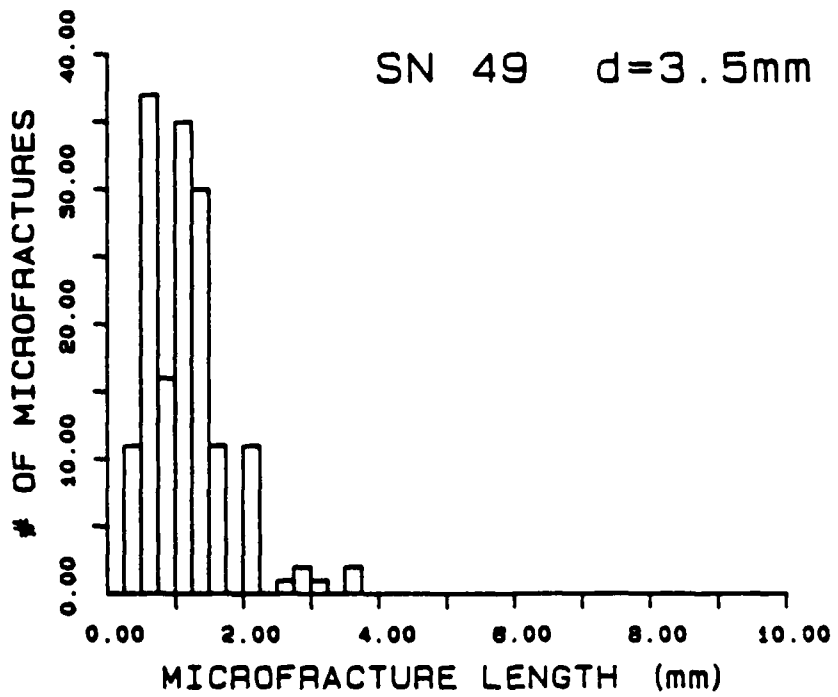
SN 49 d=3.5mm
OF MICROFRACTURES
0.00
10.00
20.00
30.00
40.00
0.00
2.00
4.00
6.00
8.00
10.00
MICROFRACTURE LENGTH (mm)

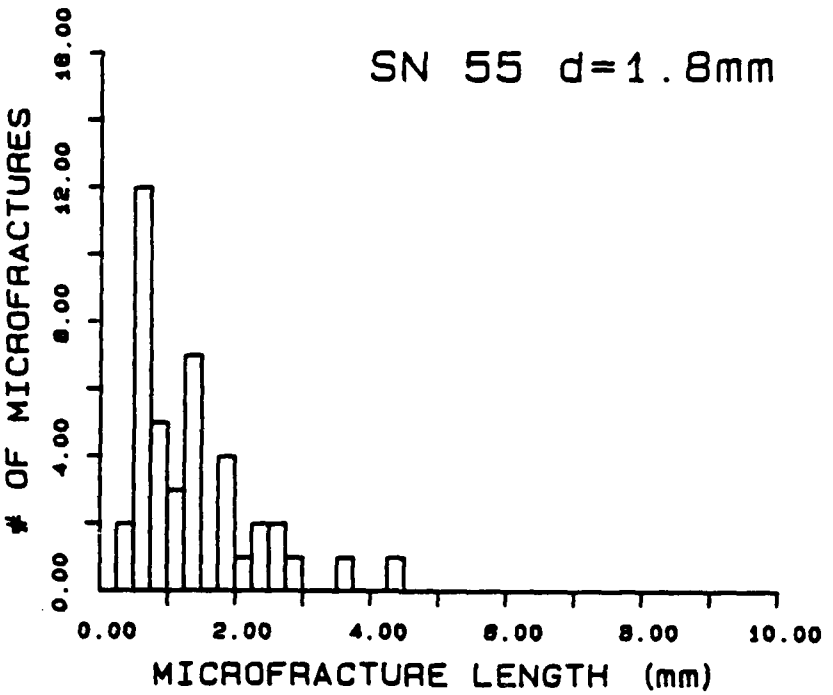
SN 55 d=1.8mm
OF MICROFRACTURES
0.00
4.00
8.00
12.00
16.00
0.00
2.00
4.00
6.00
8.00
10.00
MICROFRACTURE LENGTH (mm)

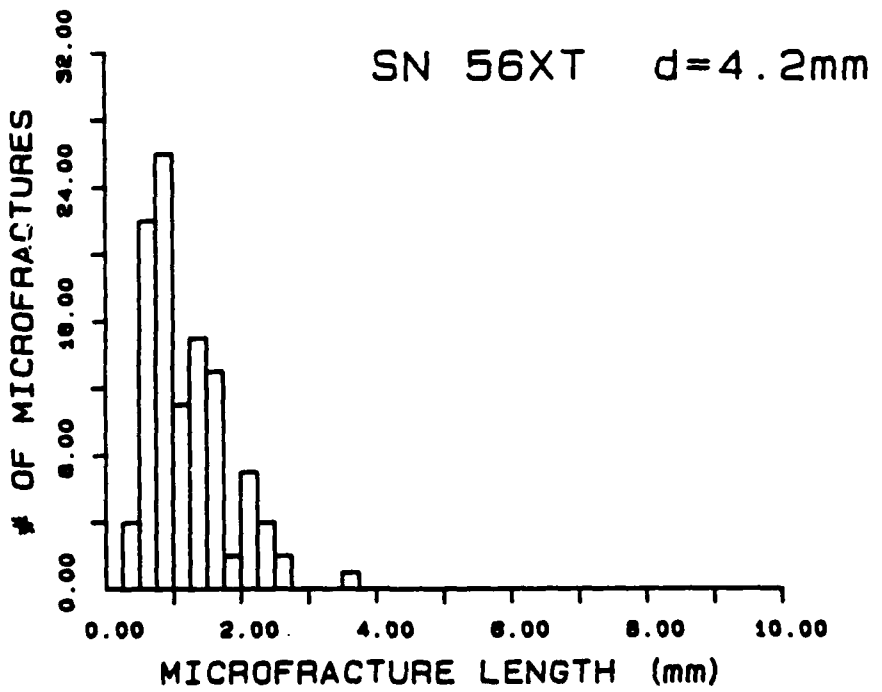
SN 56XT d=4.2mm
OF MICROFRACTURES
0.00
8.00
16.00
24.00
32.00
0.00
2.00
4.00
6.00
8.00
10.00
MICROFRACTURE LENGTH (mm)

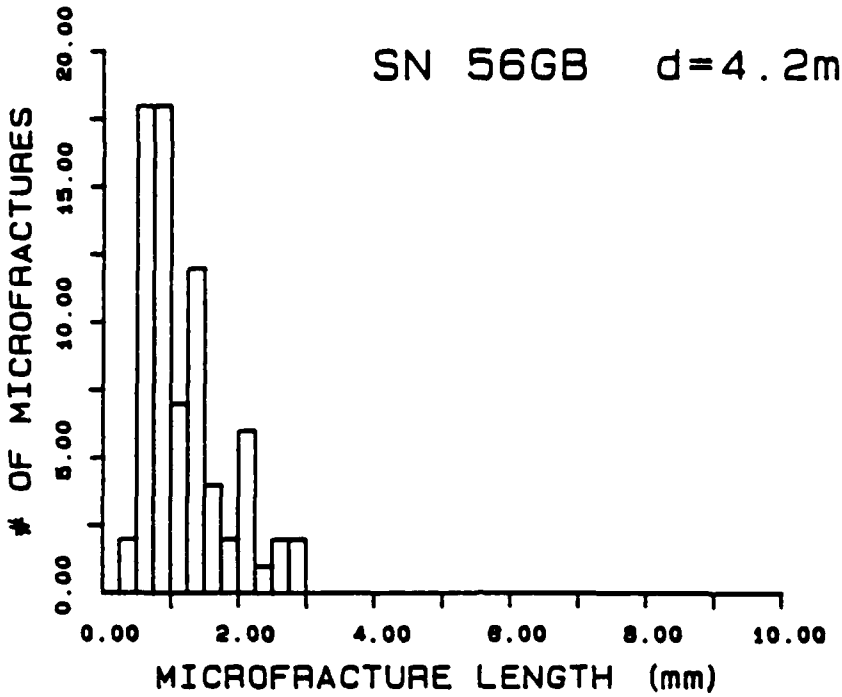
SN 56GB d=4.2mm
OF MICROFRACTURES
0.00
5.00
10.00
15.00
20.00
0.00
2.00
4.00
6.00
8.00
10.00
MICROFRACTURE LENGTH (mm)

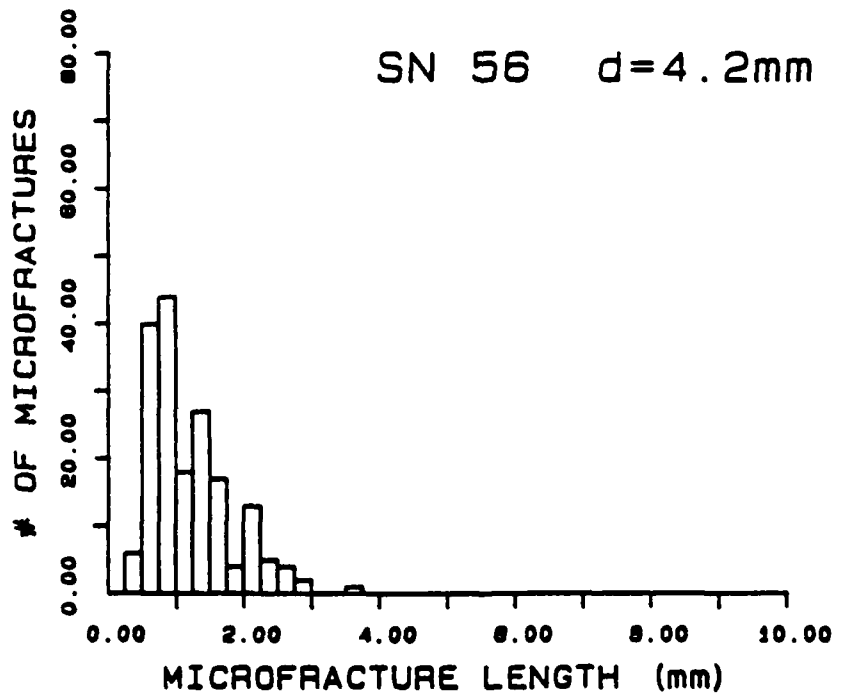
SN 56 d=4.2mm
OF MICROFRACTURES
0.00
20.00
40.00
60.00
80.00
0.00
2.00
4.00
6.00
8.00
10.00
MICROFRACTURE LENGTH (mm)

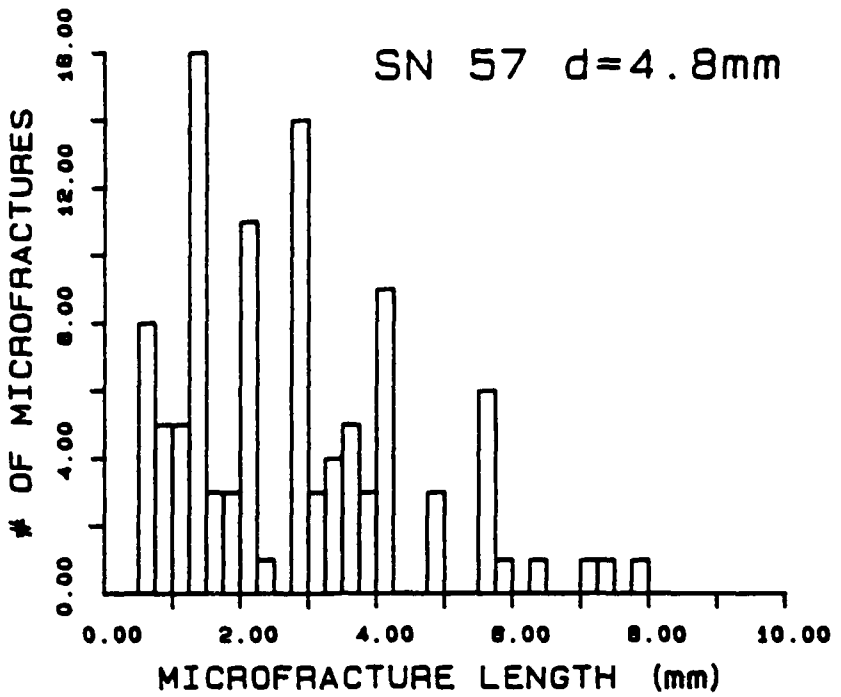
SN 57 d=4.8mm
OF MICROFRACTURES
0.00
4.00
8.00
12.00
16.00
0.00
2.00
4.00
6.00
8.00
10.00
MICROFRACTURE LENGTH (mm)

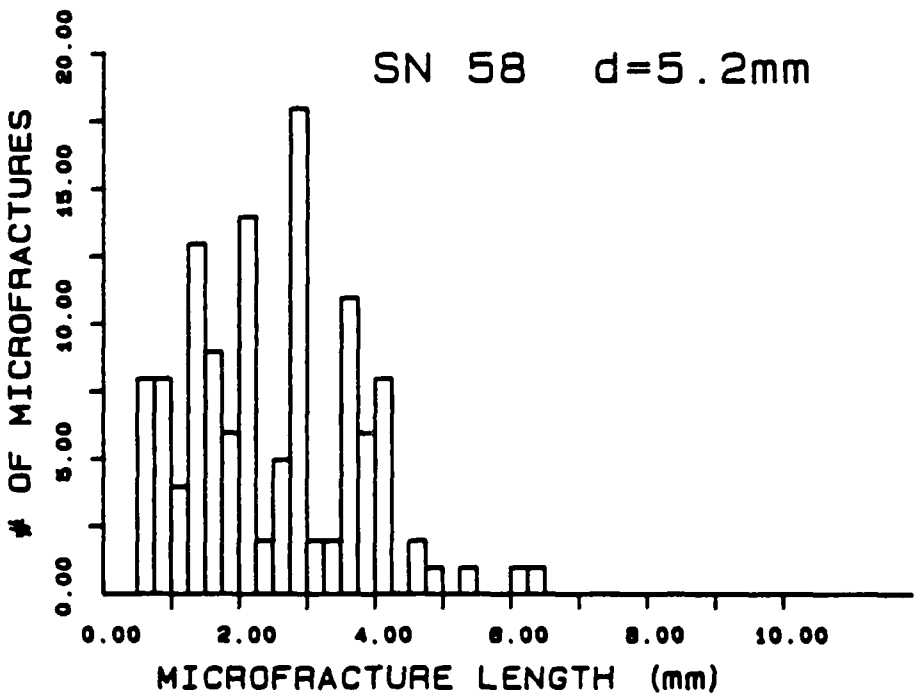
SN 58 d=5.2mm
OF MICROFRACTURES
0.00
5.00
10.00
15.00
20.00
0.00
2.00
4.00
6.00
8.00
10.00
MICROFRACTURE LENGTH (mm)

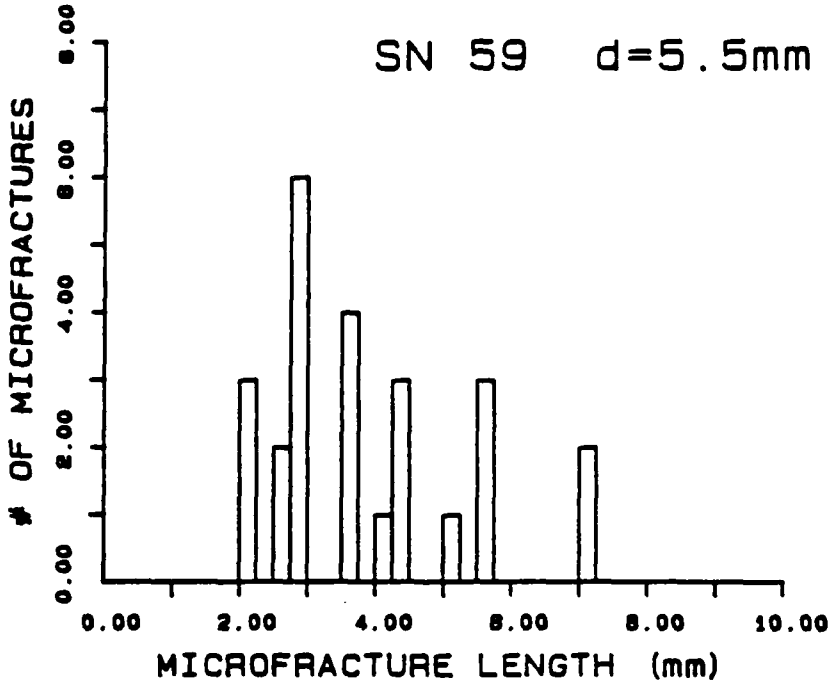
SN 59 d=5.5mm
OF MICROFRACTURES
0.00
2.00
4.00
6.00
8.00
0.00
2.00
4.00
6.00
8.00
10.00
MICROFRACTURE LENGTH (mm)

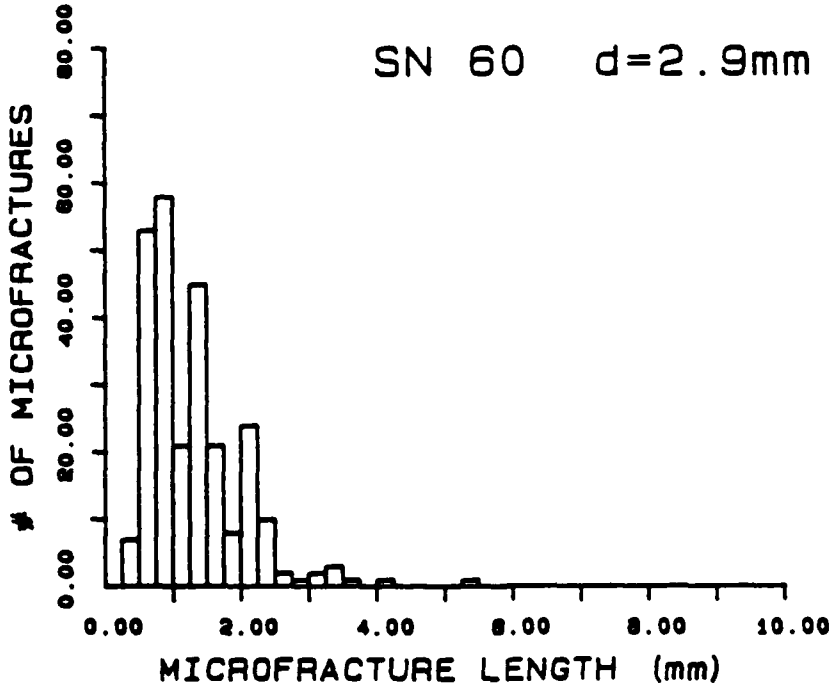
SN 60 d=2.9mm
OF MICROFRACTURES
0.00
20.00
40.00
60.00
80.00
0.00
2.00
4.00
6.00
8.00
10.00
MICROFRACTURE LENGTH (mm)

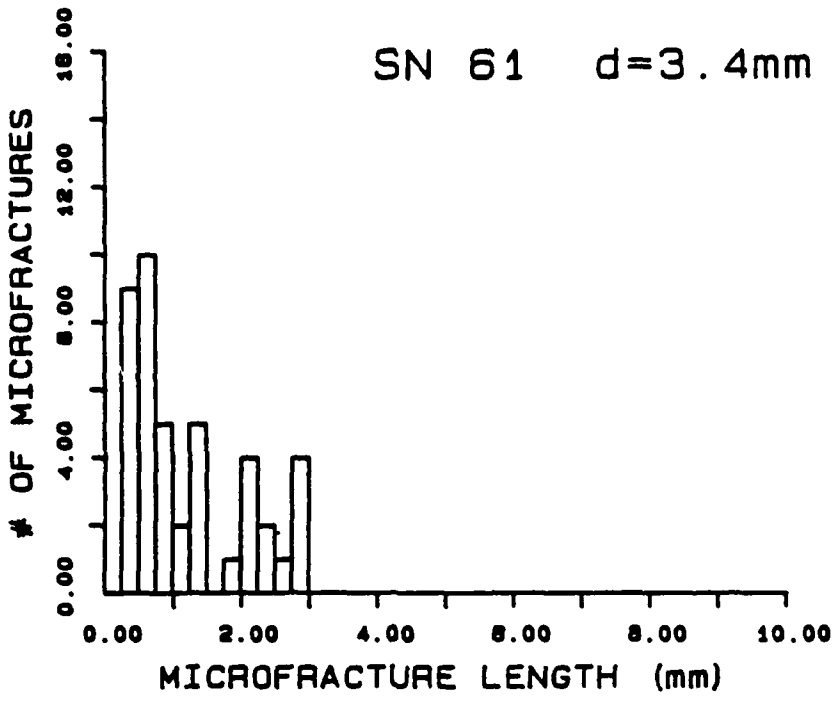
SN 61 d=3.4mm
OF MICROFRACTURES
0.00
4.00
8.00
12.00
16.00
0.00
2.00
4.00
6.00
8.00
10.00
MICROFRACTURE LENGTH (mm)

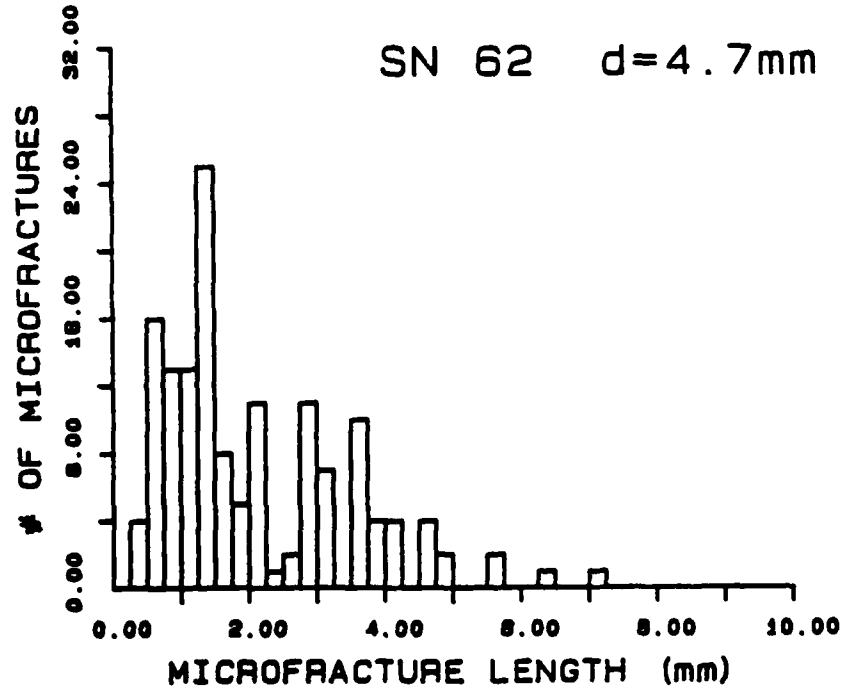
SN 62 d=4.7mm
OF MICROFRACTURES
0.00
8.00
16.00
24.00
32.00
0.00
2.00
4.00
6.00
8.00
10.00
MICROFRACTURE LENGTH (mm)

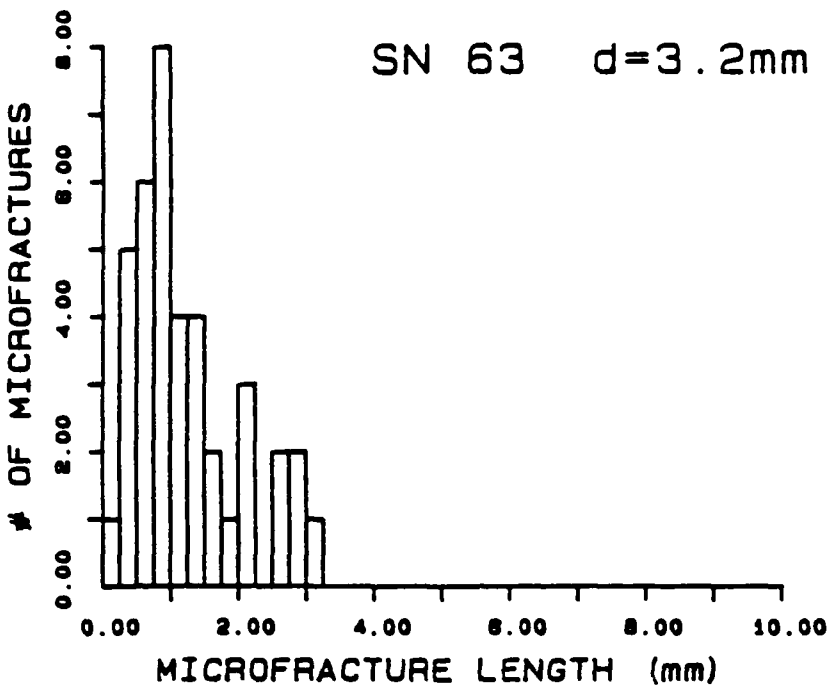
SN 63 d=3.2mm
OF MICROFRACTURES
0.00
2.00
4.00
6.00
8.00
0.00
2.00
4.00
6.00
8.00
10.00
MICROFRACTURE LENGTH (mm)

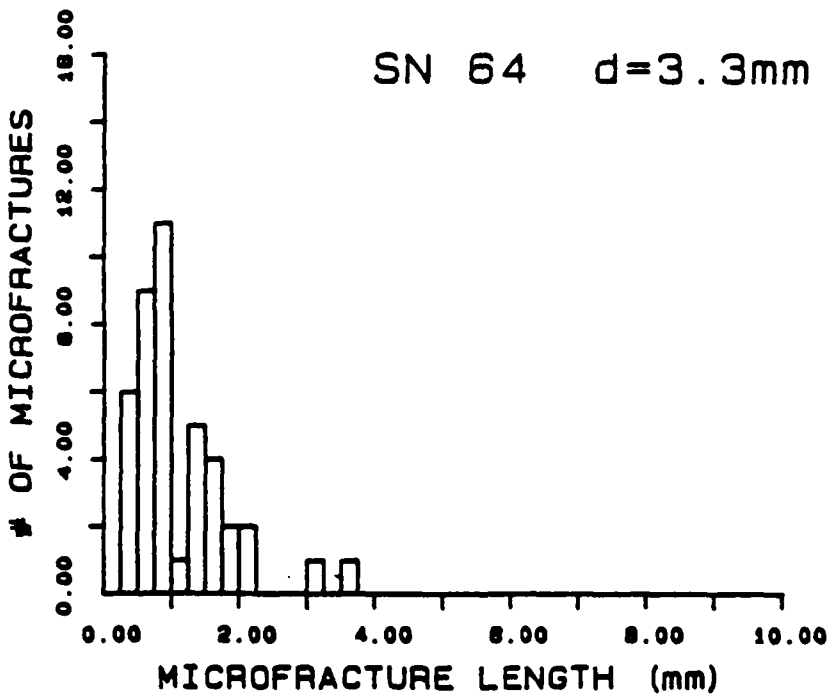
SN 64 d=3.3mm
OF MICROFRACTURES
0.00
4.00
8.00
12.00
16.00
0.00
2.00
4.00
6.00
8.00
10.00
MICROFRACTURE LENGTH (mm)

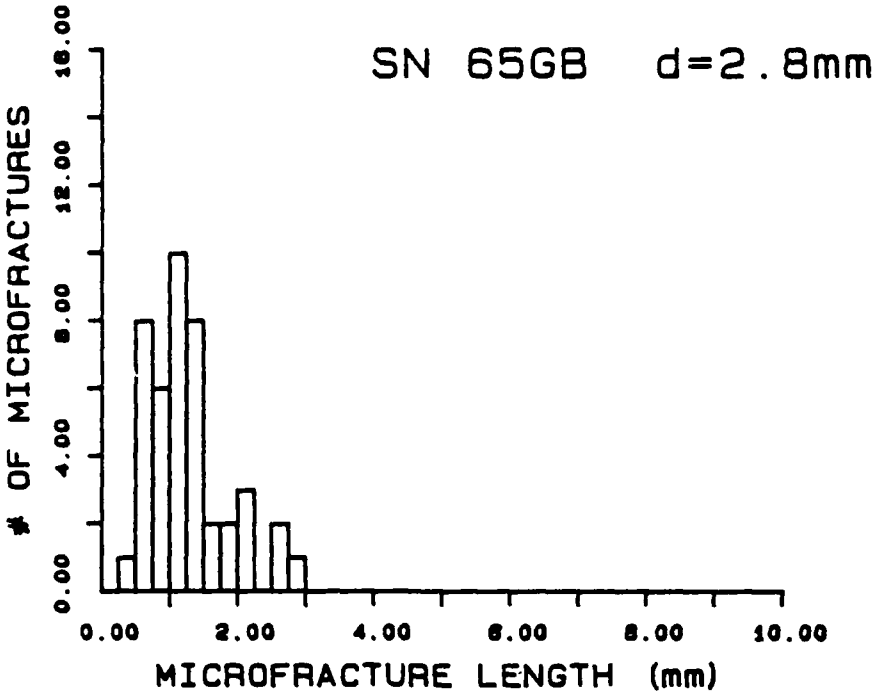
SN 65GB d=2.8mm
OF MICROFRACTURES
0.00
4.00
8.00
12.00
16.00
0.00
2.00
4.00
6.00
8.00
10.00
MICROFRACTURE LENGTH (mm)

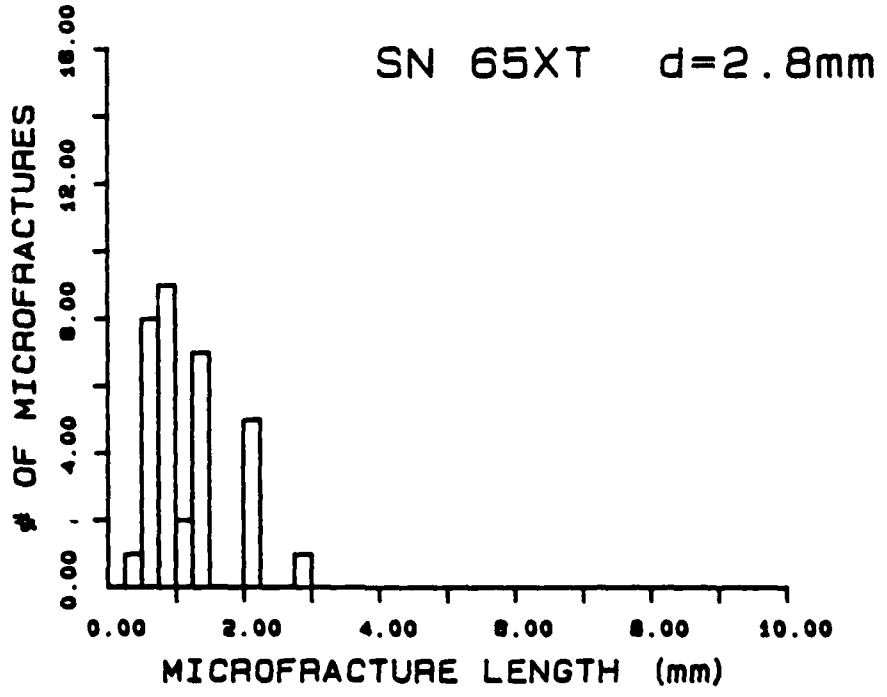
SN 65XT d=2.8mm
OF MICROFRACTURES
0.00
4.00
8.00
12.00
16.00
0.00
2.00
4.00
6.00
8.00
10.00
MICROFRACTURE LENGTH (mm)

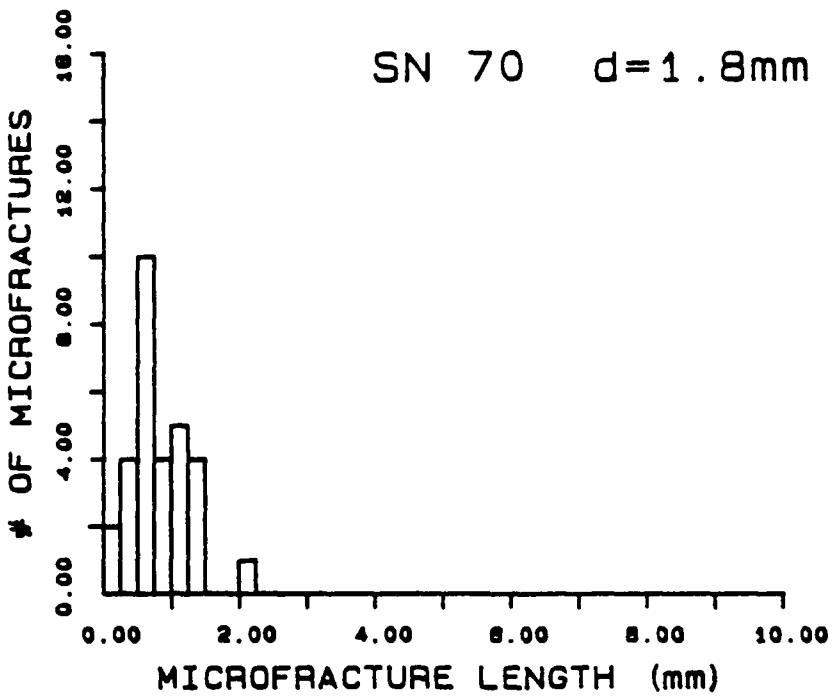
SN 70 d=1.8mm
OF MICROFRACTURES
0.00
4.00
8.00
12.00
16.00
0.00
2.00
4.00
6.00
8.00
10.00
MICROFRACTURE LENGTH (mm)

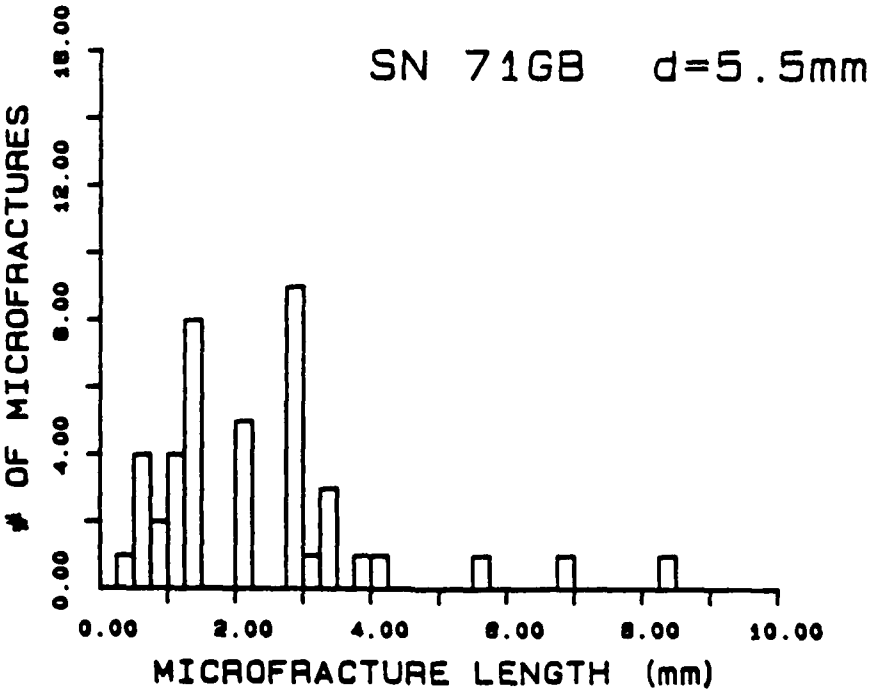
SN 71GB d=5.5mm
OF MICROFRACTURES
0.00
4.00
8.00
12.00
16.00
0.00
2.00
4.00
6.00
8.00
10.00
MICROFRACTURE LENGTH (mm)

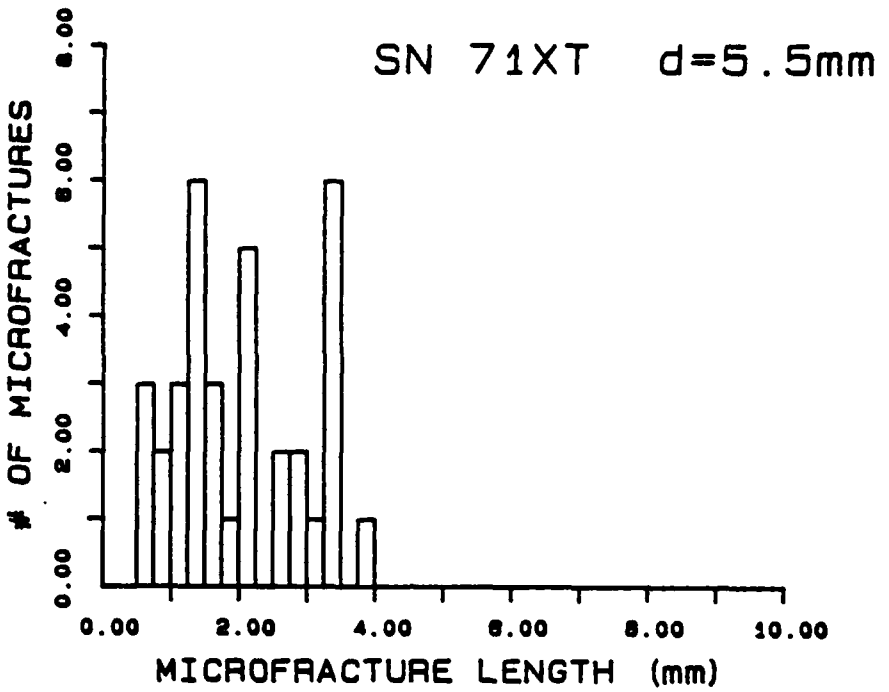
SN 71XT d=5.5mm
OF MICROFRACTURES
0.00
2.00
4.00
6.00
8.00
0.00
2.00
4.00
6.00
8.00
10.00
MICROFRACTURE LENGTH (mm)

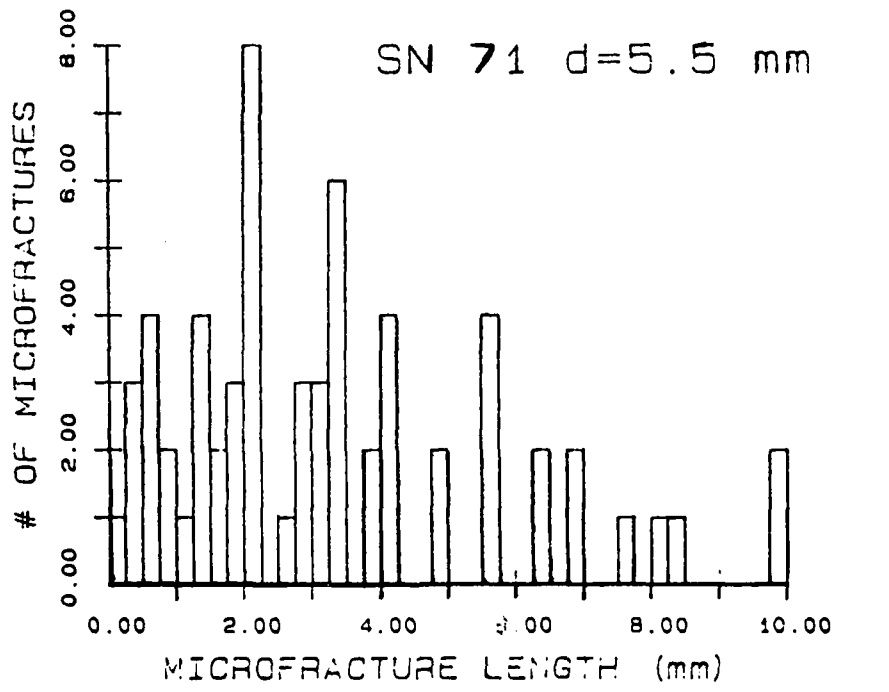
SN 71 d=5.5 mm
OF MICROFRACTURES
0.00
2.00
4.00
6.00
8.00
0.00
2.00
4.00
6.00
8.00
10.00
MICROFRACTURE LENGTH (mm)

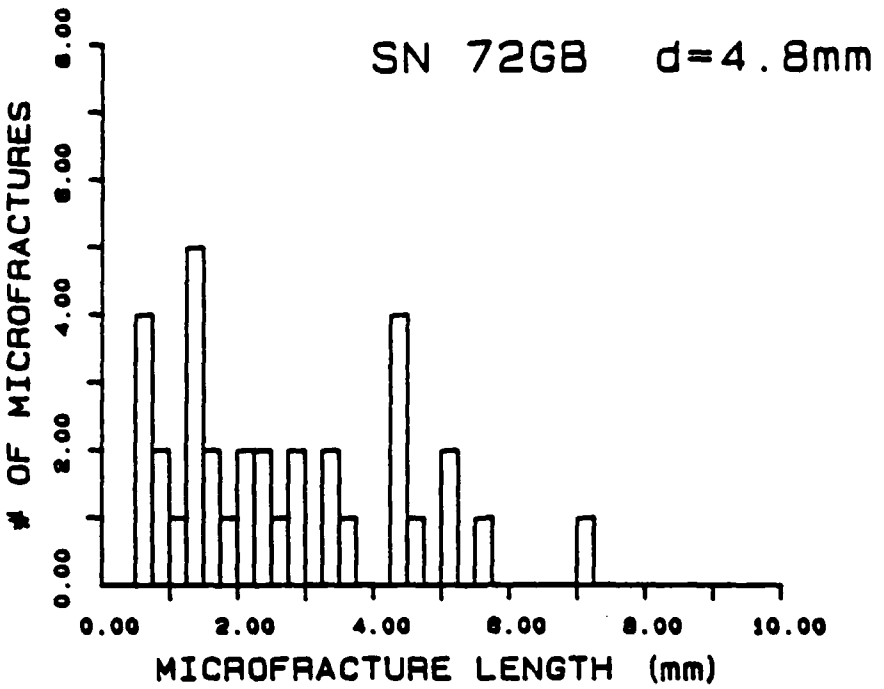
SN 72GB d=4.8mm
OF MICROFRACTURES
0.00
2.00
4.00
6.00
8.00
0.00
2.00
4.00
6.00
8.00
10.00
MICROFRACTURE LENGTH (mm)

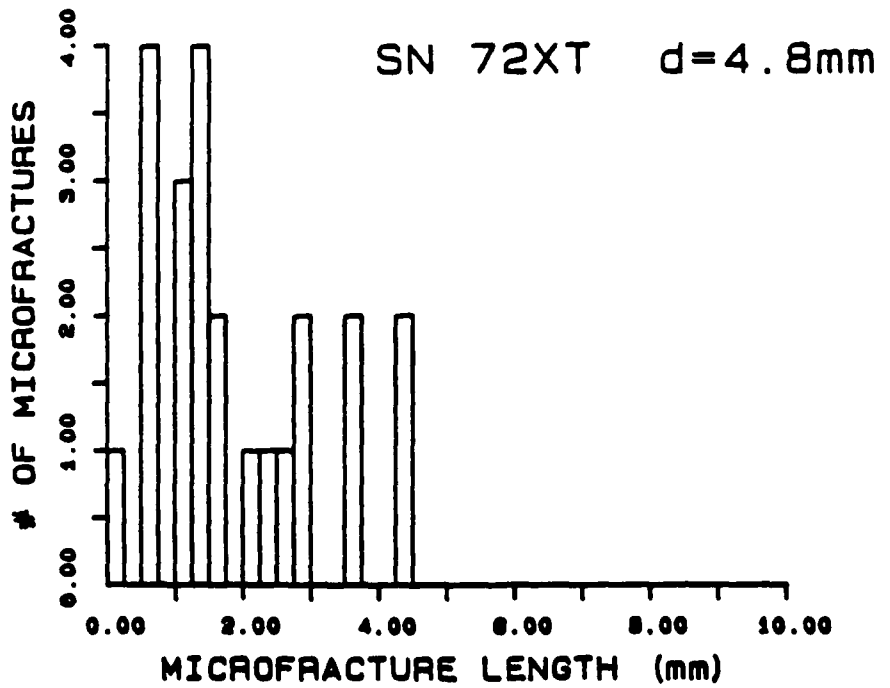
SN 72XT d=4.8mm
OF MICROFRACTURES
0.00
1.00
2.00
3.00
4.00
0.00
2.00
4.00
6.00
8.00
10.00
MICROFRACTURE LENGTH (mm)

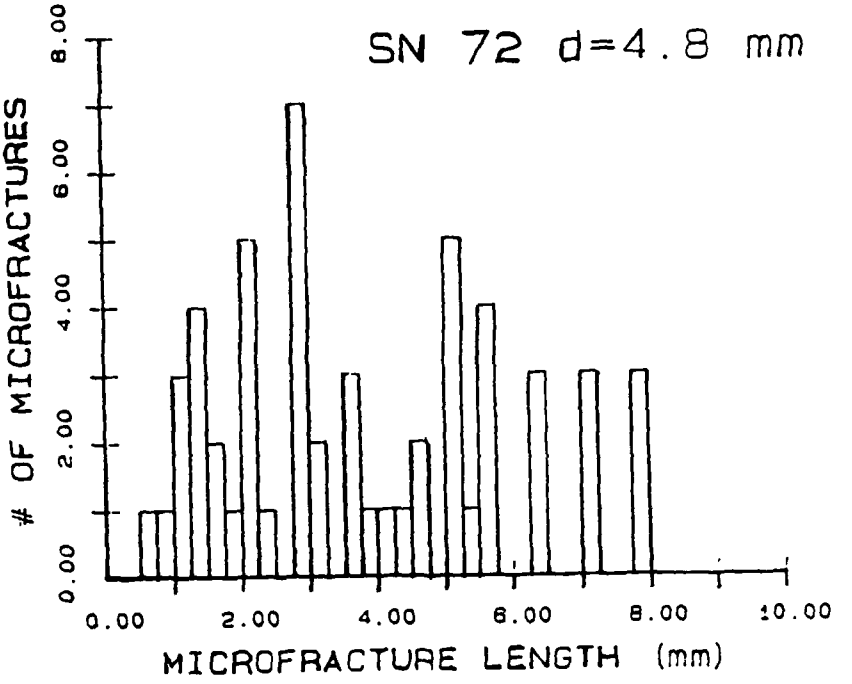
SN 72 d=4.8 mm
OF MICROFRACTURES
0.00
2.00
4.00
6.00
8.00
0.00
2.00
4.00
6.00
8.00
10.00
MICROFRACTURE LENGTH (mm)

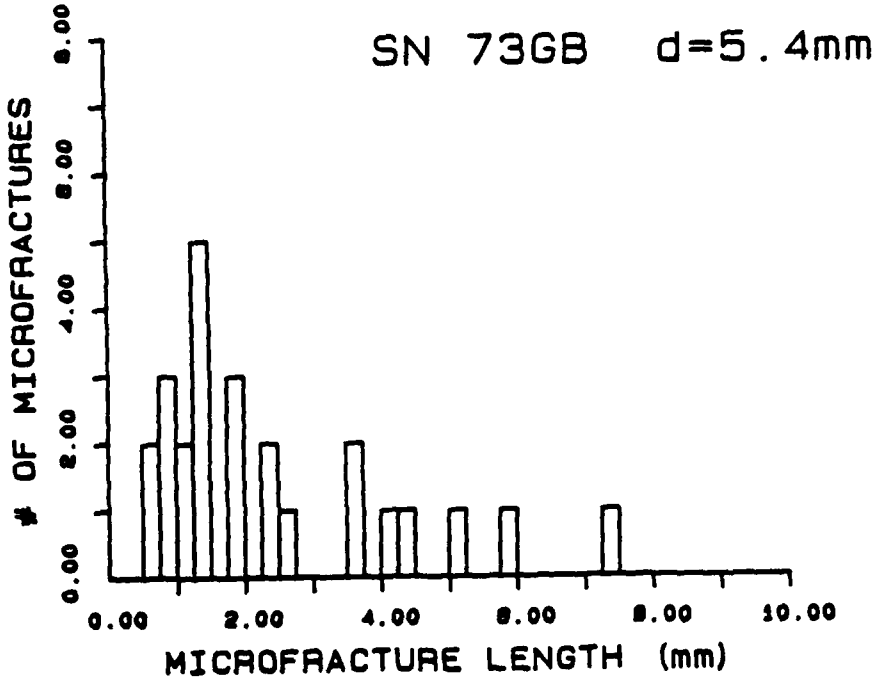
SN 73GB d=5.4mm
OF MICROFRACTURES
0.00
2.00
4.00
6.00
8.00
0.00
2.00
4.00
6.00
8.00
10.00
MICROFRACTURE LENGTH (mm)

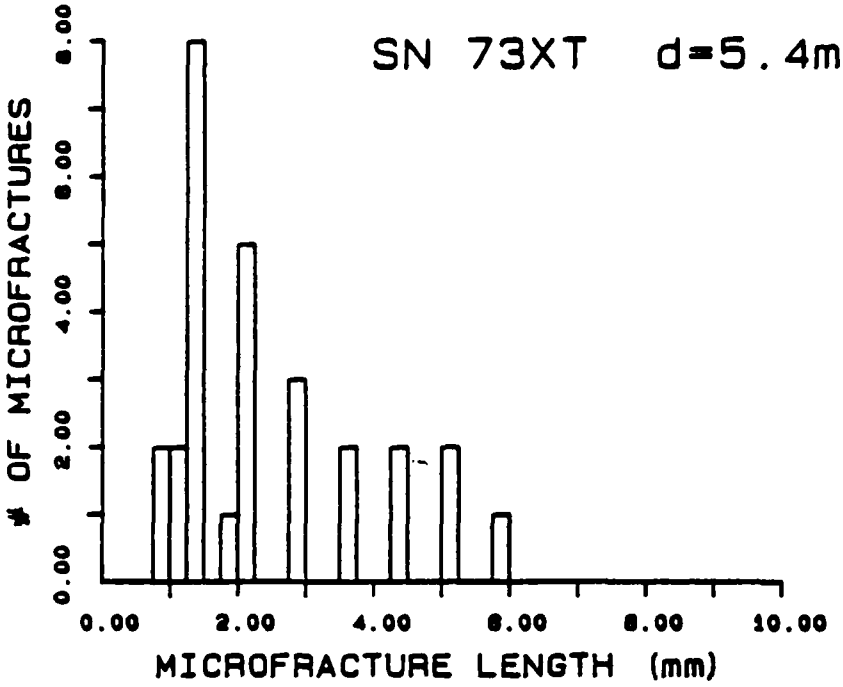
SN 73XT d=5.4mm
OF MICROFRACTURES
0.00
2.00
4.00
6.00
8.00
0.00
2.00
4.00
6.00
8.00
10.00
MICROFRACTURE LENGTH (mm)

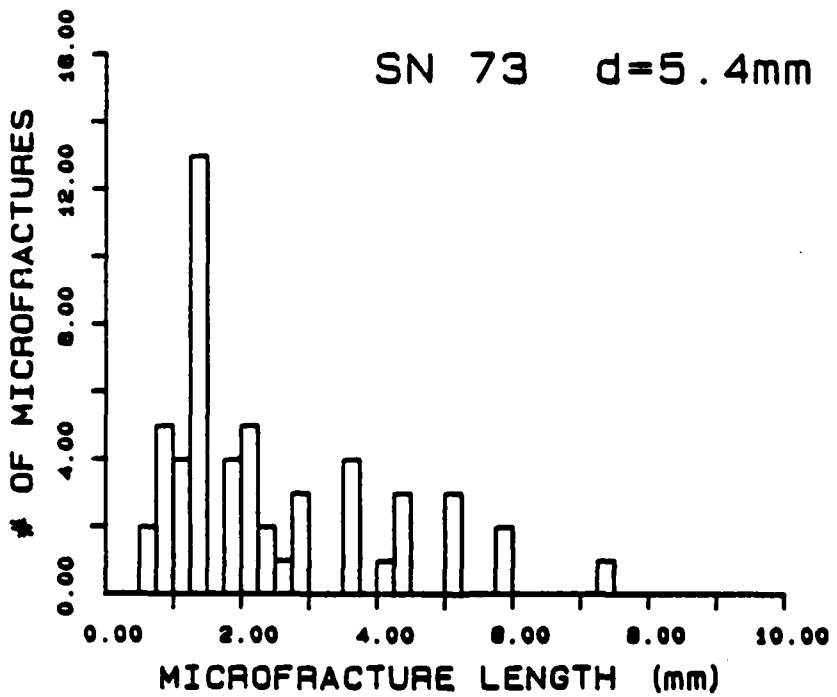
SN 73 d=5.4mm
OF MICROFRACTURES
0.00
4.00
8.00
12.00
16.00
0.00
2.00
4.00
6.00
8.00
10.00
MICROFRACTURE LENGTH (mm)

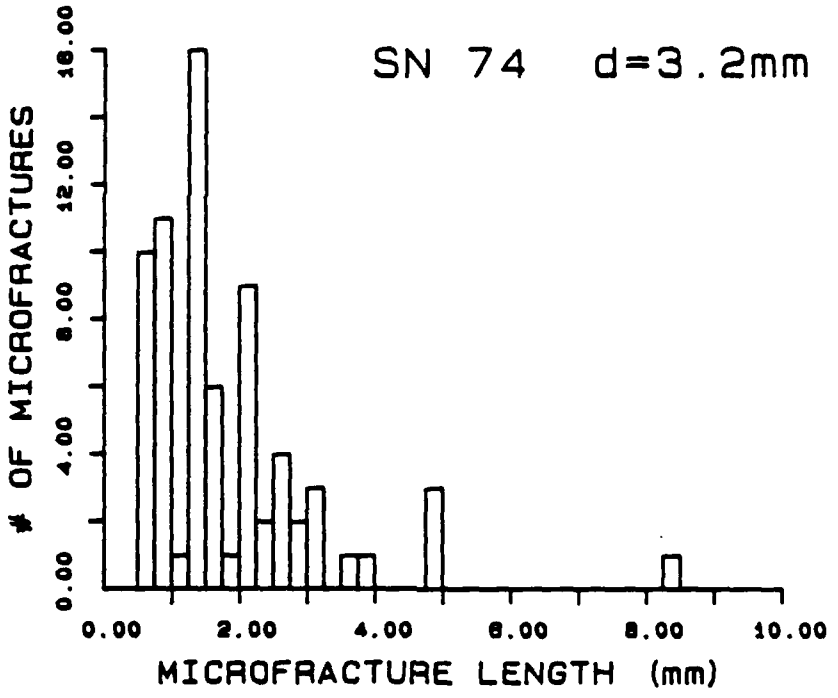
SN 74 d=3.2mm
OF MICROFRACTURES
0.00
4.00
8.00
12.00
16.00
0.00
2.00
4.00
6.00
8.00
10.00
MICROFRACTURE LENGTH (mm)

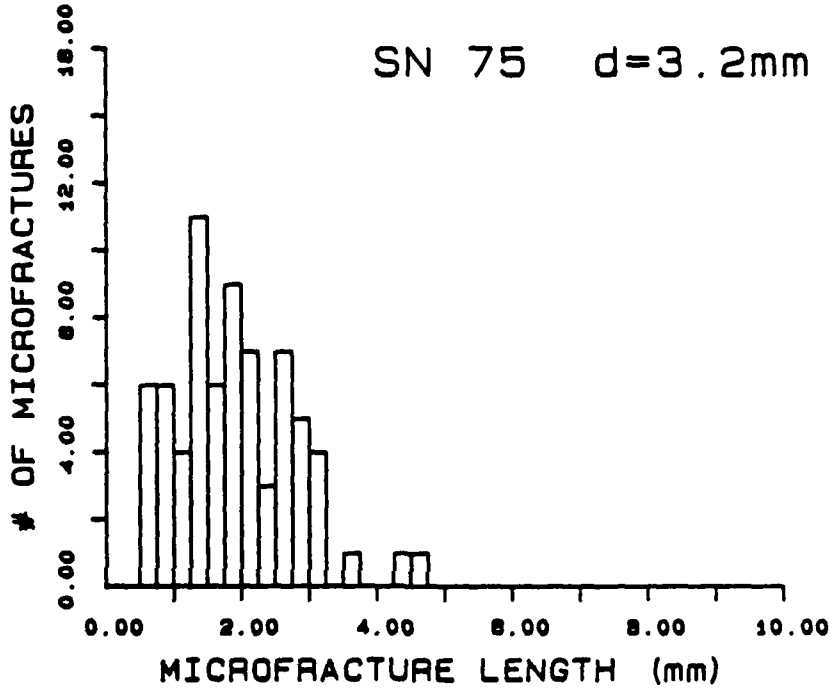
SN 75 d=3.2mm
OF MICROFRACTURES
0.00
4.00
8.00
12.00
16.00
0.00
2.00
4.00
6.00
8.00
10.00
MICROFRACTURE LENGTH (mm)

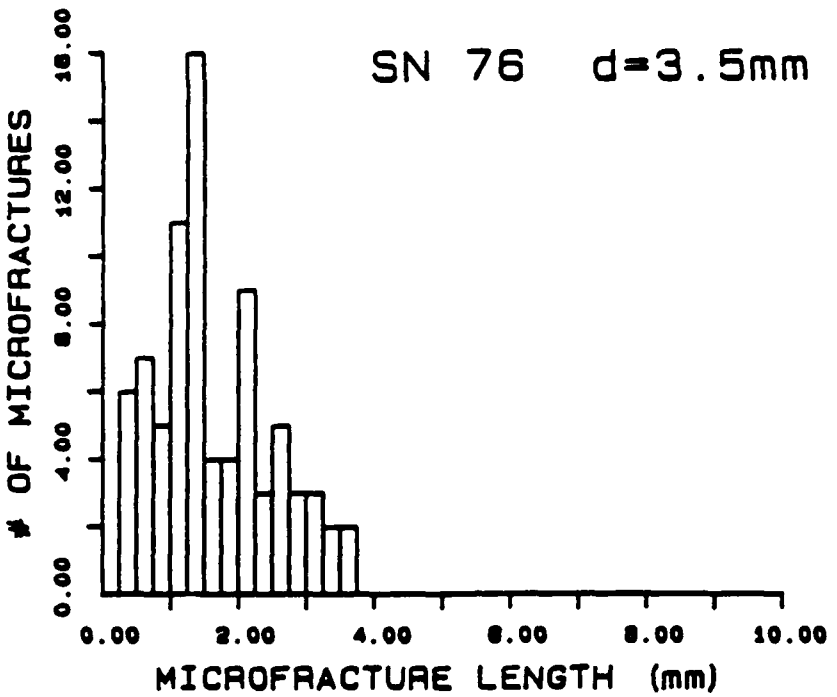
SN 76 d=3.5mm
OF MICROFRACTURES
0.00
4.00
8.00
12.00
16.00
0.00
2.00
4.00
6.00
8.00
10.00
MICROFRACTURE LENGTH (mm)

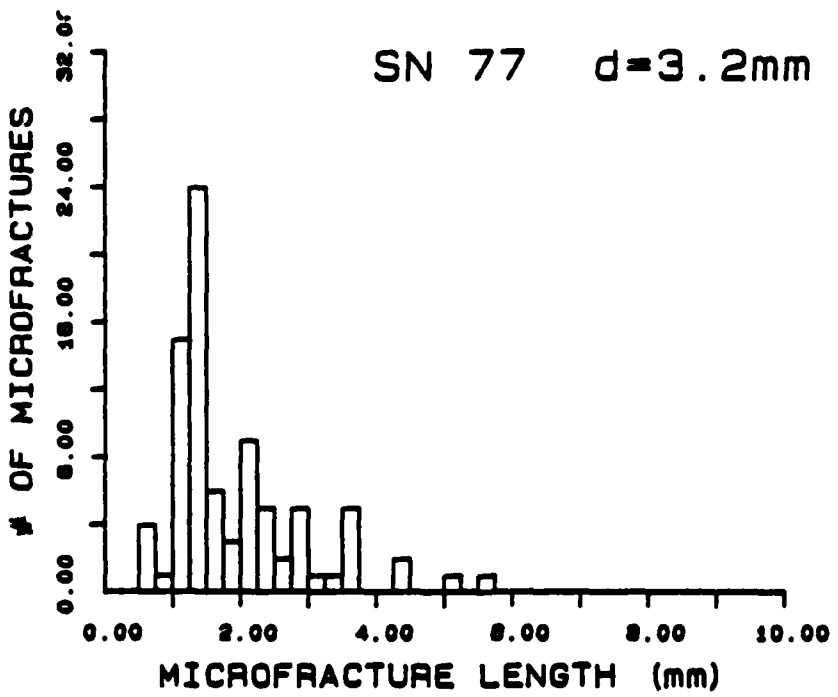
SN 77 d=3.2mm
OF MICROFRACTURES
0.00
8.00
16.00
24.00
32.00
0.00
2.00
4.00
6.00
8.00
10.00
MICROFRACTURE LENGTH (mm)

APPENDIX B: CRYSTAL ORIENTATIONS

This appendix contains pole diagrams for two specimens containing cracks. For each specimen, a number of measurements were taken to indicate the random nature of the grain orientation. In addition, the orientations of grains containing cracks are plotted separately.

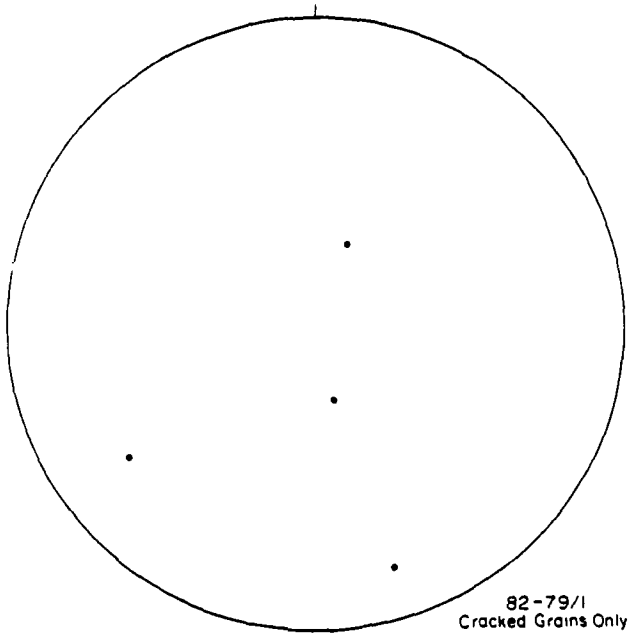

82-79/1
Cracked Grains Only

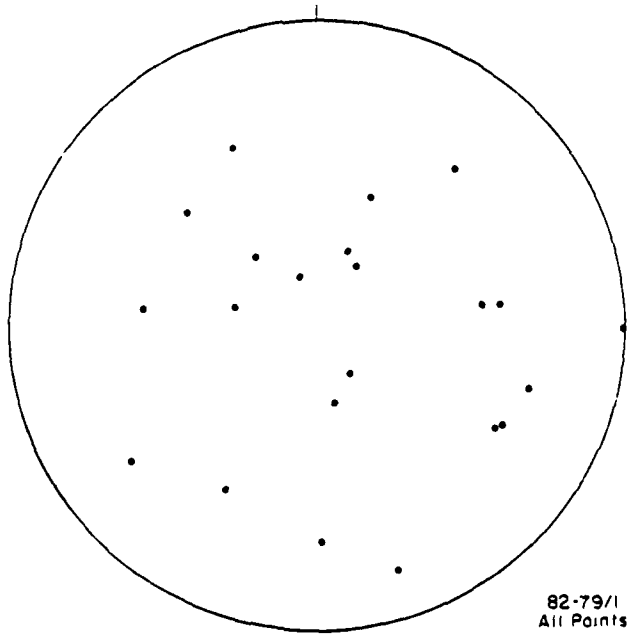

82-79/1
All Points

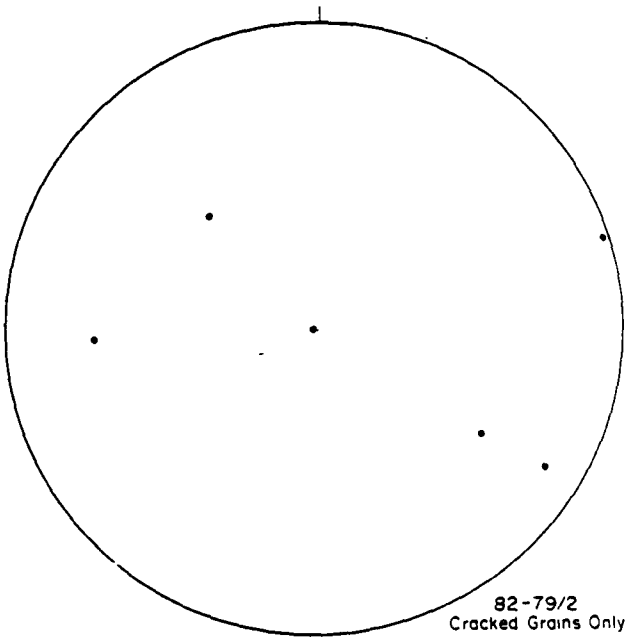

82-79/2
Cracked Grains Only

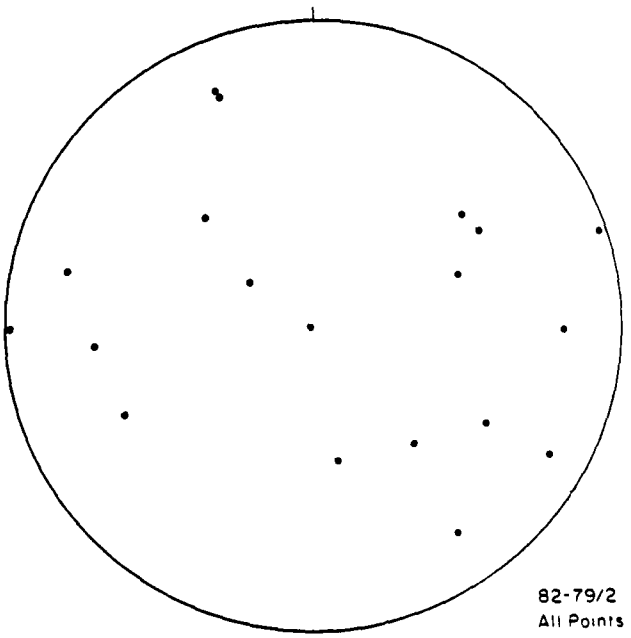

82-79/2
All Points

A facsimile catalog card in Library of Congress MARC format is reproduced below.

Cole, David M.
Effect of grain size on the internal fracturing of polycrystalline ice / by David M. Cole. Hanover, N.H.: U.S. Army Cold Regions Research and Engineering Laboratory; Springfield, Va.: available from National Technical Information Service, 1986.
v, 79 p., illus.; 28 cm. (CRREL Report 86-5.)
Prepared for the Office of the Chief of Engineers by Corps of Engineers, U.S. Army Cold Regions Research and Engineering Laboratory under DA Project 4A762730AT42.
Bibliography: p. 49.
1. Acoustic emissions. 2. Creep tests. 3. Fracture (mechanics). 4. Grain size. 5. Ice. 6. Polycrystalline. I. United States. Army. Corps of Engineers. II. Cold Regions Research and Engineering Laboratory, Hanover, N.H. III. Series: CRREL Report 86-5.

☆U.S. GOVERNMENT PRINTING OFFICE: 1986 -600 -048 / 32019

END

10-86

DTIC